EFFECT OF FORMULATION VARIABLES ON INSULIN LOCALISATION WITHIN SOLID LIPID NANOPARTICLES

LI MING THONG, MPharm (Hons)

Thesis submitted to The University of Nottingham

for the degree of Doctor of Philosophy

MARCH 2015

ABSTRACT

There has been a lot of interest on solid lipid nanoparticles (SLNs) as these colloidal submicron drug dosage forms present a promising frontier in drug delivery. It is possible to incorporate susceptible drugs such as protein intended for oral delivery. Here, we aim to develop an oral delivery system based on SLNs to deliver the peptide hormone, insulin using the double emulsion (W/O/W) solvent evaporation technique for formulating the SLNs. The choice of lipids was carefully selected to incorporate acceptability to biological milieu. The main purpose of the work was to formulate SLNs to achieve different localisation of insulin within the SLNs, based on the three hypothetical models proposed by Muller *et al.* (2000). Following that, the effect of this localisation on the propensity of the SLNs to be taken up by absorptive cells was investigated. SLNs was successfully fabricated to achieve two insulin localisation models, namely the solid solution model and the core-shell model with drug-enriched shell. The zeta potential measurements was used to indirectly indicate the appropriate insulin localisation model. The zeta potential of the unloaded SLNs, insulin-loaded SLNs and surface-adsorbed insulin SLNs were recorded as -51.7 ± 1 mV, -45.8 ± 1 mV and -40.8 ± 1 mV respectively. *In vitro* cell studies showed a notable difference in the Caco-2 cell lines when the cells were exposed to SLNs of the two different insulin localisation models. Thus, different effects seen on the Caco-2 cells suggests that the localisation of insulin within SLNs can potentially influence its uptake, stressing the importance of characterising drug localisation in nanoparticles, as this eventually affects drug bioavailability.

LIST OF PUBLICATIONS AND PRESENTATIONS

Thong Li Ming, Nashiru Billa, Mohd Cairul Iqbal Amin. Preformulation studies on insulin-loaded solid lipid nanoparticles (SLN): A preliminary investigation on insulin stability. PPT-26, Malaysian Journal of Pharmacy 2009; 1(7).

L.M. Thong, N. Billa, C.J. Roberts, J.C. Burley. Effects of formulation processing on physical properties of insulin-containing palmitin/palmitic acid nanoparticles. Journal of Pharmacy and Pharmacology 2010; 62(10): 1426.

L.M. Thong, N. Billa, C.R. Roberts & J.C. Burley. Effect of cavitation intensity and lipid composition on physical properties of insulin-loaded tripalmitin and palmitic acid nanostructured lipid crystals (NLC). Poster presented in 2nd World Congress on Bioavailability & Bioequivalence: Pharmaceutical R&D Summit 2011 - International Conference on Pharmaceutics & Novel Drug Delivery Systems, Las Vegas, USA, June 6-8, 2011.

L.M. Thong, N. Billa. Zeta potential Measurements: Potential Indicator of Insulin Location within Solid Lipid Nanoparticles (SLNs). PPT-08, Malaysian Journal of Pharmacy 2011; 1(9): 391.

[Won the Best Poster Award in the MPS-Pharmacy Scientific Conference 2011]

L.M. Thong, N. Billa, C.J. Roberts. A potential approach indicating drug location in solid lipid nanoparticles. UK-PharmSci Conference, Nottingham, United Kingdom, Sept 12-14, 2012. (Poster 187)

ACKNOWLEDGEMENTS

I would like to express my sincerest gratitude to my project supervisor, Associate Professor Dr Nashiru Billa for his invaluable assistance and guidance given to me throughout this research period. Completion of this research project would not have been made possible without his tremendous support and encouragement rendered to me during the toughest times that I have encountered.

I would also like to extend my heartfelt thanks to Professor Stephen Doughty and Professor Andrew Morris for the opportunity given to me to successfully complete this research project, as well as the academic staffs from the School of Pharmacy who have helped and supported me along this long journey. Special thanks to Professor Clive Roberts for his invaluable advice and support given to me all along. I would also like to thank the Faculty of Science administrative and technical staffs as well as the technical staffs from Faculty of Engineering for their kind assistance and advice throughout the research period.

I also would like to express my gratitude to Associate Prof Dr Cairul Iqbal and Associate Prof Dr Syahrilnizam Abdullah from the Pharmacy Faculty in Universiti Kebangsaan Malaysia and Medical Genetics Laboratory in Universiti Putra Malaysia respectively, for their kind collaboration and assistance to allow the use of their laboratories to carry out the research work.

A big thank you to my colleagues from the School of Pharmacy as well as my fellow group members who were always there to render advice and encouragement during my time here. Not forgetting those who have shared the

same office in BB01, BB47 and NLG01 whom were always supportive and ready to listen and share ideas.

I would also like to thank Ministry of Science, Technology and Innovation of Malaysia (MOSTI 01-02-12-SF0062) for their financial support in making this project a feasible one. Special thank you to everyone else who has in one way or another helped and contributed to the success of this project.

Most importantly, I would like to extend my utmost appreciation to my beloved family members, especially to my mum and my late father, who have always been there for moral support and encouragement throughout this path.

Thank you.

TABLE OF CONTENTS

CHAPTER 6 CONCLUSION AND FUTURE WORK

LIST OF FIGURES

LIST OF TABLES

LIST OF EQUATIONS

Eq. 2.1: $$RSD = \frac{\text{Standard deviation}}{\text{Mean}} \text{ x } 100\%$$

Eq. 2.2: $$\text{Percentage Error } (\%) = \frac{\text{Measured} - \text{Actual Concentration}}{\text{Actual Concentration}} \text{ x } 100\%$$

Eq. 3.1: $$d(H) = \frac{kT}{3\pi\eta D}$$

Eq. 3.2: $$\upsilon \text{E} = 4\pi\varepsilon 0\varepsilon \text{r} \frac{\zeta}{6\pi\mu} (1 + \kappa r)$$

Eq. 3.3: $$\Delta S = \frac{\Delta \text{H}}{\text{Tm}}$$

Eq. 3.4: $$\% \text{ Encapsulation Efficiency} = \frac{\text{Amount of insulin in precipitate}}{\text{Total insulin added}} \text{ x } 100\%$$

Eq. 5.1 $$\text{C} = \frac{\text{n}}{\text{v}} \text{ x } \text{d}$$

ABBREVIATIONS

ACN	Acetonitrile
ATCC	American Type Culture Collection
DSC	Differential scanning calorimetry
CO_2	Carbon dioxide
CV	Coefficient of variation
DCM	Dichloromethane
DLPC	Dilauroyl phosphatidylcholine
DPPC	Dipalmitoyl phosphatidylcholine
DLS	Dynamic light scattering
DMSO	Dimethyl sulfoxide
EDTA	Ethylenediaminetetraacetic acid disodium salt
EE	Encapsulation efficiency
FBS	Fetal Bovine Serum
FDA	Food and drug administration
FE-SEM	Field emission-scanning electron microscopy
GALT	Gut-associated lymphoid tissue
GAMA	Gas-assisted melting atomization
GIT	Gastrointestinal tract
GRAS	Generally regarded as safe
HCl	Hydrochloric acid
HPLC	High Performance Liquid Chromatography
IDF	International Diabetes Federation
LOD	Limit of Detection
LOQ	Limit of Quantification
MEM	Minimum Essential Media
MeOH	Methanol
MTT	Diphenyltetrazolium bromide
NHMS	National Health and Morbidity Survey
NLCs	Nanostructured lipid carriers
PACA	Poly(alkyl cyanoacrylate)
PBS	Phosphate-Buffered Saline
PCS	Photon Correlation Spectroscopy
PdI	Polydispersity index

Pen-Strep	Penicillin-Streptomycin
PES	Polyethersulfone
PGSS	Particles from Gas Saturated Solutions
PLGA	Poly $_{D,L}$-lactide-*co*-glycolide
PLM	Polarised light microscopy
P(MAA-g-EG)	Poly (methacrylic acid-g-ethylene glycol)
RC	Regenerated cellulose
RSD	Relative standard deviation
R_t	Retention time
SD	Standard deviation
SEM	Scanning electron microscopy
SLNs	Solid lipid nanoparticles
TEM	Transmission electron microscopy
TFA	Trifluoroacetic acid
W/O	Water-in-oil
W/O/W	Water-in-oil-in-water

CHAPTER 1

INTRODUCTION

1.1 General Overview

The rapid advances in the biotechnology sector in recent years has led to an increased production of biopharmaceuticals such as hormones, nucleic acids, peptide, protein, monoclonal antibodies and vaccines which offers great therapeutic potential. There are numerous biopharmaceuticals developed via recombinant technologies or chemical synthesis. Peptide and protein drugs are almost always administered via parenteral routes to avoid the hostile environment along the gastrointestinal tract (GIT) which include the presence of an acidic medium and proteolytic enzymes that will inactivate and digest the protein. Furthermore, due to their high molecular weights and lack of lipophilicity, proteins have poor permeability across the intestinal epithelium (Carino and Mathiowitz, 1999; Rekha and Sharma, 2009; Sarmento *et al.*, 2007a).

The oral route continues to be the most natural and convenient means to administer drugs, but also presents challenges to formulation scientists, especially for protein and other gastro-labile drugs. Nanoparticles are known to potentially improve the oral bioavailability of drugs, which are otherwise poorly absorbed from the gastrointestinal tract on their own. Nanoparticles have the highest surface area to volume ratio of any other dosage form. Furthermore, nanoparticles can potentially modify the physicochemical properties in comparison to the drug candidate itself, thus increasing gastrointestinal absorption of these peptides (Bawarski *et al.*, 2008).

1.2 Biopharmaceuticals

The terminology of biopharmaceuticals has been debated on over several years with different industry players; biotechnology and pharmaceutical businesses viewing it from their respective standpoints. However, from a broader perspective, biopharmaceuticals can be defined as the intersection of biotechnology and pharmaceuticals, in which the pharmaceutical is inherently biological in nature and is manufactured using biotechnological principles. According to the United States Food and Drug Administration (FDA), biopharmaceuticals cover a broad range of medicinal products such as recombinant proteins, monoclonal antibodies or nucleic acid-based products (Müller and Keck, 2004; Rader, 2008, 2005). According to Walsh (2010), 58 biopharmaceuticals were approved by the regulatory bodies of European Union and/or United States from January 2006 to June 2010, totalling to just over 200 products of biopharmaceuticals in the market until mid-2010 with many still in the pipeline or undergoing clinical trials (Tauzin, 2008; Walsh, 2010).

1.2.1 Challenges in Delivery of Biopharmaceuticals

Formulation of biopharmaceuticals into therapeutically effective drug delivery systems with optimal storage stability is indeed challenging. Particularly, the need to overcome barriers is crucial to improving delivery efficiency (Jorgensen and Nielson, 2009). The physical and chemical properties of biopharmaceuticals often influence how the delivery system would be developed, as no single system is feasible for all biopharmaceuticals.

A common problem of biopharmaceuticals is often associated to their chemical nature, in particular conformational issues due to their unique structural

characteristics. It is also a prerequisite for the delivery system to be able to protect the drug under harsh degradative environment in order to exert its inherent biological activity (Jorgensen and Nielson, 2009; Müller and Keck, 2004). Therefore, thorough understanding of the biopharmaceutical molecular structure, stability as well as its physical and chemical properties is crucial to develop a successful and feasible drug delivery system (Jorgensen and Nielson, 2009).

1.2.2 Insulin

Insulin is a polypeptide hormone produced by the pancreatic beta-cells, secreted into the portal vein before being transported directly into the liver. It functions as a regulator of blood sugar levels by binding to insulin receptors after extraction in the liver, exerting its role in glucose metabolism (Arbit and Kidron, 2009; Meier *et al.*, 2007; Satake *et al.*, 2002).

The introduction of biopharmaceutical recombinant human insulin therapy is indeed a major medical breakthrough in recent times, having been the mainstay of treatment for advanced-stage diabetes. Insulin was the first recombinant drug to be introduced in the 1970s as a healthcare product, marking a big milestone in the biotechnology sector (Goeddel *et al.*, 1979; Pillai and Panchagnula, 2001). Since its introduction, much research has been focused on the aspects of production, purification, stability and delivery (Arbit and Kidron, 2009; Jain *et al.*, 2006).

1.2.2.1 Physicochemical properties

Human insulin molecule consists of a total of 51 amino acid residues in two polypeptide chains, A and B, linked by two inter-disulphide bridges as shown in Figure 1.1. The A-chain contains 21 residues, with an intra-disulphide bond between A6 and A11, whilst the B-chain holds 30 amino acid residues (Fig. 1.1). The A-chain forms two nearly antiparallel α helices, whilst the B-chain forms a single α-helix and a β-strand, therefore providing a hydrophobic interior and a surface covered by both polar and non-polar amino acid residues (Brange, 1994). The molecular weight of an insulin monomer is approximately 5.8kDa.

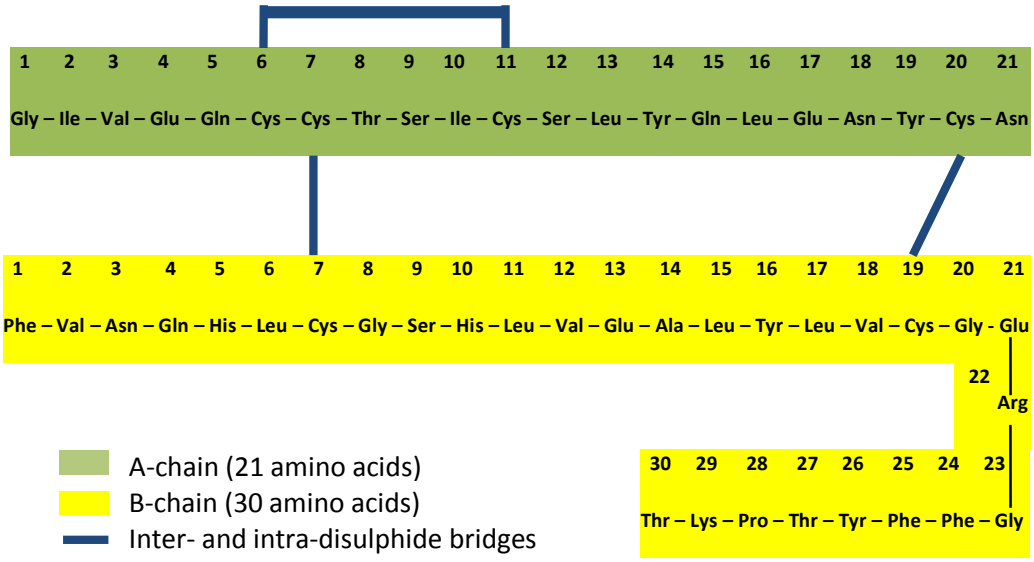

Figure 1.1 The primary structure of human insulin.
(Adapted from: Beta Cell Biology Consortium)
(Accessed on: 10th July 2014)

Monomeric insulin, the biologically active form circulating in the body, exists at low aqueous concentration (<0.1 µM - 0.6 µg/ml). Insulin dimerises in aqueous solution at concentrations higher than 0.6 µg/ml, whereas if dissolved in the range of pH 4-8 and in the presence of zinc ions, insulin is more likely to have three dimers assemble together to form a hexamer (Brange, 1994).

Figure 1.2 shows three dimers associated together with central zinc-coordination to form a hexameric assembly.

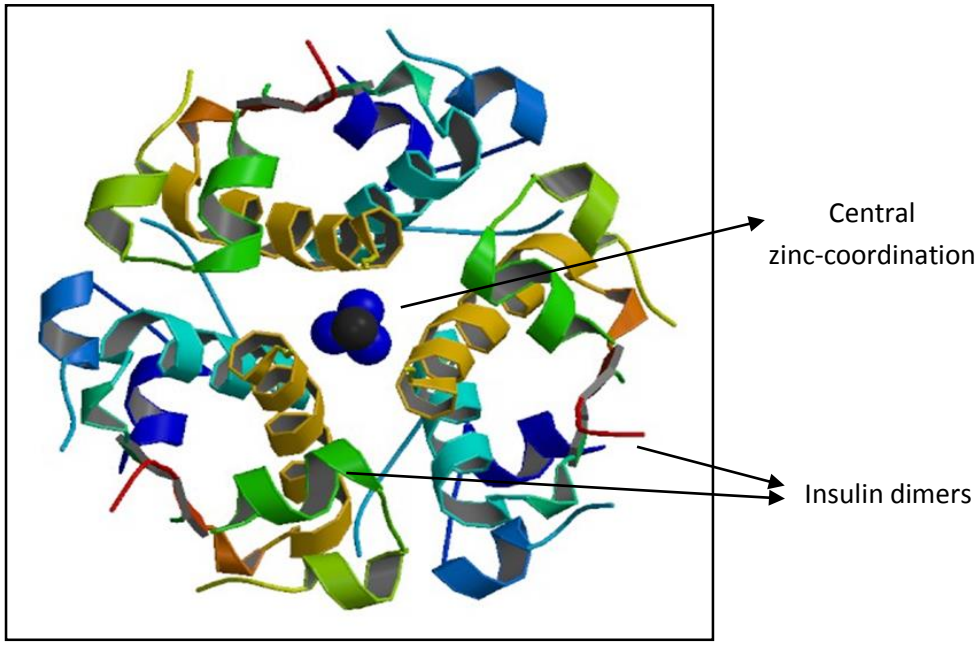

Figure 1.2 Hexameric assembly of human insulin with coordination around zinc [PDB ID: 1TRZ]. (Adapted from (Ciszak and Smith, 1994)

1.2.2.2 Pharmacological properties

Insulin plays a major role in the body's carbohydrate, fat and protein metabolism, acting primarily on the liver, muscle and fat cells. A sharp rise in postprandial blood glucose level triggers insulin secretion from the pancreatic β-cells, subsequently increasing the uptake and storage of glucose, amino acids and fats, and hence reduces blood glucose level.

Insulin binds to the insulin receptor on the surface of its target cells, causing a conformational change in the transmembrane glycoprotein complex. This activates the signal transduction mechanism which essentially decreases the blood glucose level by inhibiting glycogenolysis and gluconeogenesis and boosting glycolysis and glycogenesis. A maximum response of insulin effect can be achieved with less than 10 % of receptors being occupied with bound insulin (Rang *et al.*, 2003). The insulin-receptor complex then internalises altogether into vesicles, and subsequently insulin is degraded in lysosomes whilst the receptors are recycled to the plasma membrane. Insulin is inactivated enzymatically in the liver and kidney with an elimination half-life of about 10 minutes (Rang *et al.*, 2003).

1.3 Diabetes

1.3.1 Definition

Diabetes mellitus is a chronic disease which is developed when the pancreas does not produce sufficient insulin, or that the body is not utilising the circulating insulin effectively, resulting in hyperglycaemia (Association, 2010). Insulin is therefore necessary for maintaining normal blood sugar level in the body.

Diabetes is commonly divided into two types, characterized either by deficiency in insulin production (Type 1) or the body's inefficient use of insulin (Type 2). Type 1 *diabetes mellitus* is caused by the patient's own immune system which destroys the beta cells in the pancreas. Pancreatic beta cells are responsible for insulin production in the body. Type 2 *diabetes mellitus* is the most common form of diabetes that normally presents later in life. It occurs when either the body's cells do not respond to insulin (insulin resistance) or when the pancreas does not produce sufficient insulin in order to maintain a normal glucose level.

1.3.2 Prevalence

In Malaysia, the latest population-based survey, National Health and Morbidity Survey 2011 (NHMS 2011) reported that the prevalence of diabetes in adults ≥ 18 years of age has risen to 15.2 % from 11.6 % in 2006 (NHMS 2006) (Figure 1.3) (Ministry of Health, 2012). This survey also highlighted the prevalence of undiagnosed diabetics at 8.0 % of Malaysian adults ≥ 18 years of age in 2011, almost double of that in 2006 (Figure 1.3) (Ministry of Health, 2012).

In 2013, the International Diabetes Federation (IDF) estimated about 382 million people worldwide with diabetes in the adult population which represents approximately 8.3 % of the world's adult population, with almost 46 % of them still remained undiagnosed (Figure 1.4) (IDF, 2013).

By the year 2030, the number of people with diabetes worldwide is predicted to increase to 438 million (Unwin, 2009). A recent finding reported an estimate of 5.1 million deaths worldwide which is attributable to diabetes in the year of 2013, and that one person dies from diabetes in every six seconds (IDF, 2013). The alarming global prevalence and high mortality rate are indeed major causes of concern.

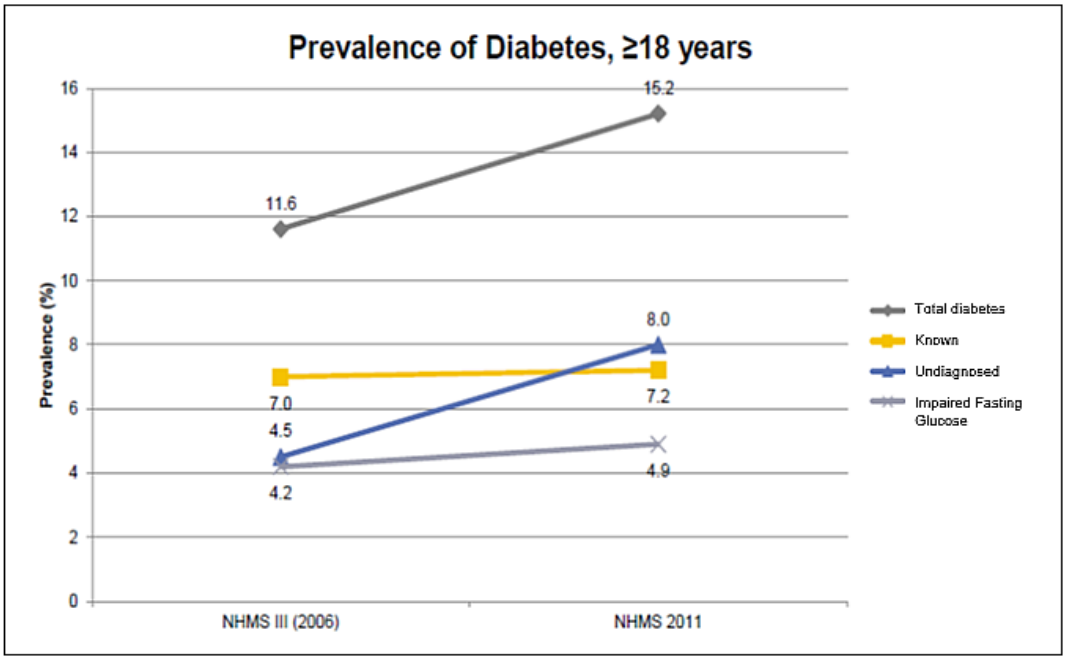

Figure 1.3 Diabetes prevalence among Malaysian adults (≥18 years) reported in NHMS III (2006) and NHMS 2011. (Adapted from (Ministry of Health, 2012)

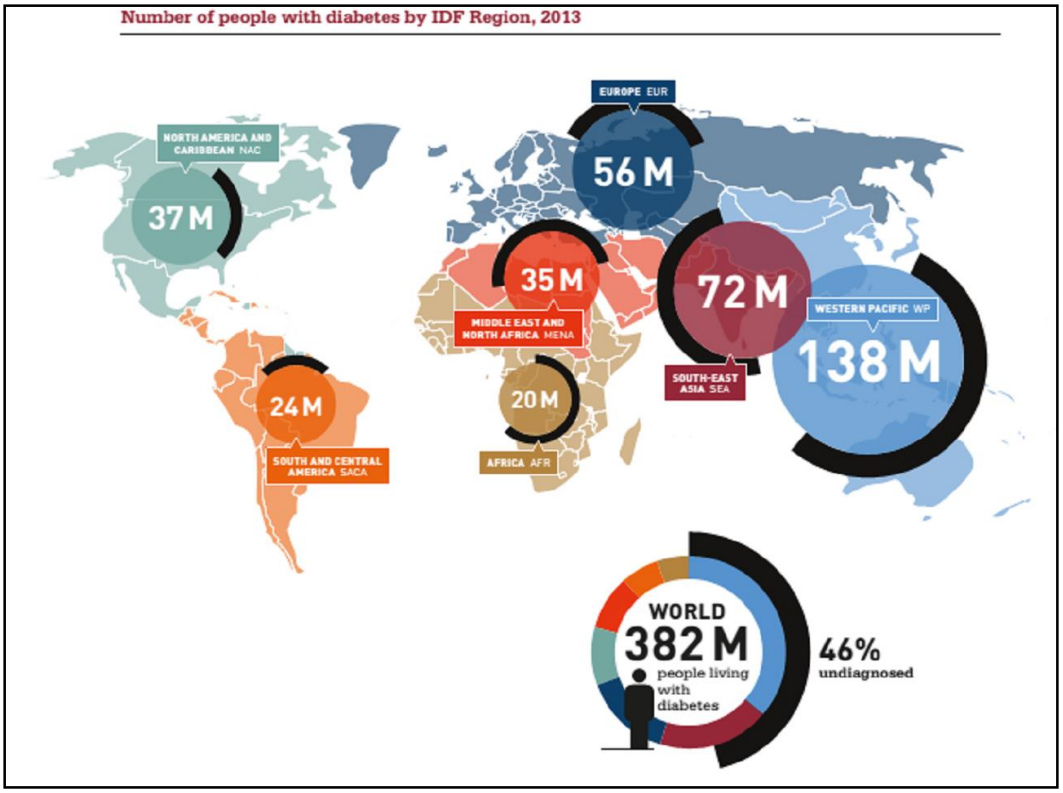

Figure 1.4 World statistics of diabetes population in different regions of the world, with estimated undiagnosed patients. (Adapted from International Diabetes Federation, IDF 2013)

1.3.3 Pharmacological Basis of the Management of Diabetes

Diabetes is a progressive, chronic metabolic disorder. Pharmacological management of diabetes in the initial stages involves the intake of oral hypoglycaemic agents such as sulphonylureas (gliclazides), biguanides (metformin), glitazones (rosiglitazone) and α-glucosidase inhibitors (acarbose) (Coustan, 2007; Krentz and Bailey, 2005; Rang *et al.*, 2003). Recently, glucagon-like peptide (GLP-1) agonist (eg. Exenatide), an incretin mimetic, was newly introduced in the market as an effective alternative management for diabetes (Coustan, 2007; Verspohl, 2012). These extensive range of oral hypoglycaemic agents differ in their mode of actions, safety profiles and tolerability. Their mode of actions vary from stimulating insulin secretion, reducing hepatic glucose production, delaying digestion and absorption of carbohydrates to improving insulin sensitivity in the cells (Krentz and Bailey, 2005).

However, all oral hypoglycaemic agents are contraindicated in patients with Type 1 *diabetes mellitus*. These patients rely solely on insulin treatment to achieve normoglycaemic levels. As for patients with Type 2 *diabetes mellitus*, the use of oral hypoglycaemic agents is unable to delay the rate of disease progression. Escalating therapy is often the case for this category of patients, reflecting a progressive loss of beta cells function and an increase in insulin resistance (Krentz and Bailey, 2005). Unfortunately, there is no cure for diabetes. Insulin is almost always the standard treatment for Type 2 diabetic patients, when other oral antidiabetic agents fail to achieve optimal blood glucose level. These patients are therefore required to utilise a life-long insulin treatment.

1.4 Current Delivery Methods for Insulin

Currently, patients requiring insulin therapy need to administer multiple daily injections of insulin subcutaneously, which can be extremely distressing. The patients may also experience local pain, itching, allergy and insulin lipodystrophy. More importantly, the strict regimen and also the unacceptability of injecting themselves on a regular basis have led to poor patient compliance, hence failure to achieve lasting glycaemic control. These disadvantages emphasise the need to find an alternative to subcutaneous injections, highlighting the possibility of oral insulin delivery as the most convenient and acceptable route of administration for chronic therapy.

Several other alternative approaches of delivering insulin have been attempted to improve patient compliance which include inhalation, intranasal, buccal/sublingual and transdermal delivery systems (Flood, 2006; Mastrandrea and Quattrin, 2006; Owens, 2002).

Delivery of insulin via pulmonary route became increasingly promising when Exubera® was approved by regulatory authorities U.S. Food and Drug Administration (FDA) to be marketed in January 2006 (Heinemann, 2012; Lassmann-Vague and Raccah, 2006; Owens, 2002). However, the excitement of the revolutionary inhaled insulin, marketed by Pfizer, was short-lived. Exubera® did not gain acceptance of patients and physicians due to safety concerns and higher cost of production, and thus was eventually withdrawn from the market in October 2007 (Heinemann, 2012; Lassmann-Vague and Raccah, 2006; Mathieu and Gale, 2008).

1.5 Future Direction for Insulin Delivery

Less invasive and alternative delivery routes of insulin therapy are being actively explored to overcome the setbacks of subcutaneous insulin injections currently available on the market. Among those alternative routes of administration being tested are intranasal administration, pulmonary, peroral, buccal and sublingual routes (Heinemann, 2012; Lassmann-Vague and Raccah, 2006; Mao *et al.*, 2009; Owens, 2002). Despite availability of these promising alternative routes, they have had limited success due to the absence of external stimuli which can facilitate absorption (Mao *et al.*, 2009).

Formulation of intranasal insulin was tested with numerous absorption enhancers such as saponin, lecithin and chitosan in gel to improve insulin absorption with minimal toxicity upon administration (Varshosaz *et al.*, 2004). Studies have shown that a burst release of insulin was achieved, however, the bioavailability was found to be largely dependent on inter-individual response resulting in variable glucose-lowering effects among patient (Lassmann-Vague and Raccah, 2006; Leary *et al.*, 2006). The setbacks of this administration route were a major concern, particularly nasal irritation, risk of immunogenicity (El-Etr *et al.*, 1987) and possible injury to the nasal mucosa and mucocilliary system (Frauman *et al.*, 1987). Hence, this route, for now, does not seem too favourable.

Pulmonary insulin delivery appears rather promising, as the lung has a large surface area with good vascularisation and thin epithelial alveoli for rapid drug absorption, making this route far more permeable to macromolecules (Mao *et al.*, 2009; Patton, 1996). Studies have shown that relative insulin bioavailability doubled when protease inhibitors such as trypsin, plasmin and kallikaren were co-administered with insulin, compared to when insulin was administered alone (Fukuda *et al.*, 1995; Okumura *et al.*, 1992). Likewise, permeation enhancers

are also usually required in pulmonary delivery to improve absorption of macromolecules across the alveoli cell layer (Hussain *et al.*, 2004).

Several inhaled insulin delivery systems have once progressed to clinical trial stages, such as AERx®, Exubera® and Technosphere® Insulin. However, the failure of Exubera® was extremely discouraging to the area of pulmonary insulin delivery, with most systems being withdrawn from clinical trials thereafter (Heinemann, 2012). Despite this, MannKind Corporation is still actively pursuing its product Technosphere® Insulin, hoping to address the constraints observed from clinical studies and obtain market approval in the near future (Heinemann, 2012; Lassmann-Vague and Raccah, 2006).

Although these delivery routes appear promising, the question of whether the delivery system is feasible and effective in patients still remains unanswered. Thus, there is still much room for understanding and research to be carried out before these insulin delivery systems arrive on the market.

Due to the limited success of alternative routes of insulin administration so far, oral insulin delivery has since gained interest among researchers as a safe and effective means of insulin delivery. Oramed® Pharmaceuticals recently claimed that a revolutionary oral insulin capsule developed by them is currently in Phase 2 clinical trials in the United States (Leichman, 2013).

1.5.1 Oral Insulin Delivery

Undoubtedly, oral delivery is the most acceptable route among patients. Improved patient compliance and adherence are among significant benefits of the oral route of delivery. However, this route of administration comes with its own limitations. Insulin delivered orally will need to overcome both the physical

and enzymatic barriers of the human gastrointestinal tract (GIT) in order to deliver insulin effectively (Arbit *et al.*, 2008; Mao *et al.*, 2009).

The physical barrier refers to the epithelial cells lining the GIT which are tightly bound with minimal leakage, thus limiting the drug absorption through the intracellular route. Due to the size constraints, permeation via intracellular route is virtually impossible. In addition, the microvilli (brush border) present on the apical surface of the epithelial cells also limits the absorption of insulin due to the presence of digestive enzymes on the microvilli. The glycoalyx and mucus layer found on top of the epithelial layer also acts as another physical barrier to oral insulin delivery (Arbit *et al.*, 2008; Carino and Mathiowitz, 1999).

The enzymatic barrier refers to the rapid presystemic enzymatic degradation due to secretion of high level of proteases in gastric and intestinal fluids as well as the membrane-bound peptidases localised on the surface of various mucosal tissues (Mao *et al.*, 2009; Woodley, 1993). This contributes to a large amount of insulin being degraded prior to being absorbed across the intestinal epithelium.

1.5.1.1 Potential Physiological Advantages of Oral Insulin Delivery

Orally delivered insulin is designed to mimic the exacted physiological route as it is taken up from the gastrointestinal tract into the portal vein. It is anticipated that the oral insulin will be transported to the liver via the portal vein; be subjected to first-pass metabolism that gives rise to the “portal signal”, hence regulating the glucose metabolism (Arbit and Kidron, 2009; Satake *et al.*, 2002).

This is contrary to what happens when it is administered parenterally, in which insulin is introduced directly into the systemic circulation, resulting in a lower portal-peripheral insulin gradient and a weaker “portal signal”. Thus, the regulation of glucose metabolism is rendered more effective in oral insulin versus parenteral insulin. In addition, oral insulin is also more likely to benefit the patient by reducing the risk of hyperinsulinaemia and hypoglycaemia, commonly associated to systemic insulin therapy (Arbit and Kidron, 2009; Satake *et al.*, 2002).

1.6 Nanoparticulate Formulations

Colloidal nanoparticulate delivery systems are defined as particulate dispersions containing nanoparticles with overall size distribution within the range of 10 – 1000 nm (Allémanna *et al.*, 1993). These common types of delivery systems include those containing lipids, such as liposomes, nanoemulsion, lipid nanoparticles; natural or synthetic polymeric nanoparticles, such as poly D,L-lactide-*co*-glycolide (PLGA) (Vonarbourg *et al.*, 2006). These delivery systems have become particularly attractive in recent years due to their ability to encapsulate and deliver new, large-molecule therapeutics such as peptides, proteins and genes (Bilati *et al.*, 2005b; Delie *et al.*, 2001; Vonarbourg *et al.*, 2006). In addition, nanoparticulate delivery systems are also well accepted for their ability to improve drug bioavailability, by means of protecting the drug against degradative substances (Allémanna *et al.*, 1998). Bonduelle *et al.* (1996) reported that the oral bioavailability of cyclosporin A-loaded nanocapsule showed a notably elevated bioavailability of cyclosporin A, a cyclic peptide, and a reduced side effect of nephrotoxicity as compared to the commercial cyclosporin A emulsion tested in the study.

Several types of nanoparticulate formulations containing insulin have been prepared to achieve an efficacious insulin oral delivery system. Such formulations have been investigated using polymeric nanocarriers, lipid-based as well as complex hydrogel nanoformulations (Ahmad *et al.*, 2011).

An example of polymeric nanocarriers, composed of chitosan, was found to be effective in transporting insulin across the intestinal epithelium primarily due to the mucoadhesive properties of chitosan that caused prolonged hypoglycaemia seen in diabetic rats, as opposed to the insulin solution form (Chen *et al.*, 2011). The modified chitosan nanoparticles, a combination of polymers chitosan and poly(γ-glutamic acid), formed a pH-responsive nanoparticle system. Recent studies reported that these nanoparticles led to a slow onset, prolonged hypoglycaemia in diabetic rats with a relative insulin bioavailability of 15 % (Sonaje *et al.*, 2010a, 2010b), and therefore may act as a suitable alternative to the subcutaneous basal intermediate-acting insulin (Sonaje *et al.*, 2010b). Studies on insulin have also shown that insulin-encapsulated poly(alkyl cyanoacrylate) (PACA) nanocapsules resulted in a reduction of glycaemia by 72 % after nine days and 48 % after 15 days of oral administration (Damgé *et al.*, 1988), as compared to only less than 0.5 % of insulin dose being detected when free (non-encapsulated) insulin was administered orally (Allémanna *et al.*, 1998). In another study, insulin-phospholipid complex loaded into PLGA nanoparticles for oral delivery recorded a 42.6 % reduction in plasma glucose with a prolonged effect of up to 12 hours post administration in diabetic rats (Cui *et al.*, 2006).

Liposomes and solid lipid nanoparticles are the different types of lipid-based nanoformulations used to deliver insulin orally. Liposomes are made up of concentric lipid bilayers, formed spontaneously by amphiphilic lipids, are

capable of protecting entrapped molecules within the aqueous core (Dapergolas and Gregoriadis, 1976). The amphiphilic lipids can be natural or synthetic phospholipids, such as phosphatidylcholine (lecithin), phosphatidylethanolamine, phosphatidylglycerol, phosphatidylserine and phosphatidylinositol (Vemuri and Rhodes, 1995). Insulin loaded into dipalmitoyl-phosphatidylcholine (DPPC)/cholesterol liposomes significantly reduced the blood glucose level in diabetic rats to 57 % of pretreatment values after 4 hours of administration (Dapergolas and Gregoriadis, 1976). However, a less pronounced hypoglycaemic effect was noted when insulin loaded phosphatidylcholine/cholesterol liposomes were administered in diabetic rats, highlighting the effects of different types of liposomes used (Dapergolas and Gregoriadis, 1976). Cetyl palmitate-based solid lipid nanoparticles (SLNs) have also been used to incorporate insulin for oral administration, achieving a significant hypoglycaemia in diabetic rats over 24 hours (Sarmento *et al.*, 2007a). In another study, insulin loaded lectin-modified solid lipid nanoparticles (SLNs) demonstrated a better protection against insulin degradation by digestive enzymes *in vitro* than that observed in insulin loaded SLNs, with relative bioavailabilities of 7.11 % and 4.99 % respectively in comparison to subcutaneous insulin, both improving the oral absorption of insulin (Zhang *et al.*, 2006).

There has also been a successful attempt to formulate oral insulin into a complex multi-layered nanoparticle preparation made from biodegradable, biocompatible, mucoadhesive and protease-protective biomaterials. Insulin incorporated into the alginate, dextran sulphate and poloxamer hydrogel, formed through ionotropic pre-gelation and polyelectrolyte complexation, was stabilised with chitosan and coated with albumin (Woitiski *et al.*, 2009). This complex hydrogel formulation demonstrated retained bioactivity of insulin *in*

vitro as well as enhanced protection against enzymatic digestion and ultimately its absorption (Woitiski *et al.*, 2009, 2011).

1.7 Solid Lipid Nanoparticles (SLNs)

Solid lipid nanoparticles (SLNs) represent lipid nanoparticulate delivery systems that combine the benefits of solid particles, emulsions and liposomes (Mukherjee *et al.*, 2009b). The SLNs are realised by exchanging the liquid lipid present in emulsions to a lipid that is solid at room and body temperature. The lipid phase will be subsequently dispersed in water or in an aqueous surfactant solution (Mukherjee *et al.*, 2009b; Müller *et al.*, 2002a). Lipids may be selected from a range of triglycerides, partial glycerides, fatty acids, steroids and waxes (Müller and Keck, 2004).

Since the beginning of nineties, many research groups have focused on the use of SLNs as an alternative colloidal carrier to polymeric nanoparticles, avoiding drawbacks pertaining to polymeric nanoparticles such as polymer cytotoxicity and the use of organic solvents (Almeida and Souto, 2007; Mehnert and Mäder, 2001; Müller *et al.*, 2000). Table 1.1 lists a range of pharmaceutical drugs having been successfully incorporated into SLNs by numerous research groups.

Moreover, SLNs have also been reported to manifest controlled and localised drug release, higher drug encapsulation, better drug bioavailability and tissue distribution with improved stability of incorporated labile drug (Cavalli *et al.*, 1993; Mehnert and Mäder, 2001; Uner and Yener, 2007). A prolonged release of prednisolone over a 5-week duration has been demonstrated in the drug release studies of prednisolone-containing SLNs (Müller *et al.*, 1995).

Table 1.1 Examples of drugs incorporated into SLNs. (Pathak *et al.*, 2007)

Drug Name	References
Clobetasol	(Hu *et al.*, 2002)
Clozapine	(Venkateswarlu and Manjunath, 2004)
Cyclosporine	(Olbrich *et al.*, 2002)
Darodipine	(Hubert *et al.*, 1991)
Hydrocortisone	(Cavalli *et al.*, 1999)
Idarubicin	(Zara *et al.*, 2002)
Indomethacin	(Calvo *et al.*, 1996)
Paclitaxel	(Chen *et al.*, 2001)
Prednisolone	(Müller *et al.*, 1995)
Progesterone	(Dufresne and Leroux, 2004)
Tobramycin	(Bargoni *et al.*, 2001)
Tretinoin	(Manconi *et al.*, 2002)
Ubidecarone	(Bunjes *et al.*, 2001)
Vitamin A	(Jenning *et al.*, 2000)

1.8 Preparation of Solid Lipid Nanoparticles

SLNs are primarily made up of solid lipid, emulsifier and water/solvent. The lipids commonly used are triglycerides (tri-stearin), partial glycerides (Imwitor), fatty acids (stearic acid, palmitic acid), sterols (cholesterol) and waxes (cetyl palmitate). Emulsifiers are an essential ingredient in SLNs formulations to stabilise the lipid dispersion by forming a protective cover over the SLNs surface (Quintanar-Guerrero *et al.*, 2005). Several emulsifiers, used alone or in

combination, can prevent particle agglomeration of SLNs efficiently to avoid Ostwald's ripening phenomenon (Cavalli *et al.*, 1993; Mukherjee *et al.*, 2009b).

1.8.1 Lipids : Palm oil

Triglycerides are the major constituents of palm oil, with over 95 % of palm oil is made up of mixture of triglycerides. Major fatty acids present in palm oil are myristic acid, palmitic acid, stearic acid and oleic acid. Table 1.2 lists the fatty acids with their corresponding chemical structures and lipid numbers.

Table 1.2 Example of fatty acids with chemical formulae and lipid numbers. (Lipid numbers presented as *C:D*; where *C* is the number of carbon atoms and *D* is the number of double bonds in the fatty acid)

Fatty acids	**Chemical formula**	***C:D***
Myristic acid	$CH_3(CH_2)_{12}COOH$	14:0
Palmitic acid	$CH_3(CH_2)_{14}COOH$	16:0
Stearic acid	$CH_3(CH_2)_{16}COOH$	18:0
Oleic acid	$CH_3(CH_2)_7CH{=}CH(CH_2)_7COOH$	18:1

Figures 1.5 and 1.6 show the chemical structures of palmitic acid and tripalmitin respectively. Most fatty acids are present as triglycerides, with tripalmitin being the predominant saturated triglyceride in palm oil (Sundram *et al.*, 2003). Tripalmitin is derived from the esterification of three palmitic acid molecules and a glycerol molecule. Since tripalmitin is made up of palmitic acids which are saturated fatty acids, it is therefore presented as a solid at room temperature.

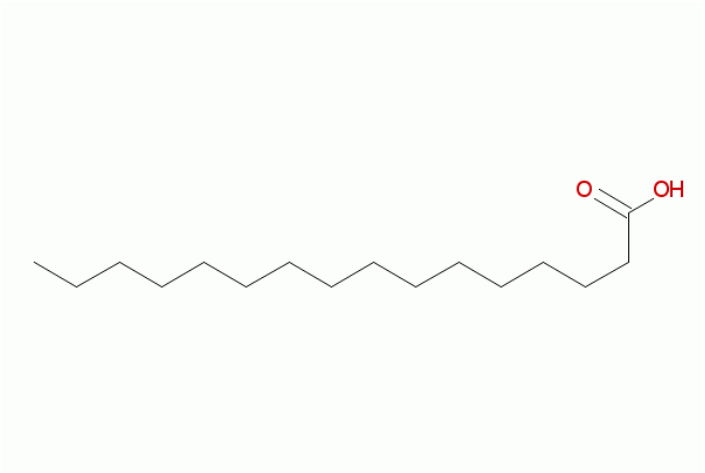

Figure 1.5 Chemical structure of palmitic acid [$CH_3(CH_2)_{14}COOH$].

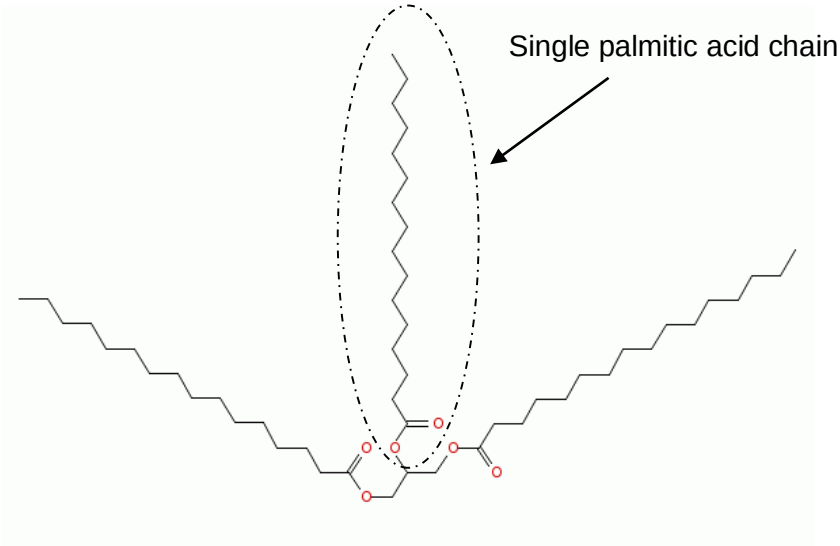

Figure 1.6 Chemical structure of tripalmitin ($C_{51}H_{98}O_6$).

1.8.2 Methods of Production of Lipid Nanoparticles

Several methods for preparing SLNs have been presented since their introduction in the 1990s (Yazan, 2008). Among the commonly used techniques is the high pressure homogenisation method which can be performed in either hot (Schwarz *et al.*, 1994; Westesen *et al.*, 1993) or cold conditions (Castelli *et al.*, 2005; Mühlen *et al.*, 1998) depending on the nature of the drug. Ultrasonication, high-speed homogenisation (Eldem *et al.*, 1991; Luo *et al.*, 2006), solvent-diffusion and solvent emulsification-evaporation methods (Siekmann and Westesen, 1996; Trotta *et al.*, 2003) have also been used to produce solid lipid nanoparticles. These methods are commonly used to encapsulate lipophilic drugs. However, a double emulsion water-oil-water (W/O/W) method based on a modified solvent emulsification-evaporation technique was used to prepare SLNs for the incorporation of hydrophilic drug substances (Cortesi *et al.*, 2002). The hydrophilic drug is encapsulated with a stabiliser to minimize partitioning of the drug into the external water phase during solvent evaporation (Mukherjee *et al.*, 2009b).

1.9 Basic Physiology and Function of Gastrointestinal Tract (GIT)

Orally administered insulin will pass down the stomach, in which the environment is very acidic and it also contains high amount of proteolytic enzymes which destroys the physiological activity of the protein (Figure 1.7). It is widely reported that low gastric pH and the presence of pancreatic enzymes lead to extensive particle aggregation and lipid degradation of non-coated SLNs (Carino and Mathiowitz, 1999; Garcıa-Fuentes *et al.*, 2003). Insulin is therefore effectively stopped by the natural barriers to protein delivery as the large aggregated particles will not be taken up by Peyer's patches and the insulin will be prematurely digested by the enzymes. To avoid this from happening, insulin should be protected from release within the hostile environment of the stomach. As it moves down the stomach into the duodenum, the pH increases to 7.4 and the enzymatic activity decreases, making it a more suitable location for insulin absorption.

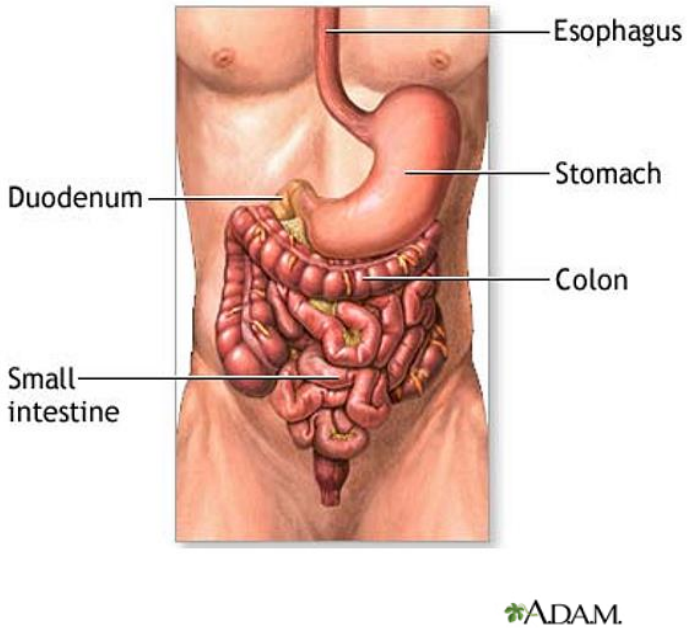

Figure 1.7 Human gastrointestinal tract.
(Adapted from A.D.A.M. Inc.)
(Accessed on 30th July 2014)

1.10 Present Research Theme

The present research theme focuses on utilising lipid from palm oil which is rich in saturated and unsaturated fatty acids and triglycerides. There is a lot of potential in this area of oral drug delivery system using palm oil constituents, considering the fact that palm oil lipids have the potential for gastrointestinal uptake via the lymphatic route. Moreover, these physiological lipids are versatile and are non-toxic to humans.

Palmitic acid and tripalmitin were thus investigated as potential SLNs lipid matrix for the delivery of insulin. Several studies have reported, either a single type of solid lipid or a combination of a solid and a liquid lipid as their lipid core of the nanoparticles (Garcıa-Fuentes *et al.*, 2003; Trotta *et al.*, 2003; Zhang *et al.*, 2006). Liu *et al.* (2007) attempted to utilise a combination of two different solid lipids, palmitic acid and stearic acid, as the lipid core of the nanoparticles.

To our knowledge, there has not been any attempt to investigate the combination of solids, a fatty acid (palmitic acid) and a triglyceride (tripalmitin), which are structurally different but share the same fatty acid chain in the formulation of solid lipid nanoparticles. This area of research is not new but is certainly intense and appears to be very promising, especially from the data reported in the literature. Previous studies have developed SLNs containing insulin to be delivered orally using various preparation methods, for example, solvent evaporation (Garcıa-Fuentes *et al.*, 2003), solvent emulsification-diffusion (Trotta *et al.*, 2005), reverse-micelle double emulsion technique (Liu *et al.*, 2007). These studies were mainly aimed at developing lipid nanoparticles encapsulating peptides and studying their physicochemical properties as well as *in vitro* stability.

However, little attempt has been directed towards establishing the localisation of insulin within the fabricated nanoparticles, and none towards correlating the localisation of the insulin within the SLNs with the gastrointestinal uptake of these SLNs.

1.11 Research Aims and Objectives

The ultimate aim of the present project was to establish whether the location of peptide hormone insulin formulated within the SLNs influenced the *in vitro* uptake of the nanoparticles by absorptive cells.

The above objective was realised by firstly formulating the SLNs in order to achieve the three drug localisation models as proposed by Müller *et al.* (2000) (Fig. 1.8). This was done by manipulating formulation and processing parameters. The three possible drug localisation models proposed by Müller *et al.* (2000) are (a) solid solution model (with the drug molecularly dispersed within the lipid matrix), (b) the core-shell model (with a drug-enriched shell and a lipid core) and (c) the drug-enriched core model (with the lipid matrix shell encapsulating the drug core) (Müller *et al.*, 2000).

It is believed that the location of insulin within the SLNs has a direct impact on the rate of uptake of the nanoparticles by the enterocytes as well as Peyer's patches into the lymph and the ultimate rate of assimilation of the same in the lymph (Sarmento *et al.*, 2007b). These two processes, namely the rate of uptake and the rate of assimilation of SLNs will influence the eventual bioavailability of the ultimate prototype. The above pursuit has not be reported in the literature and forms the core basis of this research.

The final objective was to investigate the difference, if any, between the different localisation models of insulin within the solid lipid nanoparticles and the uptake of such lipid nanoparticles by the absorptive cells.

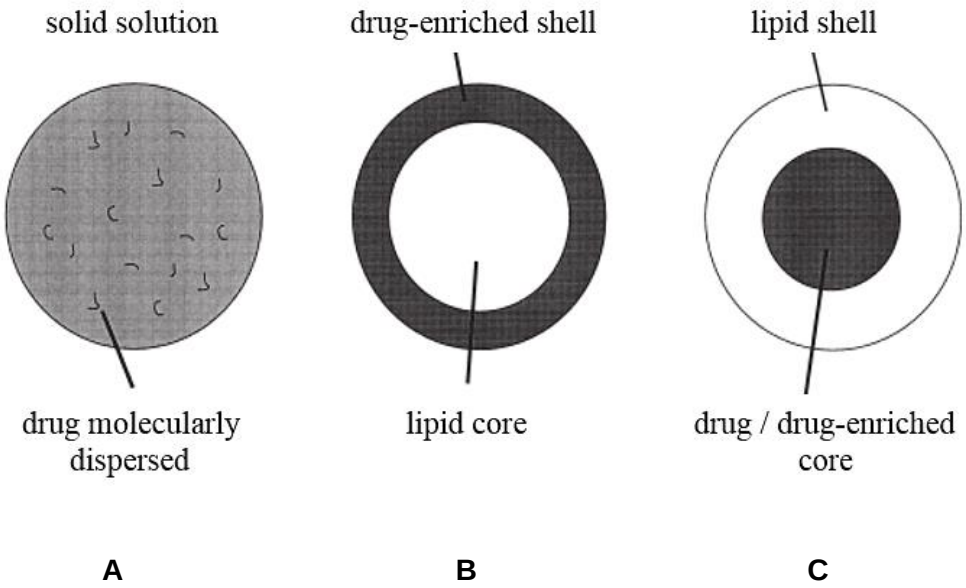

A : **solid solution model (dispersion within matrix)**

B : **core-shell models with drug enriched shell**

C : **core-shell models with drug-enriched core**

Figure 1.8 A schematic diagram showing the three hypothesised models of drug localisation :- A, B and C.
(Adapted and modified from (Müller *et al.*, 2000)

CHAPTER 2

Stability Studies on Recombinant Human Insulin

2.1 Introduction

This section details the preformulation work to establish a reliable and robust analytical method for insulin analysis as well as to address its stability in response to appropriate challenges.

The main aim of this phase of work was to subject insulin to perceived stresses encountered during formulation. Therefore, a short-term accelerated stability testing was conducted on human recombinant insulin at various temperatures and pH as part of preformulation studies. A high performance liquid chromatography (HPLC) method was used to determine the extent of deamidation of insulin by measuring the degradation products. This was done at various storage conditions. We also utilised dynamic light scattering technique to detect protein aggregates or changes in particle sizes of insulin molecule as an indication of protein physical instability induced by different storage temperatures. Hence, the most suitable conditions would be used for the handling, storing and processing of insulin during the formulation work.

Like any other globular proteins, insulin has a tendency to adopt a folding and assembly of the individual molecules, with the hydrophobic surfaces being buried inside and the hydrophilic residues being exposed (Brange *et al.*, 1997). Any change in the native conformation will render it unstable. Therefore, stability issue of insulin is crucial since any inappropriate handling can potentially accelerate its degradation.

Extensive studies on the physicochemical stability of insulin have been reported in the literature. These studies have highlighted the importance of understanding the drug nature in order to preserve its biological potency (Brange, 1994). Apart from stability and efficacy issues, maintaining the safety and non-immunogenicity of the protein formulation is of utmost importance

especially if it is to be self-administered directly by the patients (McNally and Hastedt, 2013; Wakankar and Borchardt, 2006).

Insulin is subjected to chemical and physical instabilities during storage and usage, which can compromise the efficacy of the drug. It is known to undergo degradation via deamidation and aggregation (Brange *et al.*, 1997; Lai and Topp, 1999; McNally and Hastedt, 2013).

Chemical instability mainly manifests as deamidation which is hydrolytic and involves the deamidation of the asparagine amino acid residues to aspartic acid (Lai and Topp, 1999; McNally and Hastedt, 2013). HPLC is commonly used to separate and detect presence of insulin as well as its degradation products (Hoyer *et al.*, 1995; Oliva *et al.*, 1996).

Physical instability often refer to changes in the protein conformational structure including denaturation, aggregation (fibrillation) and precipitation (Brange *et al.*, 1997; Lai and Topp, 1999; Manning *et al.*, 1989; McNally and Hastedt, 2013). Insulin may also undergo transformation by forming intermolecular covalent bonds with other insulin molecules resulting in higher molecular weight transformation products (Brange, 1994; Oliva *et al.*, 2000). High temperature, exposure to hydrophobic surfaces (air-water interface) and organic solvents can lead to physical instability of insulin (Brange *et al.*, 1997; Lai and Topp, 1999; McNally and Hastedt, 2013). Several approaches have been used to characterise physical instabilities of protein samples, including size-exclusion chromatography (Clodfelter *et al.*, 1999), light scattering technique (Oliva *et al.*, 2000) and fluorescence microscopy technique to detect protein aggregates (Demeule *et al.*, 2007).

To address the issues of chemical instabilities of proteins, reversed-phase HPLC is probably the most utilised analytical method in the literature for the separation and determination of proteins and peptides (Aguilar, 2004; Geng and Wang, 2008; Sarmento *et al.*, 2006). This technique, used for separating proteins by exploiting hydrophobic interactions between the column packing and the hydrophobic regions of the protein, is a powerful and robust method which has been used for quantifying insulin accurately in both artificial and biological environments (Moslemi *et al.*, 2003; Oliva *et al.*, 2000; Rajan *et al.*, 2006; Sarmento *et al.*, 2006; Xu *et al.*, 2006). Moreover, the United States, British as well as the European Pharmacopoeias have also recommended separating and determining insulin contents by using the HPLC method.

A comprehensive literature review was done on previously developed HPLC assay methods for insulin and its degradation product A-21 desamidoinsulin in order to select a suitable HPLC method for the current work.

Moslemi *et al.* (2003) developed a reversed-phase HPLC method with UV detection at room temperatue to simultaneously determine insulin and its main degradation product, A-21 desamidoinsulin. The ion-pair RP-HPLC approach, using tetramethylammonium hydroxide as the ion-pairing reagent, was chosen in order to get a well-resolved peak and reproducible retention time. Despite the peak shape being symmetrical, the resolution was poor. The retention time for this method was long, with insulin eluting at 16.76 minutes and the degradation product at 19.99 minutes. This would not be popular if it is necessary to analyse multiple samples. Some other HPLC methods also suffered the same setback of being too time consuming (Klyushnichenko *et al.*, 1994; Yomota *et al.*, 1996).

Several proposed HPLC methods in the literature have reported effective separation of insulin from its principal degradation products, A-21 and B-3 desamidoinsulin, with a high specificity and precision demonstrated. However, their limitations lie in the chromatographic conditions which involved elevated temperature at 40°C, which was not very desirable and compromises drug stability and also required a column temperature controller to maintain the temperature (Farid *et al.*, 1989; Xu *et al.*, 2006; Yomota *et al.*, 1996).

Prior to performing stability studies, this section of studies was therefore designed to develop and validate a simple yet robust HPLC method capable of identifying insulin and its degradation products.

2.2 Materials

Pure crystalline recombinant human insulin (lyophilised powder) was manufactured by EMD Biosciences (San Diego, U.S.A.) and purchased from Merck Malaysia. HPLC-grade methanol, acetonitrile (ACN) and trifluoroacetic acid (TFA) were purchased from Fisher Scientific (Loughborough, UK). Both anhydrous sodium sulphate and phosphoric acid were purchased from Systerm (Belgium). Purified water was used for all solutions and dilutions. Regenerated cellulose (RC) 0.2 µm syringe filter membranes were purchased from Titan (Tennessee, U.S.A.) to filter each insulin sample prior to sample injection.

The HPLC system comprised of a Series 200 Quaternary LC Pump Model 200Q/410 with Series 200 Autosampler, connected to the UV/Vis Detector (LC200UV) from the manufacturer Perkin Elmer (U.S.A.). A TotalChrom® software, linked to the HPLC system, allowed chromatograms to be viewed and analysed on the computer. HPLC columns used were Apex™ ODS (C18, 5 µm, 100 Å pore size, 4.6 x 150 mm) (Jones Chromatography, U.S.A.), Hypersil™ ODS (C18, 5 µm, 120 Å pore size, 4.6 x 250 mm) (Thermo Scientific™, U.S.A.) and Jupiter (C18, 5 µm, 300 Å pore size, 4.6 x 250 mm) (Phenomenex®, U.S.A.).

Particle size analysis based on dynamic light scattering technique was carried out using Zetasizer Nano-ZS (Malvern Instrument, U.K.). Samples were loaded in disposable polystyrene cuvettes (DTS 0012) prior to analysis.

2.3 Methods

2.3.1 High Performance Liquid Chromatography (HPLC) Assay Method Development for Recombinant Human Insulin

In this part of study, reported HPLC methods were reviewed in the literature for suitability and adaptability. We aimed to select relevant parameters that would enable us to produce a method that is sensitive, selective and specific with short retention times. Table 2.1 summarises the different parameters which were explored.

Table 2.1 HPLC methods used at different stages of optimisation trials.
(Words in *italic* indicate modifications done to the previous method)

Trial	Method	HPLC Conditions	Insulin Samples	HPLC Column
1	Adapted from (Sarmento *et al.*, 2006)	1) Mobile phase : ACN ; 0.1 % TFA 2) Eluent : • 1^{st} – 5^{th} minute (gradient elution) - ACN:TFA 30:70 to 40:60 (v/v) • 6^{th} – 10^{th} minute (isocratic elution) - ACN:TFA 40:60 (v/v) 3) Flow rate : 1 ml/min 4) UV detection wavelength: 214 nm	Dissolved in pH 4.5 sodium acetate buffer (BP, 2007)	Apex ODS (C_{18}), 5 µm, 4.6 x 150 mm (Jones Chromatography, U.S.A.)
2	Adapted and modified from (Sarmento *et al.*, 2006)	1) Mobile phase : ACN ; 0.1 % TFA 2) Eluent : • 1^{st} – 5^{th} minute (gradient elution) - ACN:TFA 30:70 to 40:60 (v/v) • 6^{th} – 10^{th} minute (isocratic elution) - ACN:TFA 40:60 (v/v) 3) Flow rate : 1 ml/min 4) UV detection wavelength: 214 nm	*Dissolved in pH 2 citrate buffer*	Apex ODS (C_{18}), 5 µm, 4.6 x 150 mm (Jones Chromatography, U.S.A.)
3	Adapted and modified from (Sarmento *et al.*, 2006)	1) Mobile phase : ACN ; 0.1 % TFA 2) Eluent : • 1^{st} – 5^{th} minute (gradient elution) - ACN:TFA 30:70 to 40:60 (v/v) • 6^{th} – 10^{th} minute (isocratic elution) - ACN:TFA 40:60 (v/v) 3) Flow rate : 1 ml/min 4) UV detection wavelength: 214 nm	Dissolved in pH 2 citrate buffer	*ODS Hypersil C18, 5 µm, 4.6 x 250 mm* *(Thermo Scientific, UK)*

Trial	Method	HPLC Conditions	Insulin Samples	HPLC Column
4	Adapted and modified from (Sarmento *et al.*, 2006)	1) Mobile phase : ACN ; 0.1 % TFA 2) Eluent : • 1^{st} – 5^{th} minute (gradient elution) - ACN:TFA 30:70 to 40:60 (v/v) • 6^{th} – 10^{th} minute (isocratic elution) - ACN:TFA 40:60 (v/v) 3) Flow rate : 1 ml/min 4) UV detection wavelength: 214 nm	*Dissolved in 0.01 M HCl (pH 2)*	ODS Hypersil C18, 5 µm, 4.6 x 250 mm (Thermo Scientific, UK)
5	Adapted and modified from (Oliva *et al.*, 2000)	*1) Mobile phase :* *a. 74 % 0.2M sodium sulphate (adjusted to pH 2.3 with phosphoric acid)* *b. 26 % ACN* 2) Flow rate : 1 ml/min 3) UV detection wavelength: 214 nm	Dissolved in 0.01 M HCl (pH 2)	ODS Hypersil C18, 5 µm, 4.6 x 250 mm (Thermo Scientific, UK)
6	Adapted and modified from (Oliva *et al.*, 2000)	1) Mobile phase : *a. 73-75 % 0.2M sodium sulphate (adjusted to pH 2.3 with phosphoric acid)* *b. 25-27% ACN* 2) Flow rate : 1 ml/min 3) UV detection wavelength: 214 nm	Dissolved in 0.01 M HCl (pH 2)	ODS Hypersil C18, 5 µm, 4.6 x 250 mm (Thermo Scientific, UK)
7	Adapted and modified from (Bradshaw, 2000)	1) Mobile phase : (A) 0.1 % TFA in water; (B) 0.1 % TFA in ACN A/B : 75/25 to A/B : 35/65 in 20 minutes (gradient elution) 2) Flow rate : 1 ml/min 3) UV detection wavelength: 214 nm	Dissolved in 0.1 % TFA (pH 2)	*Jupiter C18, 5 µm, 300 Å pore size, 4.6 x 250 mm* (Phenomenex, U.S.A.)

2.3.2 Validation of HPLC Method

The selected HPLC method deemed most reliable and suitable was subjected to method validation. The suitable criteria for selection are as outlined in 2.3.1. A primary stock solution of 1000 µg/ml was accurately prepared in 0.1 % TFA, followed by a series of dilutions using 0.1 % TFA to obtain seven secondary standard solutions. The seven insulin standard solutions were prepared over the following concentrations: - 100 µg/ml, 50 µg/ml, 25 µg/ml, 12.5 µg/ml, 6.75 µg/ml, 3.125 µg/ml and 1.5625 µg/ml. Each solution was carefully filtered through cellulose acetate membrane syringe filter with 0.2 µm pore size.

The linearity, accuracy and precision of the developed HPLC assay method were determined. For linearity, seven data points (*n=3*) were used for the calibration curve and the regression line was calculated using least squares method. Insulin solutions at 100 µg/ml, 12.5 µg/ml and 1.5625 µg/ml were accurately prepared and were injected six times for within day determinations of precision and accuracy. A further six injections were made for calculation of the inter-day precision and accuracy. In either case, the precision was calculated as percentage coefficient of variation (% CV) or relative standard deviation (RSD) (Eq. 2.1), whilst the accuracy was calculated as the percentage (%) error or relative standard error (Eq. 2.2).

$$\text{RSD} = \frac{\text{Standard deviation (SD)}}{\text{Mean}} \text{ x } 100\% \quad \text{(Eq 2.1)}$$

$$\text{Percentage (\%)Error} = \frac{\text{Measured} - \text{Actual Concentration}}{\text{Actual Concentration}} \text{ x } 100\% \quad \text{(Eq 2.2)}$$

The limit of detection (LOD) and limit of quantification (LOQ) of this HPLC method were calculated based on the standard deviation of the response (S_y) of the calibration and the slope (S). The LOD was calculated as 3.3 x (S_y/S), whilst LOQ was calculated as 10 x (S_y/S).

2.3.3 Effects of pH and Temperature on Stability of Insulin

2.3.3.1 HPLC

Insulin samples were prepared at 100 µg/ml in 0.1 % TFA (pH~2.2) and stored in clear glass vials at various storage conditions :- a) -20 ºC (freezer) ; b) 2 ºC (refrigerator) ; c) 25 ºC in darkness ; d) 25 ºC in bright light (laboratory room illumination) ; e) 45 ºC (processing temperature). Samples a) to d) were left for 11 days at the respective storage conditions. For exposure at storage temperature 45 ºC, 30 minutes of run time was deemed sufficient to match similar processing times during formulation work.

Samples were analysed based on the optimised chromatographic conditions of the validated HPLC method as described in Section 2.3.1 and 2.3.2.

2.3.3.2 Particle Size Analysis

The average hydrodynamic size (z-average) of insulin in samples was measured by photon correlation spectroscopy using Zetasizer Nano-ZS (Malvern Instrument, U.K.). Samples were loaded in disposable polystyrene cuvettes (DTS 0012). All measurements were performed at 25 ºC, with an equilibrium time of 2 minutes. Each value reported is the average of three measurements, consisting of 10 subruns per measurement.

Samples for stability studies were freshly prepared in pH 2 and pH 7 buffers at a concentration of 1 mg/ml and were each divided into three portions and stored at temperatures :- a) 2 ºC (refrigerated); b) 25 ºC (room temperature); c) 45 ºC (processing temperature).

100 µL aliquots were withdrawn from each sample at specified sampling time intervals over 14 days and frozen at -20 ºC until analysis. Samples were thawed to room temperature prior to particle size measurements. Each sample was diluted to 1 ml with respective buffer, which had already been filtered with 0.2 µm Sartorius Polyethersulfone (PES) membrane filter.

2.4 Results and Discussion

2.4.1 Optimisation of HPLC Methods

Initially, HPLC runs were performed according to the method described in Table 2.1, as adapted from Sarmento *et al.* (2006). Insulin peaks appeared inconsistently at various retention times, due to carry-over from previous sample injections. For example, some peaks appeared prior to the mobile phase front, whilst some chromatograms did not display any drug peak throughout the run, even at high concentrations of 1000 µg/ml.

Insulin was prepared in sodium acetate buffer pH 4.5, where a non-homogenous suspension was formed instead of a clear solution. It has been reported that pH has much influence on the chemical stability of insulin during storage, since it can potentially affect the charge on insulin as well as the folding and association of insulin molecules (Brange and Langkjaer, 1992). Chemical transformation involving the formation of covalent dimers and oligomers is favoured at around pH 4 (Brange, 1994), hence compromising the stability of insulin which is likely to have contributed to the inconsistencies of the insulin peaks.

In the second trial, insulin was dissolved in pH 2 citrate buffer instead of pH 4.5 buffer as used in the first trial. Solutions were prepared carefully to obtain the exact pH to avoid any fluctuations which may result in unwanted insulin phase changes (Brange and Langkjaer, 1992). Here, insulin dissolved readily in pH 2 citrate buffer to form a solution. The chromatogram revealed no peaks during a run time of 20 minutes.

It was unlikely that the insulin had degraded, since it had been freshly prepared and kept at 2 °C between runs. Previous studies had indicated that insulin was stable at 2 °C over a period of up to 72 hours (Hoyer *et al.*, 1995). The HPLC analytical method reported by Sarmento *et al.* (2006) which was adapted and modified for the present study, utilised a column with 250 mm in length. However, the column utilised for our study was 150 mm. Subsequently, a 250 mm ODS Hypersil™ (C18, 5 µm, 4.6 mm x 250 mm) was used but the peaks obtained were inconsistent as shown in Figure 2.1. Furthermore the retention time of insulin was not consistent between the morning and afternoon runs. The peaks obtained during the afternoon analysis (Fig. 2.1B) appeared totally different from the peak seen in the morning (Fig. 2.1A). In addition to these inconsistencies, the retention time for insulin using this method was about 20 minutes, which was significantly longer as compared to approximately 6 minutes as reported in the literature by Sarmento *et al.* (2006).

In an attempt to improve this method, insulin was dissolved in 0.01 M hydrochloric acid (HCl) (pH 2) instead of pH 2 citrate buffer and the HPLC conditions were retained. A peak resulting from this modification was seen at approximately 19 minutes with prominent tailing (Fig. 2.2) and therefore not satisfactory.

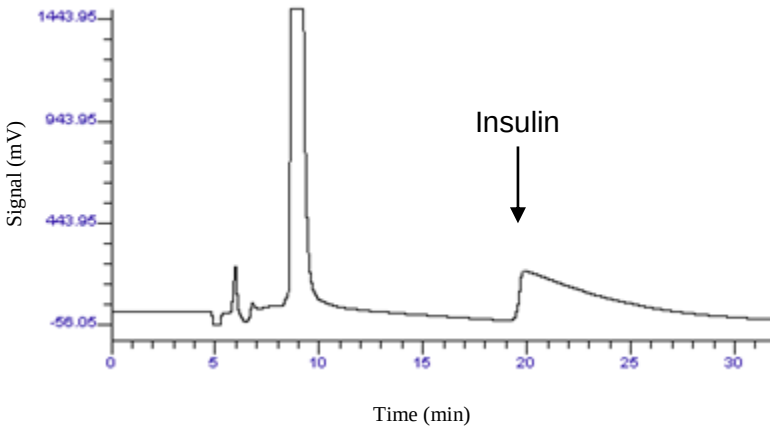

(A)

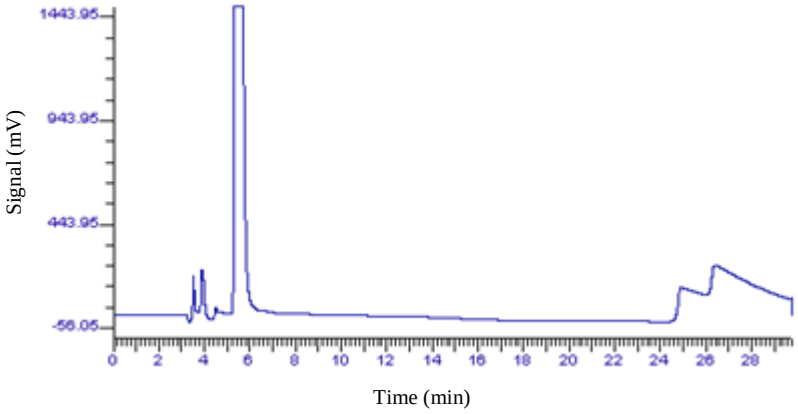

(B)

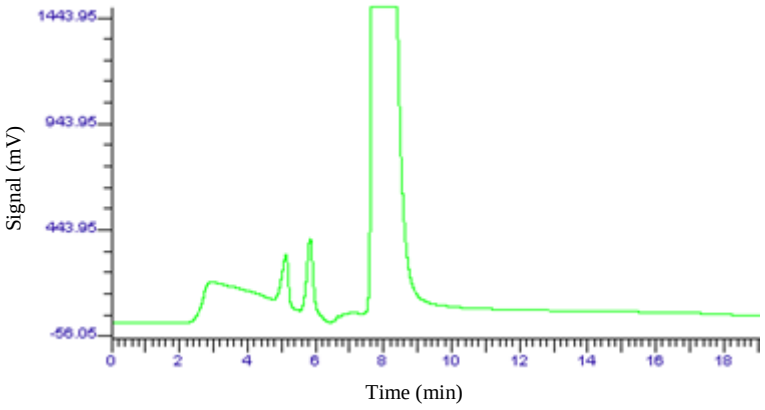

(C)

Figure 2.1 Sample chromatograms (A-C) obtained from Trial 3.

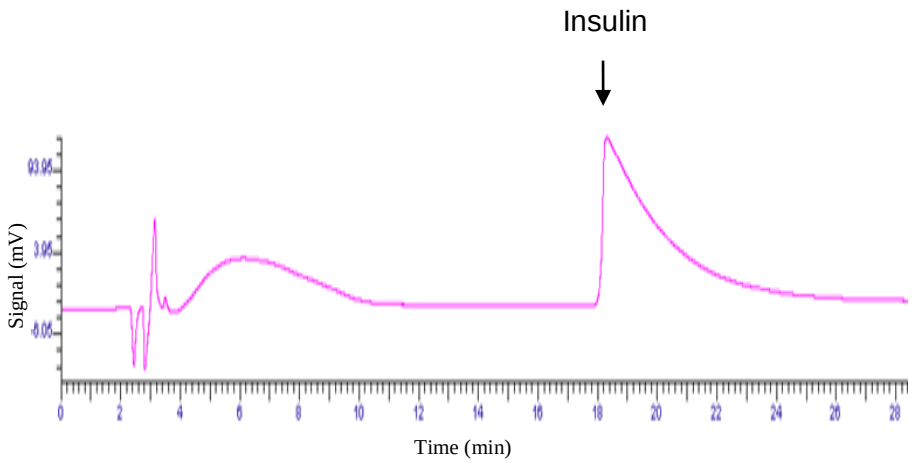

Figure 2.2 Chromatogram of insulin from Trial 4.

Oliva *et al.* (2000) reported an HPLC method in which both insulin and degradation peaks were well-resolved and highly selective at retention times of approximately 8 and 9 minutes respectively. Using this method, we obtained a single insulin peak with no degradation peaks (Fig. 2.3). For the first sample injection of insulin, the peak eluted at approximately 6 minutes, with minimal peak tailing. However, in subsequent runs the tailing effect seemed to be more pronounced. The first injection produced a retention time of approximately 6 minutes (Fig. 2.3A), the second injection eluted at approximately 7 minutes (Fig. 2.3B), and subsequent injections eluted at approximately 9.4 minutes (Fig. 2.3C) and 11.4 minutes (Figure. 2.3D). A trend of drifting of approximately 2 minutes of the retention time was observed between each injection.

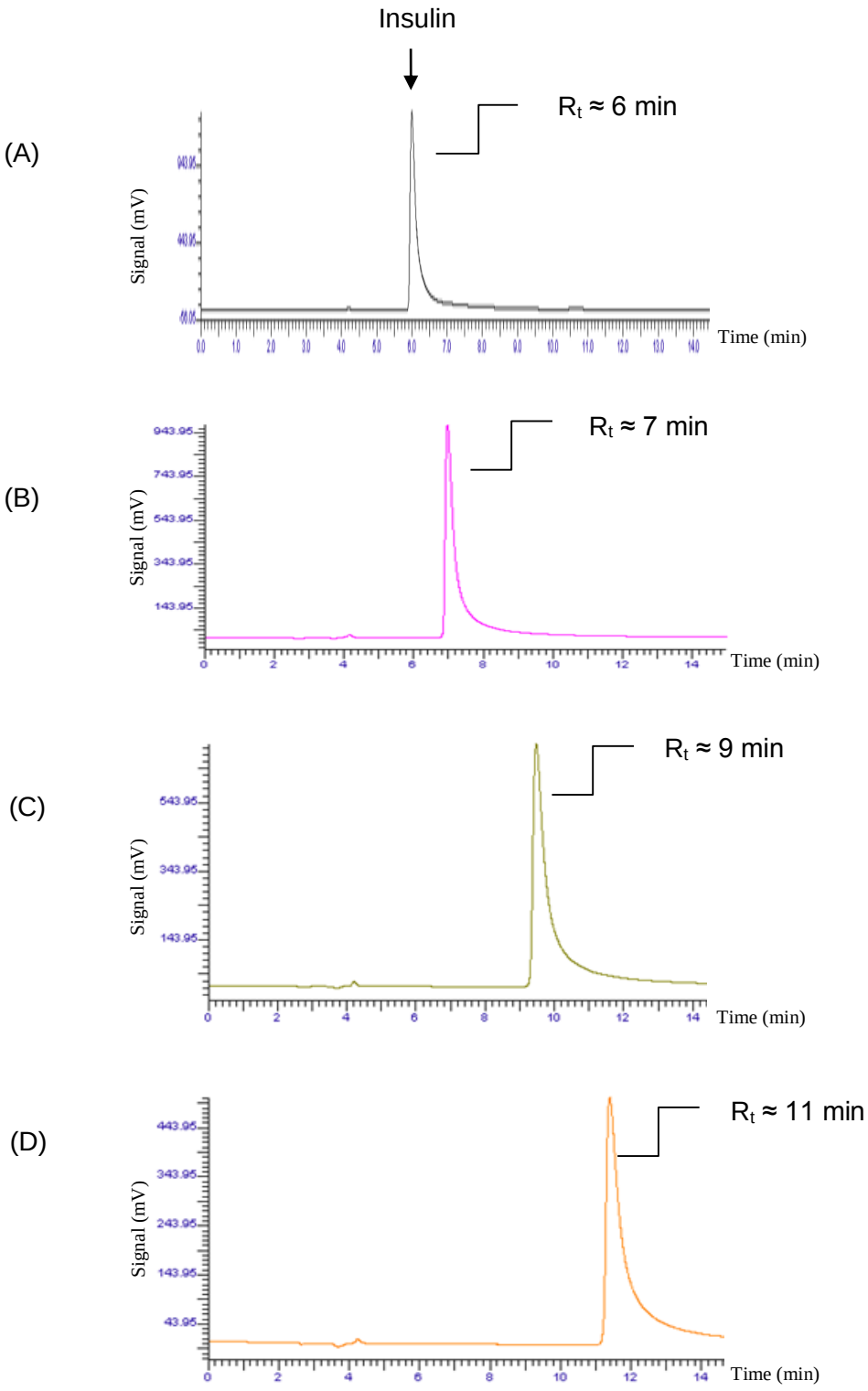

Figure 2.3 Chromatograms of insulin from Trial 5.
Note the drifting retention times (R_t) by approximately 1 to 2 minutes for each subsequent insulin injection from (A) to (D).

The effect of temperature on elution of analytes is well documented (Dolan, 2002; Hertzog *et al.*, 2002). Temperature changes are associated with poor reproducibility of retention times. It was noted that the room temperature was 28 °C in the afternoon and 23 °C in the morning, and this difference in temperature could be the cause of the drifting of the retention time. This further emphasises the sensitivity of the protein insulin to temperature.

During the preparation of mobile phases 76 % 0.2 M sodium sulphate and 24 % ACN in Trial 5 previously, it was observed that a white precipitate was formed upon mixing of both solutions. Preparation of mobile phase for HPLC assay has been detailed in the monograph for human insulin in the British Pharmacopoeia, 2007. Here, the method for preparing the mobile phase was adapted from BP, 2007 in order to address the inconsistency of the retention times and also to avoid the formation of the precipitates. Being an endothermic process, precipitation will occur during the mixing of mobile phases sodium sulphate with acetonitrile, hence it is necessary to keep the solutions at least above 20 °C (British Pharmacopoeia Commission, 2007).

With this modification, intraday injections were more consistent, although the retention time was still not optimal. Therefore, the flow rate was increased in order to achieve a shorter elution time. The retention time for insulin was approximately 13 minutes and 10 minutes at flow rates of 1 ml/min and 1.5 ml/min respectively.

The composition of mobile phases 0.2 M sodium sulphate and ACN were varied at different ratios of Na_2SO_4/ACN, namely 76/24, 74/26 and 73/27, in order to increase the polarity to achieve shorter retention times. The peaks obtained from this modification (Fig. 2.4) appeared inconsistent for composition of Na_2SO_4/ACN mobile phase at 76/24. No elution was observed for mobile phase

composition of 73/27 and 74/26. Figure 2.4 demonstrates poor inter- and intra-days repeatability for mobile phase composition 76/24, highlighting the issue of inconsistency of the HPLC method.

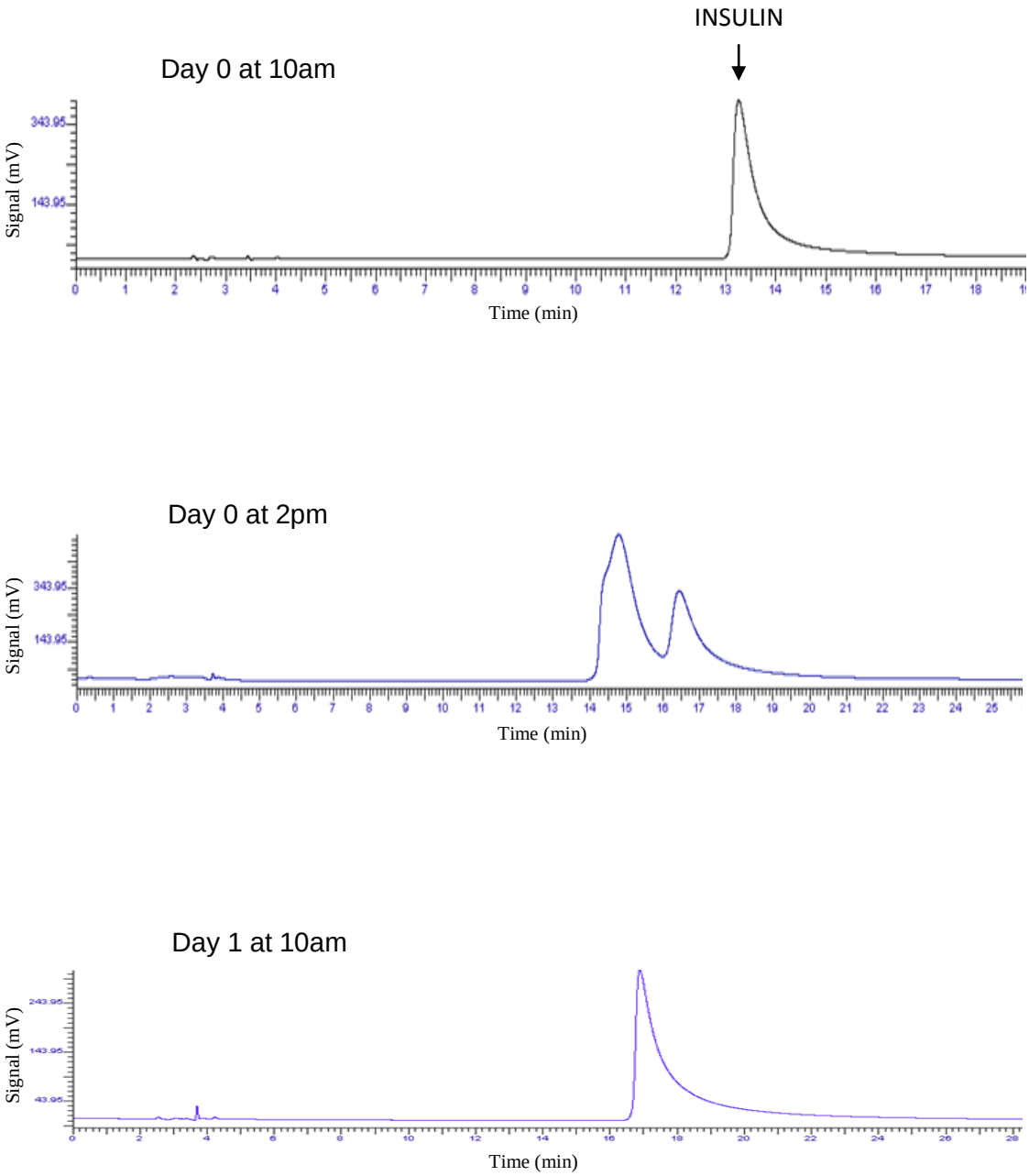

Figure 2.4 Inconsistent peaks for mobile phase at composition 76/24 (Na_2SO_4/ACN).

A review of the literature indicates that not much work has been ascribed to the effect of pore size of the column on elution efficiency. Only a handful of reports have specified that the HPLC column used for separating proteins and peptides had pore sizes in the order of 300 Å (Hoyer *et al.*, 1995; Oliva *et al.*, 1996; Purcell *et al.*, 1995). This pore size specification is much larger than those used in the present study. After careful consideration of various HPLC columns, a Phenomenex Jupiter C18, 5 µm, 300 Å pore size, 4.6 x 250 mm column was chosen for further analysis based on reports on its ability to separate proteins and peptides efficiently, in particular, the model drug insulin. The HPLC conditions used to separate insulin were adapted and modified from Bradshaw (2000) as described in Table 2.1.

With the new column, the retention time was more consistent at approximately 10 minutes. Furthermore, it was possible to separate insulin from its degradation product (A-21 desamidoinsulin) as shown in Figure 2.5, which was useful for stability studies of insulin.

Subsequently, attempts were made to achieve better peak resolution and therefore several parameters including flow rate and mobile phase gradient were varied (Fig. 2.6). A flow rate of 1 ml/min was found to be optimal at a mobile phase gradient of 2 % per minute (from 75 % to 49 %) for mobile phase 0.1 % TFA in water over the run time of 13 minutes. These parameters were optimal for a good peak resolution.

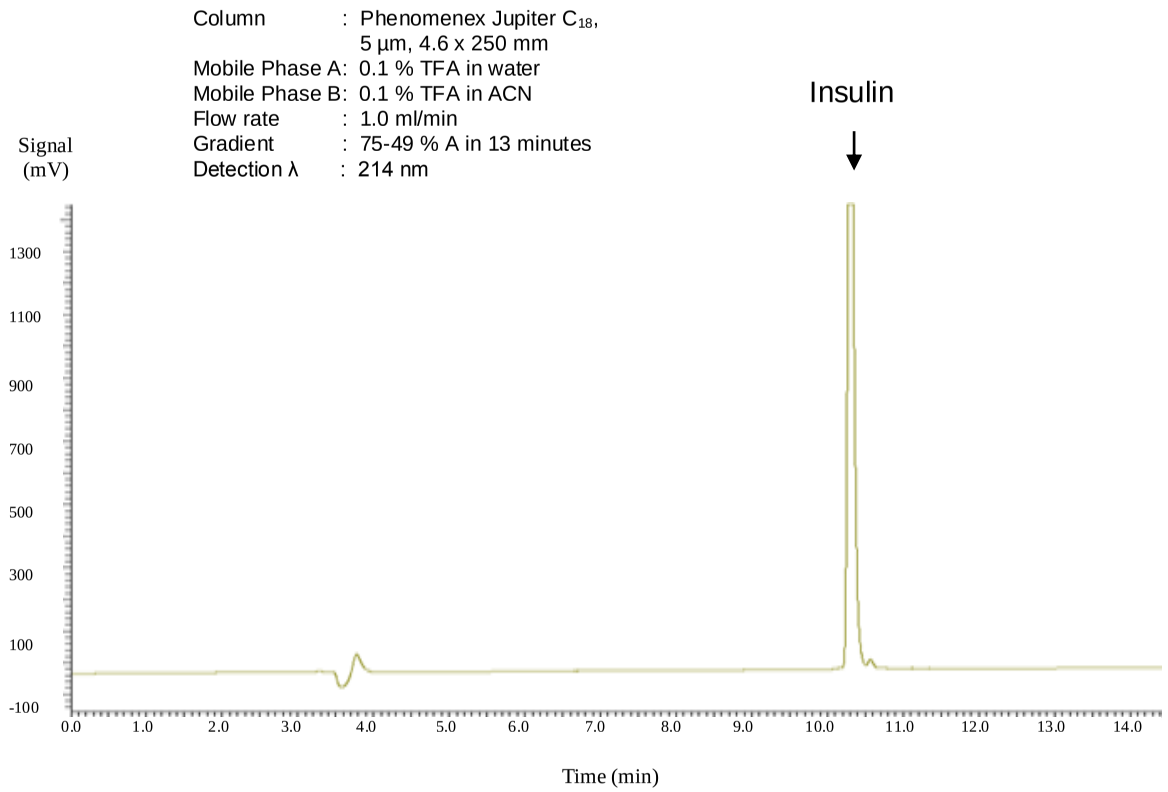

Figure 2.5 Chromatogram showing well-resolved peaks of insulin and its degradation product.

(A) Mobile phase gradient : 2 %/min (0.1 % TFA in water)
Flow rate : 1 ml/min

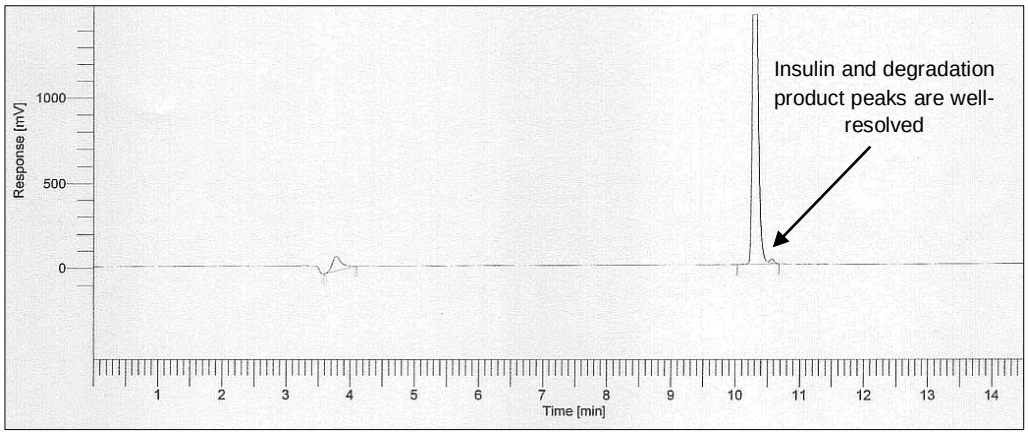

(B) Mobile phase gradient : 3 %/min (0.1 % TFA in water)
Flow rate : 1 ml/min

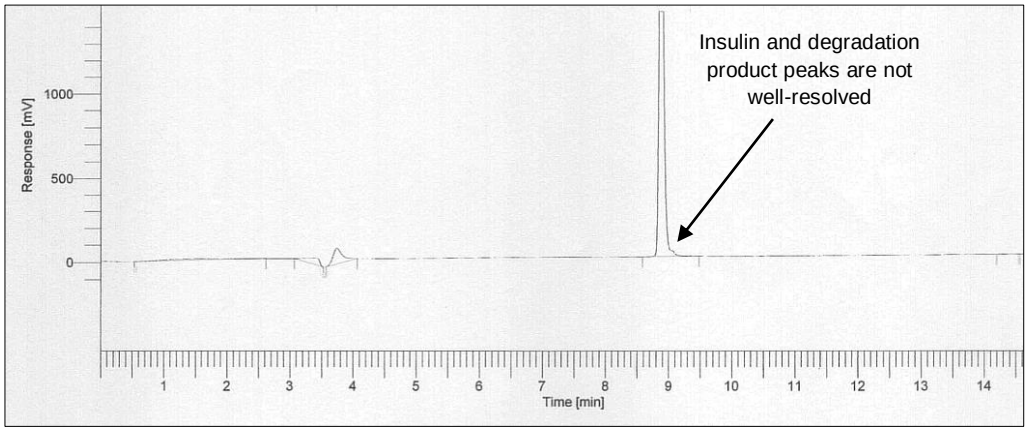

(C) Mobile phase gradient : 4 %/min (0.1 % TFA in water)
Flow rate : 1 ml/min

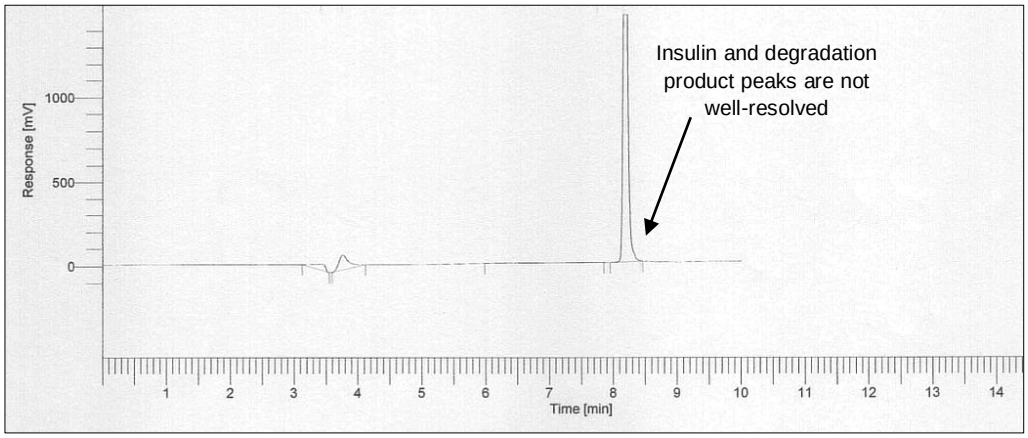

Figure 2.6 Chromatograms from optimisation of HPLC conditions showing well-resolved insulin peaks for (A) mobile phase gradient 2 %/min.

2.4.2 Validation of HPLC Method

Subsequent to the optimised procedure, the method was validated using seven insulin standard solutions at different concentrations:- 1.5625 µg/ml, 3.125 µg/ml, 6.25 µg/ml, 12.5 µg/ml, 25 µg/ml, 50 µg/ml and 100 µg/ml. These standard solutions were prepared in 0.1 % trifluoroacetic acid. Analyses were done in triplicates using the peak area.

A good linearity ($R^2 > 0.99$) was achieved in the range of study as shown in the calibration curve in Figure 2.7.

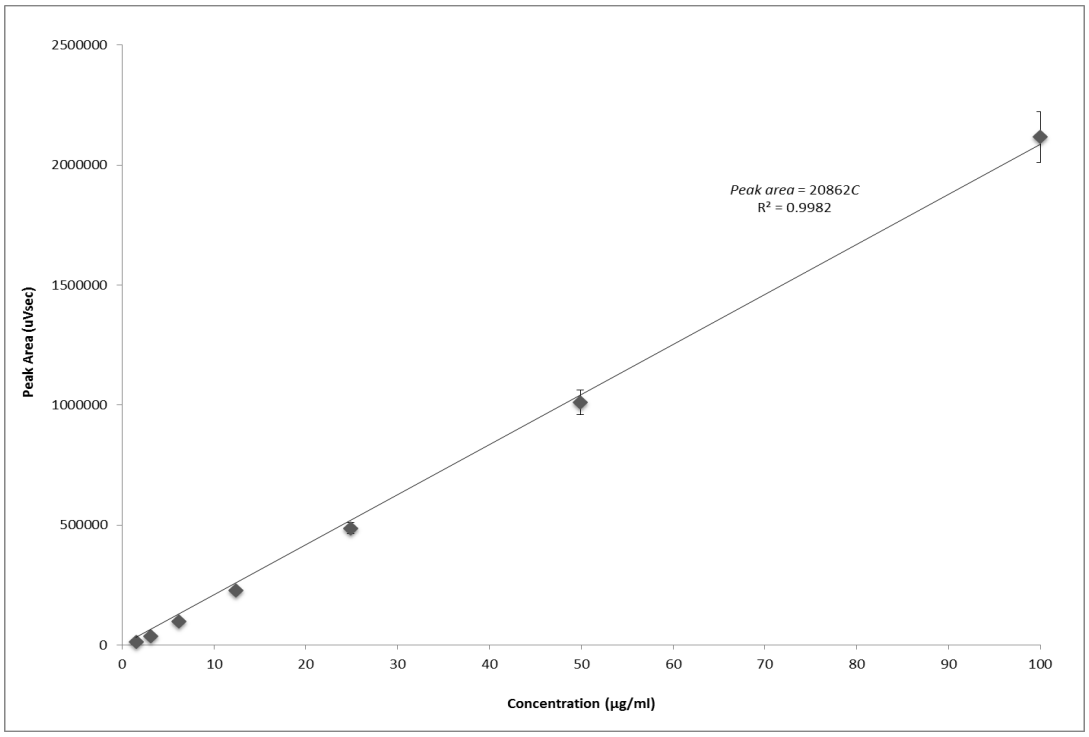

Figure 2.7 Calibration curve demonstrates the linearity of the HPLC method.

Table 2.2 Precision and accuracy of this HPLC method.

	Standard insulin concentration (µg/ml)	Concentration of insulin measured (µg/ml)					
		Day 1	**Day 2**	**Day 3**	**Day 4**	**Day 5**	**Day 6**
Intra-day	**1.5625**	0.60	0.61	0.62	0.61	0.58	0.61
	12.5	10.95	10.83	10.60	10.78	10.62	10.75
	100	103.00	99.94	101.48	98.25	98.36	101.45
Inter-day	**1.5625**	0.60	0.61	0.67	0.65	0.65	0.77
	12.5	10.91	10.92	10.86	10.88	10.52	10.68
	100	98.62	100.01	98.23	100.05	98.06	99.60

Three concentrations of insulin, namely 1.5625 µg/ml, 12.5 µg/ml and 100 µg/ml, were analysed with six injections for each concentration within the same day and over six different days under the same conditions (Table 2.2). The precision of the assay, calculated as RSD, was determined from the analyses of the intra-day and inter-day variation samples. The intra-day RSD was found to be at 2 %, 1.2 % and 1.9 % for concentrations 1.5625 µg/ml, 12.5 µg/ml and 100 µg/ml respectively. For the same insulin standard concentrations, inter-day RSD values of 9.4 %, 1.5 % and 0.9 % were registered respectively. These RSD values are within the acceptable limits of 15 %, indicating that this analytical method is very precise at these concentration (Bressolle *et al.*, 1996). Our RSD values were close to those reported by Sarmento *et al.* (2007) for concentrations 12.5 µg/ml and 100 µg/ml, as their inter-day RSD were recorded as 2.55 % and 0.25 % respectively.

As for accuracy of this method, the relative standard errors were calculated as 14 % and 0.4 % (intra-day) and 13.6 % and 0.9 % (inter-day) for concentrations 12.5 µg/ml and 100 µg/ml respectively. These results demonstrated that this method is very accurate at both these concentrations, as they are within ±15 % deviation of the nominal value (Bressolle *et al.*, 1996). However, for the concentration of 1.5625 µg/ml, the relative standard errors in both intra-day and inter-day measurements were calculated to be rather high at above 50 %, demonstrating a low accuracy of this method at this concentration. The LOD and LOQ values for this HPLC method were found to be 2.2 µg/ml and 6.7 µg/ml respectively.

All in all we can conclude that the method is precise and accurate for the concentrations (12.5 µg/ml and 100 µg/ml) analysed and is comparable to those reported in the literature.

2.4.3 Stability-indicating studies using HPLC analyses

Stability-indicating HPLC methods for the assay of insulin and its importance in separating and identifying insulin degradation products have been previously described in the literature (Hoyer *et al.*, 1995; Moslemi *et al.*, 2003; Oliva *et al.*, 2000). The optimised and validated HPLC method as described in the present study was deemed suitable for a stability indicating study on insulin since it was possible to resolve degradation peak as well. In this context, the extent of insulin degradation after exposure to different stresses will be correlated with the extent of reduction of the insulin peak area in the chromatogram. Figure 2.8 shows the HPLC chromatogram of freshly prepared insulin. Prior to the stability studies, the freshly prepared insulin concentration was 100 µg/ml. It can be observed that negligible degradation product (A-21 desamidoinsulin) was present when the freshly prepared insulin was injected.

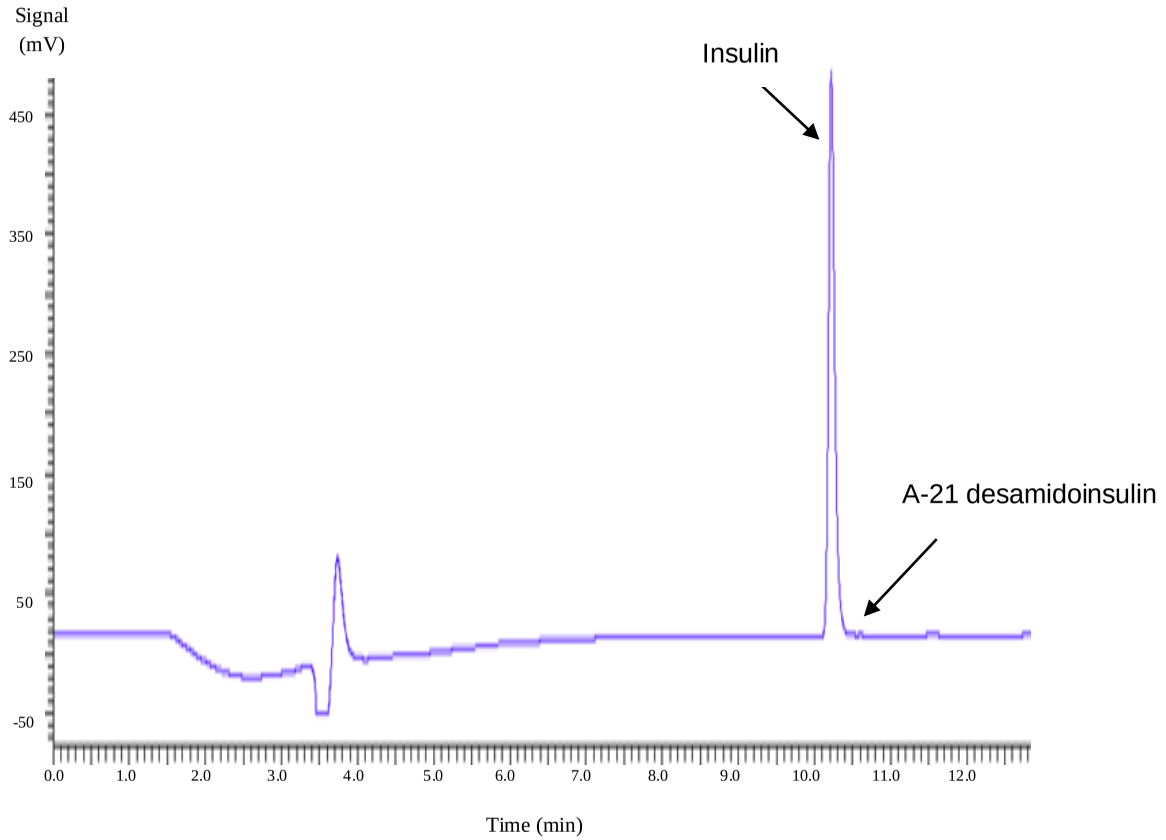

Figure 2.8 HPLC chromatogram of freshly prepared insulin (Day 0).

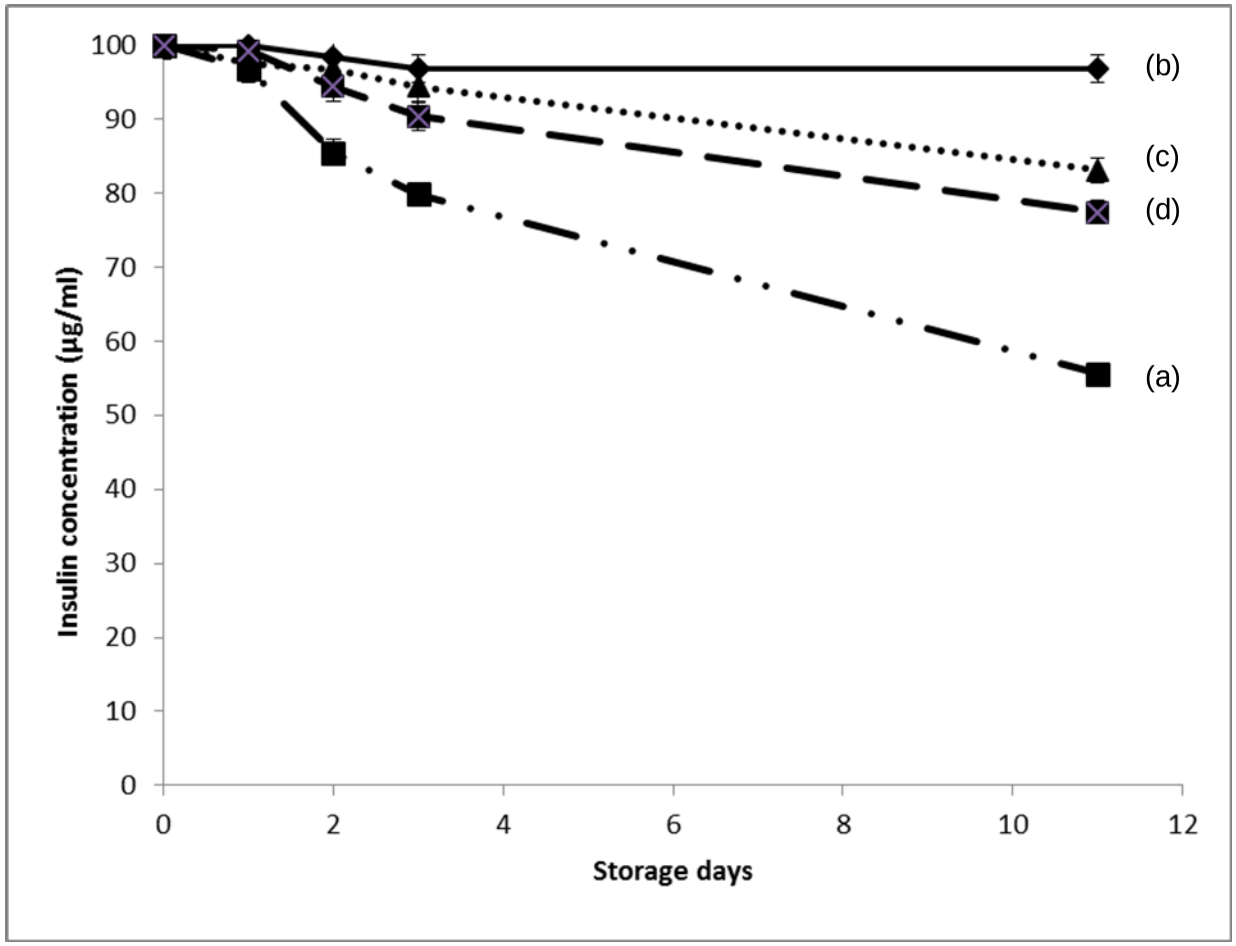

Figure 2.9 Effects of various storage conditions :- (a) -20 ºC, (b) 2 ºC, (c) 25 ºC in dark, (d) 25 ºC in light on the amount of insulin over 11 days of storage period.

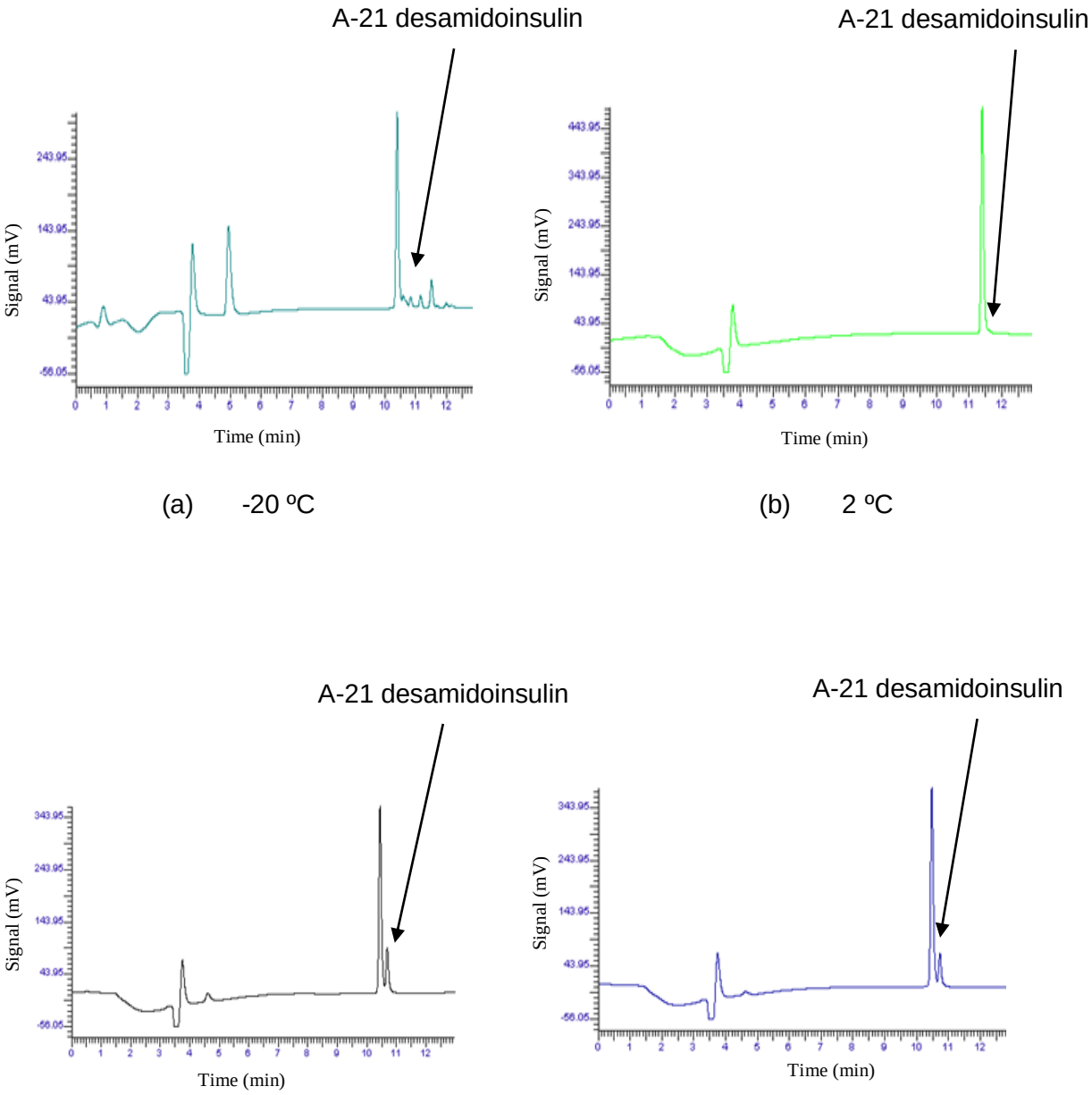

Figure 2.10 HPLC chromatograms of insulin at various storage conditions :- (a) -20 ºC, (b) 2 ºC, (c) 25 ºC in dark, (d) 25 ºC in light, on Day 11 of study period.

The average room temperature was 24.8 ºC and the average refrigerator and freezer temperatures were 2.5 ºC and -20.2 ºC respectively. Figure 2.9 shows the decrease in amount of insulin over 11 days of storage at the various temperatures, whilst Figure 2.10 shows the chromatograms of insulin and the degradation products at the respective temperatures.

It was observed in Figure 2.10(b) that insulin solution stored in the refrigerator at 2 ºC remained relatively stable during 11 days of storage, with a negligible degradation peak. Insulin was stable at 2 ºC throughout the duration of study of 11 days (Fig. 2.10b). On the other hand, at -20 ºC, degradation peaks in the chromatogram were observed (Fig. 2.10a) which did not appear in others (Fig. 2.10b, c, d). This observation has not been reported in the literature and indicate that freezing and thawing insulin solution may lead to the production of degradation products. Therefore, storing insulin solution at sub-zero temperatures should be avoided.

Referring to Figure 2.10(c) and 2.10(d), both HPLC chromatograms displayed a significant A-21 desamidoinsulin degradation peak for insulin stored at room temperature in the dark and light respectively. It was found that the insulin peak decreased at a faster rate when stored at 25 ºC in light (Fig. 2.9d), as compared to being stored at 25 ºC in the dark (Fig. 2.9c) with peak signals of 1,999,304 mV versus 2,140,795 mV respectively at day 11 of the stability studies. This data is in good agreement with the findings of Hoyer *et al.* (1995), demonstrating that presence of light does affect the stability of insulin solution.

For stability studies carried out at 45 ºC, it was found that after 30 minutes of exposure, insulin remained relatively stable with concentration analysed at approximately 99 µg/ml from an initial concentration of 100 µg/ml. However, the concentration of the peak for A-21 desamidoinsulin increased with time as well (Fig. 2.11), indicating that exposure to heat also speeds up the rate of degradation of insulin. Interestingly, as shown in Figure 2.11, there was a linear (R^2 > 0.99) increase in the percentage change in the concentration of A-21 desamidoinsulin over the duration of 30 minutes of storage at 45 °C. This indicates that the formation of A-21 desamidoinsulin increased linearly as a function of time, despite the fact that the insulin concentration was not much affected by the heat during the study period.

Another interesting finding was that the rate of chemical degradation was not directly related to a decrease of insulin concentration. This points to a possible complex degradation kinetics (Jacob *et al.*, 2006; Pearlman, 1993). Thus, the decrease in insulin concentration was not solely contributed by deamidation reaction and thus insulin concentration remained relatively stable over the study period of 30 minutes, although the amount of A-21 desamidoinsulin had increased. We may conclude that insulin solution will remain stable during subsequent formulation work, when exposed to a temperature of 45 ºC for less than 30 minutes.

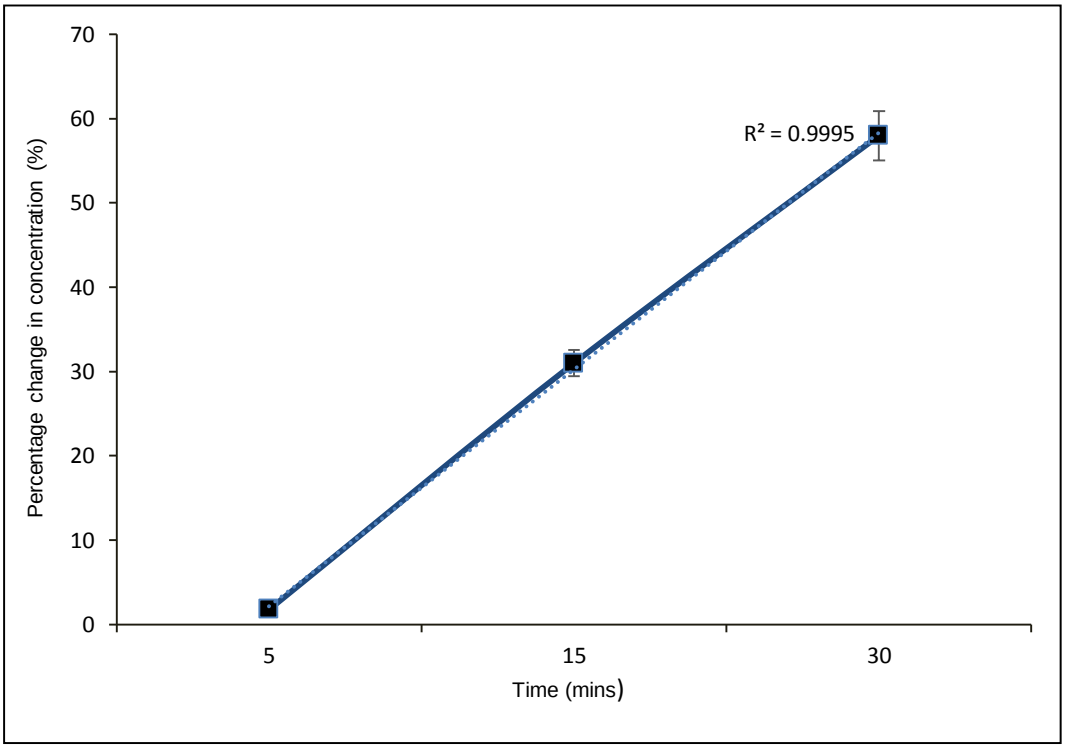

Figure 2.11 Percentage changes of A-21 desamidoinsulin concentration as a function of time for insulin solution stored at 45 °C *(n=3)*.

2.4.4 Stability-indicating studies using Dynamic Light Scattering analyses

Dynamic light scattering technique is not routinely used for stability studies. However, it was utilised here due to the ability of this method to discriminate between particles of protein aggregates or changes in particle sizes, which can be used to infer physical instabilities. Insulin was observed to be completely soluble in pH 2 buffer (clear solution). However, it was practically insoluble in pH 7 buffer, appearing as suspension. It has been reported that insulin exists in different oligomeric forms as a result of variation in pH. Monomeric or dimeric conformation was reported to be favoured at low pH, whilst at neutral pH, insulin exists largely in hexameric form (Darrington and Anderson, 1995; Whittingham *et al.*, 2002). These different configurations are related to relative size, with monomers being smaller and hexamers larger in size.

The z-average values for insulin in pH 2 buffer, measured using Zetasizer, at 3 different storage temperatures as a function of time at 2 °C, 25 °C and 45 °C are shown in Figure 2.12.

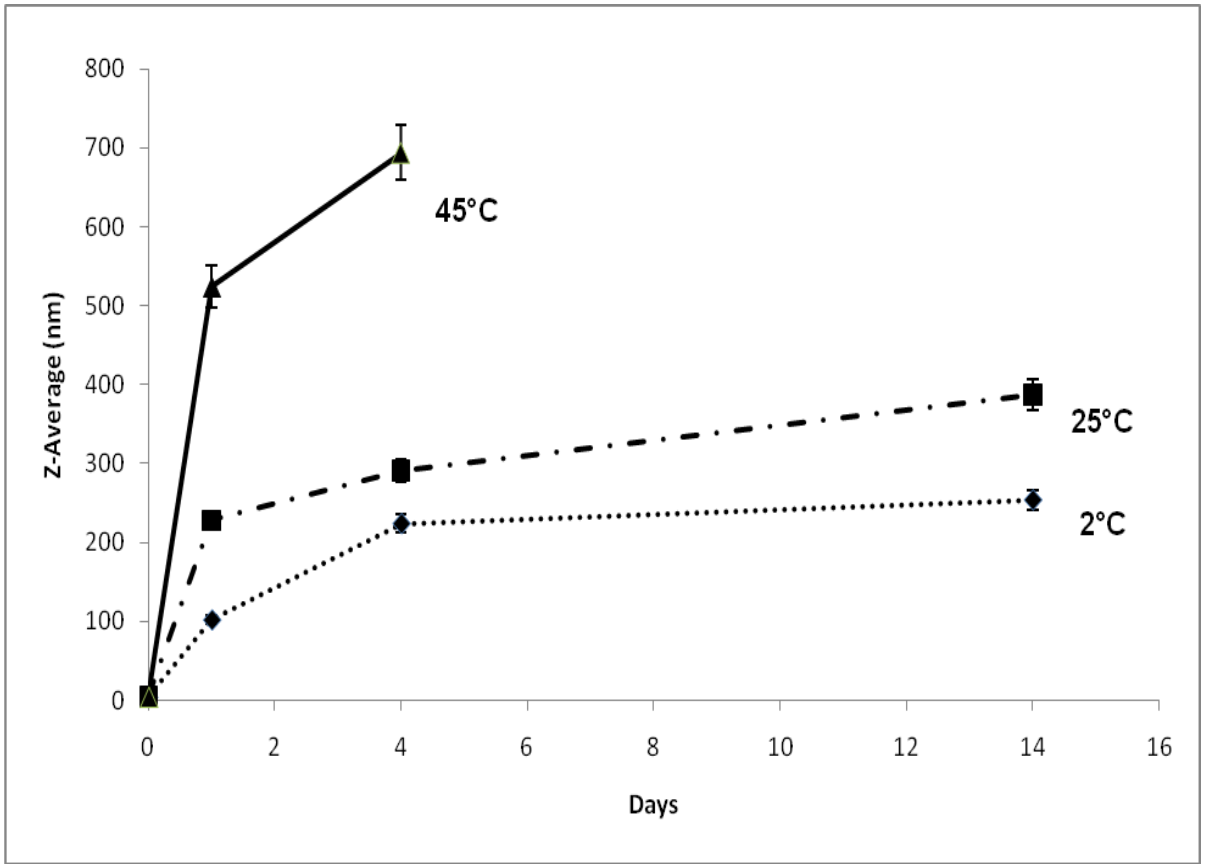

Figure 2.12 Z-average values of insulin in pH 2 as a function of time at temperatures 2 °C, 25 °C and 45 °C *(n=3)*.

An increase in z-average values was observed with increasing storage temperatures as well as duration. Protein aggregation is indicated by an increase in intensity-weighted mean particle sizes. This clearly indicates that protein aggregates were formed over the experimental period and is in concert with what has been reported in the literature. High temperature with prolonged storage or mechanical shaking of insulin can result in the formation of high molecular weight aggregates, observed as larger-sized particles (Oliva *et al.*, 1996). The insulin sample kept in the refrigerator (2 °C) showed the slowest rate of protein aggregation, followed by those stored at room temperature, then at 45 °C. It is important to note that protein aggregation (physical instability) would occur over storage irrespective of the temperature. The difference in the extent and rate of protein aggregation is determined by the storage temperature as observed.

Table 2.3 Z-average values for insulin sample in pH 7 buffer stored at 3 different temperatures 2 °C, 25 °C, 45 °C taken at fixed sampling days *(n=3)*.

Day	**Z-Average (nm)**		
	2 °C	**25 °C**	**45 °C**
0	Undetectable	Undetectable	Undetectable
1	Undetectable	417 ± 39.8	160 ± 9.5
4	604 ± 37.9	357 ± 12.4	
14	459 ± 34.1		

Table 2.3 summarises the z-average values for insulin in pH 7 buffer stored at various temperatures (2 °C, 25 °C and 45 °C). Contrary to the results shown earlier, the particle sizes of insulin in pH 7 decreased with time and storage temperature. At day 0, particle sizes were too large to be detected. Due to its poor solubility in pH 7 buffer, insulin remained suspended upon addition to the buffer solution. The decrease in particle size over storage period could be due to an increase in dissolution of the particles in the buffer with time. There is also the possibility of hydrolysis at B3-asparagine residues in the neutral pH 7 buffer (Pearlman, 1993). The decrease in size was most rapidly seen at 45 °C, followed by 25 °C and 2 °C.

From the results obtained, it can be concluded that insulin samples stored at all temperatures displayed a certain degree of protein degradation, with the most occurring at 45 °C, whilst samples stored at refrigeration (2 °C) were relatively the more stable.

2.5 Concluding remarks

A simple and reliable HPLC method for detecting insulin was developed and validated with respect to linearity, precision, accuracy, limit of detection and limit of quantification. The HPLC method parameters are summarised as follows:

Column	:	Phenomenex Jupiter C_{18}, 5 µm, 4.6 x 250 mm
Mobile Phase A	:	0.1 % TFA in water
Mobile Phase B	:	0.1 % TFA in ACN
Flow rate	:	1.0 ml/min
Gradient	:	75-49 % mobile phase A in 13 minutes
Detection λ	:	214 nm

The rate of degradation of insulin depends on the storage conditions, with exposure to heat and light being observed to be one of the main contributing factors that speed up the degradation reaction. HPLC and dynamic light scattering technique have been useful in detecting physically or chemically degraded products of insulin.

On the basis of above, pH 2 was considered most suitable to dissolve insulin and a storage temperature of 2 °C most optimal for insulin storage.

CHAPTER 3

Formulation and Characterisation of Optimised Insulin-containing Solid Lipid Nanoparticles (SLNs)

3.1 Introduction

3.1.1 SLNs from palm oil lipid constituents

Solid lipid nanoparticles (SLNs) are colloidal drug delivery systems which have received increasing attention of late because they are made from physiologically compatible lipids and therefore are a promising alternative to polymeric nanoparticles (Garcıa-Fuentes *et al.*, 2003; Hu *et al.*, 2006; Liu *et al.*, 2007; Müller *et al.*, 2000; Ruckmani *et al.*, 2006; Souto and Müller, 2010; Zhang *et al.*, 2006). Commonly used lipids can be highly purified triacylglycerols, complex acylglycerol mixtures or waxes (Souto and Müller, 2007). Many studies have demonstrated that the safest lipids are glycerides composed of fatty acids and lecithin (Fangueiro *et al.*, 2013; Souto *et al.*, 2011). Palm oil lipid constituents have been used in the fabrication of SLNs lipid matrix, namely tripalmitin (Helgason *et al.*, 2009; Weiss *et al.*, 2008) and palmitic acid (Xie *et al.*, 2011b). SLNs are favoured over conventional polymeric particulate systems due to better safety, tolerability and release profile attributes as well as their ability to protect labile drugs (Müller *et al.*, 2000; Sarmento *et al.*, 2007a).

In particular, the successful incorporation of hydrophilic drugs in SLNs have been reported to improve bioavailability of drugs, prolong residence time as well as increase the propensity of uptake of nanoparticles and transport through the intestinal mucosa (Garcıa-Fuentes *et al.*, 2003). Studies have previously used insulin, salmon calcitonin, lysozyme and bovine serum albumin as model hydrophilic peptide drugs encapsulated in SLNs for either oral or pulmonary delivery systems (Garcıa-Fuentes *et al.*, 2003; Hu *et al.*, 2006; Liu *et al.*, 2008; Sarmento *et al.*, 2007a; Trotta *et al.*, 2005; Xie *et al.*, 2008; Zhang *et al.*, 2006).

The present work utilises palm oil lipidic components: triacylglycerol (tripalmitin) and single chain fatty acid (palmitic acid) to form the lipid matrix of the SLNs, as these offer potential advantages as described above in the incorporation of protein insulin which is hydrophilic in nature. Specifically, the solid mixture of single chain fatty acid with the triacylglycerol offers the potential of conforming to a disordered matrix upon formation, which can help prevent the expulsion of insulin from the SLNs during storage, as observed in nanostructured lipid carriers (NLCs).

3.1.2 SLNs preparation technique

There are several methods used to prepare nanoparticles reported in the literature including high pressure homogenisation, either hot (Al-Haj and Rasedee, 2009) or cold (Mehnert and Mäder, 2001), solvent emulsification evaporation method (Garcıa-Fuentes *et al.*, 2003) as well as solvent diffusion technique (Trotta *et al.*, 2005). Other methods include gas-assisted melting atomisation (GAMA) (Salmaso *et al.*, 2009) and particles from gas saturated solutions (PGSS) process using supercritical carbon dioxide (Elvassore *et al.*, 2001).

Hot homogenisation technique has inherent disadvantages which include exposure to high shear stress and high temperatures as well as formation of microparticles. Cold homogenisation on the other hand minimises thermal exposure but also produces particles with larger particle size and broader size distribution (Trotta *et al.*, 2003). The broad particle size distribution can lead to Ostwald ripening, resulting in physical instabilities during storage.

Solvent emulsification evaporation technique involves evaporating-off water-immiscible organic solvent which is included in the formulation to dissolve lipidic components, hence leaving precipitates of SLNs in an aqueous environment after evaporation. Besides, this method does not involve any heat exposure for long durations, hence an efficient way of loading unstable and hydrophilic drugs (Liu *et al.*, 2007; Morel *et al.*, 1998).

In the present study, ultrasonic energy was utilised in the production of the SLNs due to the higher efficiency of dissipated energy when this method is employed and the ability to produce nanoparticles of narrower particle size distribution. Although temperature of the entire formulation could rise during the process of ultrasonication, the duration of thermal exposure is relatively short and any heat generated is rapidly dissipated.

3.1.3 Particle size and zeta potential

For a nanoparticulate colloidal dispersion system, particle size distribution and zeta potential are crucial parameters which influence the formulation stability (Goeddel *et al.*, 1979; M. Hu *et al.*, 2004) as well as the *in vivo* fate of the nanoparticles (He *et al.*, 2010). Dynamic light scattering (DLS) technique, also known as the photon correlation spectroscopy (PCS), is commonly employed to measure the size of the particles, dispersed in a liquid. DLS measurements are calculated based on the random Brownian motion of particles (Kaszuba *et al.*, 2008; Pecora, 2000). The size of a particle is termed the hydrodynamic diameter as it refers to how a particle diffuses within a fluid. It is calculated from the translational diffusion coefficient by using the Stokes-Einstein equation (Eq. 3.1):-

$$d(H) = \frac{kT}{3\pi\eta D}$$

(Eq. 3.1)

where d(H) = hydrodynamic diameter; D = translational diffusion coefficient; k = Boltzmann's constant; T = absolute temperature; η = viscosity.

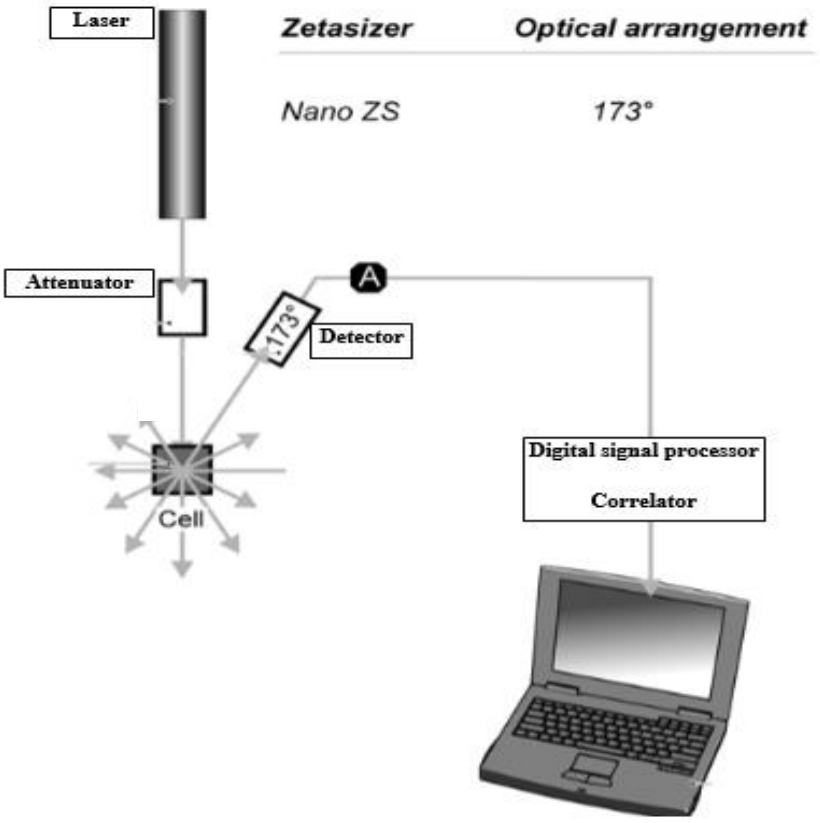

Figure 3.1 Optical configuration of the Zetasizer Nano-ZS.
[Adapted and modified from (Malvern Instruments Ltd., 2014a)]

Figure 3.1 shows the optical configurations of the Zetasizer Nano-ZS system. The laser beam provides a light source that illuminate the sample contained in a cuvette. The particles present within the sample scatter the laser beam at all angles. A detector, positioned at 173°, will measure the intensity of the scattered light.

Polydispersity index (PdI) values as measured by DLS can indicate the heterogeneity of the nanoparticle sample. PdI is represented by the width of the size distribution profile. A low PdI value represents a monodisperse sample, whilst a polydisperse sample is indicated with a high PdI value. PdI values are very sensitive to the presence of aggregates or dust (Kaszuba *et al.*, 2008).

An interfacial charge is formed instantly when a solid surface is in contact with aqueous media. A layer of immobile counter-ions adjacent to the charged particle surface at the solid-liquid interface is known as the compact layer, whilst the mobile balancing counter-ions in the liquid outside the compact layer is called the diffuse layer. Both compact layer and the diffuse layer form the electrical double layer. The electrostatic potential at the interface of the compact layer and the diffuse layer is known as the zeta potential, which is an important parameter especially in nanoparticle characterisation, as it acts as an indicator of particle surface charge (Sze *et al.*, 2003). The magnitude of zeta potential is able to predict the potential long-term stability of the colloidal system. It is generally accepted that zeta potentials for stable suspensions falls within the region of +30 mV or -30 mV. Thus, particles with zeta potentials greater than ± 30 mV are normally considered as stable colloidal system (Malvern Instruments Ltd., 2014b).

Zeta potential values are calculated based on Smoluchowski equations (Eq. 3.2) to determine the electrophoretic mobility of nanoparticulate samples (Sze *et al.*, 2003).

$$\upsilon \mathrm{E} = 4\pi\varepsilon 0\varepsilon \mathrm{r} \frac{\zeta}{6\pi\mu} (1 + \kappa r) \qquad \text{(Eq. 3.2)}$$

Where υ_E = mobility; ε_0 = relative dielectric constant; ε_r = electrical permittivity of vacuum; ζ = zeta potential; μ = viscosity; κ = Debye–Hückel parameter; r = particle radius.

3.1.4 Thermal analysis

Differential scanning calorimetry (DSC) is one of the most commonly used methods of thermal analysis in pharmaceutical science. Melting behaviour is often studied, where the change in state is accompanied by a change in the temperature dependence of the free energy, as the system changes from solid to the liquid state at the melt temperature (Craig and Reading, 2006).

Change in entropy (ΔS) at the onset of melt (T_m) is calculated from the change in enthalpy (ΔH), using the equation below (Eq. 3.3) (Folmer and Franzen, 2003):-

$$\Delta \mathrm{S} = \frac{\Delta \mathrm{H}}{\mathrm{Tm}} \qquad \text{(Eq. 3.3)}$$

The magnitude of entropies at melt (ΔS) gives an indication of the disruptive index within the system, being higher for more orderly structures (York and Grant, 1985).

3.1.5 Microscopy imaging

With polarised light microscopy (PLM) technique, we are able to obtain information on particle aggregation and colloidal stability indicated by sample homogeneity. This technique is also used for checking the presence of nanometric lipid structures (Fangueiro *et al.*, 2013; Severino *et al.*, 2012). Particle size measurements made using static light scattering techniques such as laser diffractometry can sometimes overlook larger-sized particles or aggregated particles (Keck and Müller, 2008). Therefore, light microscopy with or without polarised light is useful to provide additional characterisation insights on possible large particles apart from being able to view the shape of the particles (Fangueiro *et al.*, 2013; Obeidat *et al.*, 2010).

However, to view particles at a submicron level, scanning electron microscope (SEM) and transmission electron microscopy (TEM) are used to characterise and examine the nanoparticulate samples. SEM uses a focused beam of high-energy electrons to generate a range of signals at the surface of solid particles. The signals acquired from the interaction between the electrons and the particle surface can provide information about the sample, such as the external microstructure morphology (texture) as well as chemical composition of the material.

TEM, on the other hand, work on the principle of a beam of electrons transmitted through an ultrathin specimen. These electrons interact with the specimen as it passes through it to form a high-resolution image. TEM is routinely used in the area of nanotechnology owing to its capability to allow examination of fine details of the particles.

3.1.6 Aims and objectives

This part of study was aimed at formulating SLNs delivery system containing insulin using solvent emulsification evaporation technique. Processing and formulation parameters of the SLNs were studied in order to achieve desirable physical properties, which were then characterised appropriately.

3.2 Materials

Crystalline recombinant human insulin (lyophilized powder) was manufactured by EMD Biosciences (San Diego, USA) and purchased from Merck Malaysia. Solid lipids tripalmitin (99 % purity) and palmitic acid (98 % purity) were both purchased from Acros Organics (Geel, Belgium). L-α-phosphatidyl choline (soy lecithin) and Poloxamer 188 (Lutrol F68) were purchased from Fluka (Australia) and BASF (Germany) respectively, both used as surfactants. Analytical-grade dichloromethane (DCM) was purchased from R&M Chemicals. Trifluoroacetic acid (TFA) and methanol (MeOH) were purchased from Fisher Scientific (Loughborough, UK).

3.3 Methods

3.3.1 Preparation of SLNs Formulations

The SLNs were prepared using the W/O/W double emulsion solvent evaporation technique as described by García-Fuentes *et al.* (2003) with slight modification. Lipid nanoparticle formulations without insulin, referred to as

insulin-free SLNs, were prepared as follows. Different amounts of solid lipids and lecithin was dissolved in 1 ml of dichloromethane (DCM) to form the oily phase of the pre-emulsion. For the inner aqueous phase, 100 µL of distilled water was added to the oily phase. On the other hand, 100 µL of insulin solution (1 mg insulin dissolved in 100 µL of 0.1 % TFA) was added to the oily phase for the insulin-containing SLNs. The mixture was dispersed using an ultrasonic probe (750 W Vibra Cell VCX Series, Sonics Inc., U.S.), equipped with a titanium 13 mm diameter probe, for 15 seconds at 20 W to produce a primary W/O emulsion. 2 % Poloxamer 188 solution (outer aqueous phase) was added into the primary emulsion and was further ultrasonicated for 1 minute at 20 W, forming a W/O/W double emulsion. The double emulsion was diluted to 10 ml with 1 % Poloxamer 188 solution. Finally, the solvent was evaporated and nanoparticles were isolated and stored until characterisation.

3.3.2 Particle size analysis

The average diameter (z-average) and polydispersity index (PdI) of SLNs were measured using Zetasizer Nano-ZS (Malvern Instruments Ltd., U.K.), which was equipped with a 4 mW He-Ne laser (633 nm). The measurements were performed at 25 °C at a measurement angle of 173°. Freshly prepared samples were diluted with purified water at a dilution factor that was optimised, prior to loading into a clear disposable zeta cell (DTS 1060C). Each sample was analysed in triplicates at 10 subruns of 10 seconds each. Each z-average value reflects the intensity mean diameter, whilst the polydispersity index (PdI) indicates the particle size distribution of the SLNs.

3.3.3 Determination of Zeta potential

The same sample as described in Section 3.3.2 was also subjected to zeta potential determination using Zetasizer Nano-ZS® (Malvern Instruments Ltd., U.K.). Each measurement was carried out at 25 °C in triplicates and the zeta potential values were calculated based on Smoluchowski equations (Eq. 3.2) using Malvern Zetasizer Software 6.01®, as determined by the electrophoretic mobility of the samples.

3.3.4 Differential scanning calorimetry (DSC) analyses

DSC analyses were performed using a Mettler Toledo Differential Scanning Calorimeter 823E. The change in enthalpy (ΔH) of the endothermic peak was integrated with the built-in STARe software Version 9.01®. The melting endotherms were used to assess the entropies at melt for the nanoparticles, which were calculated using Equation 3.3. Approximately 5 mg of lipid nanoparticle samples were placed on standard aluminium pans, covered and then hermetically sealed. The sample was scanned at a heating rate of 5 °C/minute from 25 °C to 100 °C. Analysis was performed in triplicates under a nitrogen purge. An empty sealed pan was used as a reference pan.

3.3.5 Determination of encapsulation efficiency

The encapsulation of insulin within the SLNs was estimated by dissolving 5 mg of freeze-dried insulin-SLNs samples in 1 ml of 0.1 % TFA and 0.5 ml methanol (MeOH) in 2 ml microcentrifuge tubes. The sample was vortex-mixed for 1 minute. The supernatant was separated from the precipitate by centrifugation (Microfuge® 16, Beckman-Coulter Inc., U.S.A.) at a speed of 14800 rpm for 15

minutes to precipitate the lipids. The supernatant was then decanted and filtered through 0.2 µm regenerated cellulose (RC) membrane syringe filters. Thereafter, the filtered sample was analysed for insulin content within the SLNs using the validated HPLC method as described in Section 2.4.2. Analyses were performed in triplicates and the percentage encapsulation efficiency (%EE) of the insulin-SLNs was calculated as follows:-

$$\%\ \text{Encapsulation Efficiency} = \frac{\text{Amount of insulin in precipitate}}{\text{Total insulin added}} \times 100\% \quad \text{(Eq. 3.4)}$$

3.3.6 Polarised light microscopy (PLM) analysis

For the test of sample homogeneity, a drop of SLNs was placed on a clean glass slide and air-dried prior to viewing under an Olympus CX 31-P Student Polarised Light Microscope (PLM) at a magnification of 100x.

3.3.7 Field emission - Scanning electron microscopy (FE-SEM)

The size and morphology of insulin-containing and insulin-free SLNs were ascertained using a FE-SEM (Supra 55VP Gemini, Zeiss, Germany) at an accelerating voltage of 3 kV. Each sample was placed on a carbon tape and was air-dried for 24 hours. Thereafter, the sample was gold-coated using Biorad SC500 sputter coater (U.K.) for 1.5 minutes in argon to impose a conductivity of 30 mA on the sample. Each sample was prepared once on the aluminium stub.

3.3.8 Transmission electron microscopy (TEM)

The internal structure of the SLNs was viewed using a TEM (912AB Energy Filter, LEO). Prior to observation, the samples were negatively stained using 1% phosphotungstic acid (PTA). Thereafter, the fixed samples were placed on Formvar-film copper grids and allowed to air-dry for an hour. Each sample was prepared once on the Formvar-film copper grids.

3.3.9 Statistical analyses

Statistical analyses were performed using GraphPad Prism Software Version 5.02® to determine statistical significance by means of Student's t-test. In all cases, results with *p*-values < 0.05 are considered statistically significant.

3.4 Results & Discussion

3.4.1 Selection of lipid core compositions

The selection of suitable lipid core composites during the initial stages of formulation development is particularly important to identify the most appropriate combination for the most desirable properties of the nanoparticulate formulations.

In this part of the study, nanoparticles were prepared using different compositions of the solid portions of palm oil lipids, namely tripalmitin (triglyceride) and palmitic acid (single-chain fatty acid) as shown in Table 3.1.

Table 3.1 Lipid nanoparticle formulations Fa1 – Fa5 containing varying amounts of tripalmitin and palmitic acid.

Formulation	Lipids (mg)		Lecithin (%w/w of total lipid)	Poloxamer 188 (2 %w/w) (ml)	Poloxamer 188 (1 %w/w) (ml)
	Tripalmitin	Palmitic acid			
Fa1	100	0	50	3.5	to 10
Fa2	75	25	50	3.5	to 10
Fa3	50	50	50	3.5	to 10
Fa4	25	75	50	3.5	to 10
Fa5	0	100	50	3.5	to 10

The unique feature in the chemical structures of tripalmitin and palmitic acid is that the fatty acid chains in both the lipids are identical, ie. contain a C_{16} saturated fatty acid chain (Section 1.8.1).

The influence of lipid composition on physical properties of the SLNs formulations was investigated by employing either tripalmitin (formulation Fa1) or palmitic acid (formulation Fa5) as the sole lipid, or a combination of both at different ratios (formulations Fa2, Fa3 and Fa4).

It has been reported that SLNs based on a single lipid entity may exhibit a limitation to drug loading capacity as a result of possible crystallisation of the lipid into the more stable β-configuration and subsequently, drug expulsion from the SLNs (Westesen *et al.*, 1997). This is annotated in Figure 3.2(a). This limitation has led to the evolution of the so-called nanostructured lipid carriers (NLCs) in an attempt to address this constraint. NLCs, in contrast to SLNs, are produced by controlled association of liquid lipid within the solid lipid domain (Fig. 3.2b). As a result, the solid lipid crystalline network is disrupted, hence minimising drug expulsion and favouring higher drug loading (Müller *et al.*, 2002a, 2002b). A prerequisite for good drug loading is the presence of larger distances between the fatty acid chains of the triglyceride. This can be achieved by using glycerides which are structurally different (Müller *et al.*, 2002a, 2002b) or by incorporating liquid lipids into the solid lipid composites so that as the nanoparticles are formed at solidification, crystallisation is impeded.

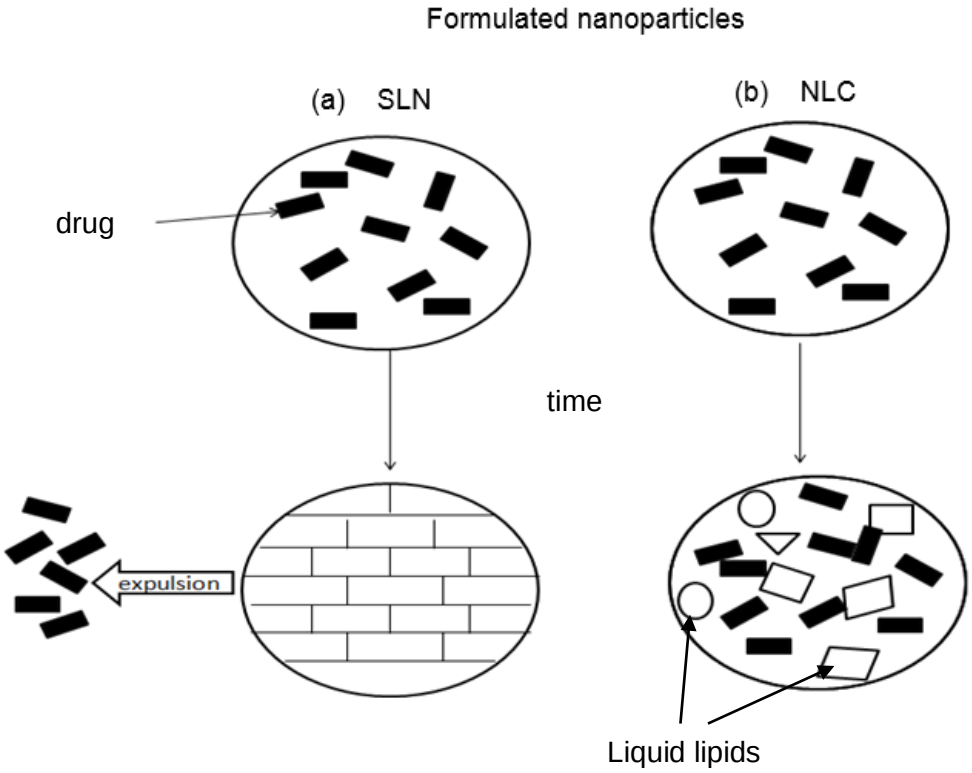

Figure 3.2 Crystallisation process during storage over time in (a) SLNs and (b) NLCs.
[Adapted and modified from (Müller *et al.*, 2002b)]

The ratio of solid lipid compositions were varied, in this instance a triglyceride and a single chain fatty acid, to investigate whether composites of structurally different solid lipids but having identical fatty acid chains (C_{16}), could be utilised in creating mutual disorder in the solidified matrix. Here, the single chain palmitic acid will act as a substitute to the liquid lipid, which is the case in NLCs.

We theorised that the association between both these lipids would be weak and, if any, could arise only between the polar moieties of both lipids. Triglycerides, are polar, and therefore can participate in hydrogen bonding with the carboxylic

group of the fatty acids. Such interactions would leave more room between the fatty acid chains (C_{16}), which could potentially manifest more disorder and hence favour drug loading.

A possible model of association between the lipids which generates spatial freedom between the chains is shown in Figure 3.3.

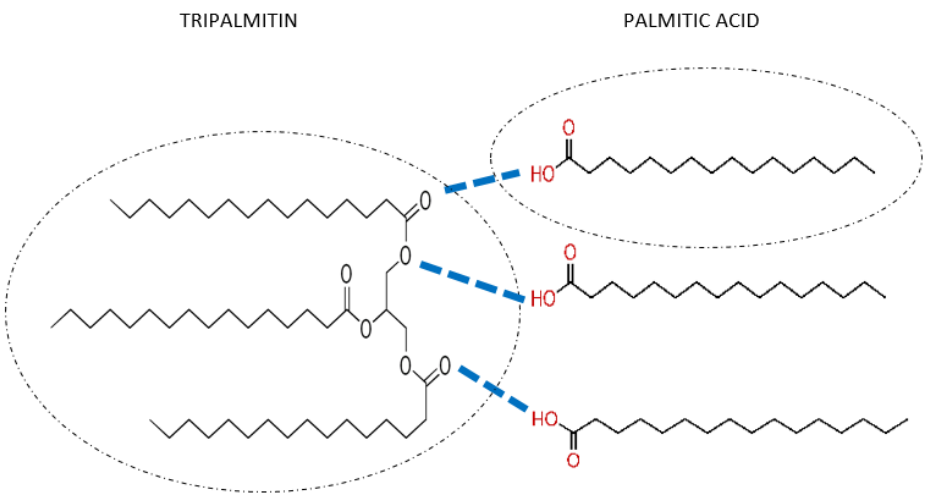

Figure 3.3 A possible model of association between tripalmitin and palmitic acid chain.
(blue dotted line represent possible weak dynamic interactions)

3.4.1.1 Particle size and zeta potential

The intensities of size distribution of these SLNs formulations (Fa1 – Fa5) are shown in Figure 3.4. It is important to note that the scale on the abscissa-axis is not linear, hence as the particle size increases, the sample polydispersity seemed less apparent in the size distribution profile. As shown in Figure 3.4, the use of tripalmitin as the sole lipid (Fa1) produced a smaller-sized particle population with lower PdI values. Conversely, when the sole lipid was palmitic acid (Fa5), the z-average was significantly higher than Fa1 and also a slightly higher PdI value was obtained. A similar trend was also observed when the two lipids were used in combination, in which increasing palmitic acid content from Fa2 through to Fa4 led to a shift in z-average values to the right indicating an increase in mean particle diameters and relatively polydispersed samples as opposed to formulation Fa1 containing solely tripalmitin.

Table 3.2 shows the recorded z-average, PdI values and zeta potentials for formulations Fa1 to Fa5 (insulin-free SLNs). The data is presented graphically in Figure 3.5 which indicates that as the ratio of palmitic acid to tripalmitin was increased (Fa2 – Fa4), the z-average particle size also increased significantly ($p<0.05$). It is also observed that inclusion of palmitic acid in these formulations (Fa2 – Fa4) produced more polydispersed samples, as seen from the larger PdI values, in contrast to that from formulation Fa1($p<0.05$). For the same formulations (Fa2 – Fa4), however, there was a reduction in PdI for formulation Fa4, though it was still more polydispersed than formulation Fa1 containing solely tripalmitin. Zeta potentials recorded for all formulations investigated (Fa1 – Fa5) followed a trend similar to that of z-average (Table 3.2), where the inclusion of palmitic acid in these formulations (Fa2 – Fa5) led to an increase in the magnitude of zeta potentials.

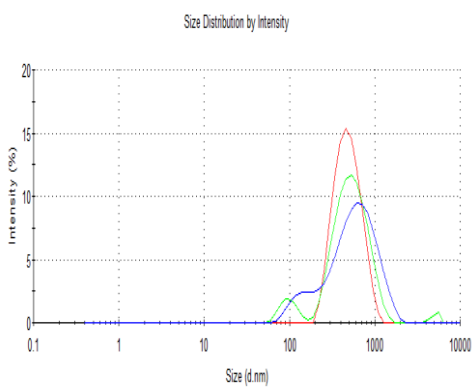

Fa1

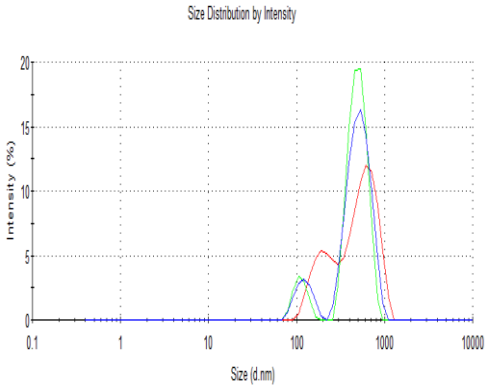

Fa2

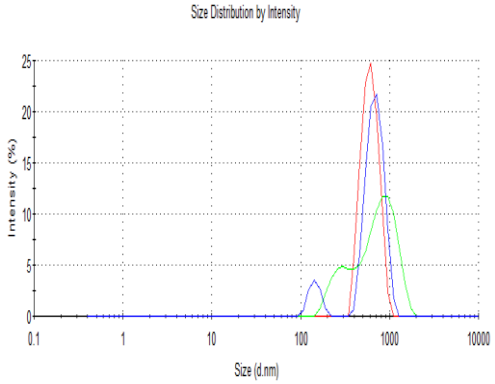

Fa3

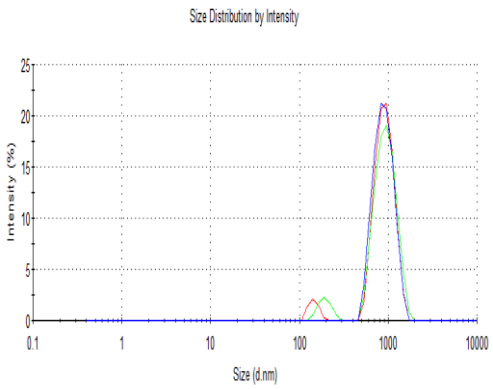

Fa4

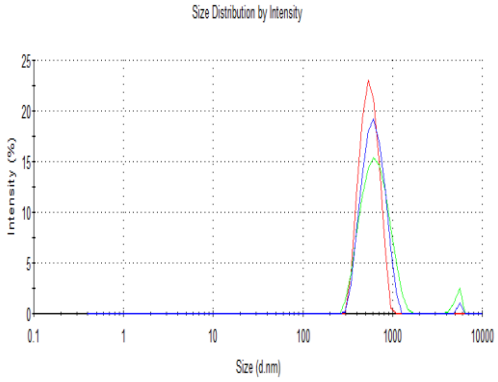

Fa5

Figure 3.4 Size distribution profiles (*n*=3) of SLNs formulations Fa1 – Fa5.

Table 3.2 Z-average(nm), polydispersity index and zeta potential (mV) for formulations Fa1 – Fa5 (insulin-free SLNs) (*n=3*).

Formulation	**Z-average (nm)** [mean ± SD]	**PdI** [mean ± SD]	**Zeta potential (mV)** [mean ± SD]
Fa1	293.3 ± 5.2	0.30 ± 0.03	-39.9 ± 1.3
Fa2	610.4 ± 7.1	0.62 ± 0.06	-39.6 ± 1.7
Fa3	847.0 ± 7.5	0.66 ± 0.07	-40.0 ± 1.2
Fa4	1028.7 ± 7.8	0.46 ± 0.05	-44.0 ± 1.3
Fa5	699.0 ± 6.5	0.33 ± 0.03	-50.6 ± 1.6

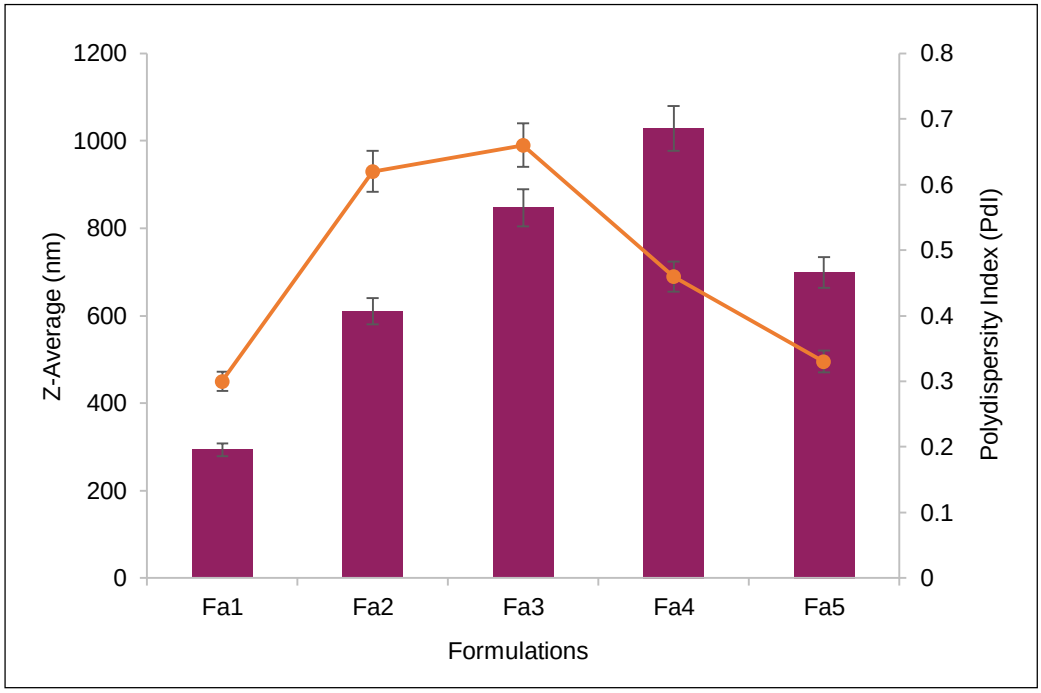

Figure 3.5 Z-average (bars) and PdI values (line) for SLNs formulations (Fa1 – Fa5) (*n=3*).

Studies have previously indicated that the physicochemical properties of SLNs are largely affected by the lipid nature and composition (Mehnert and Mäder, 2001). The fatty acids (tetradecanoic acid (C_{14}), palmitic acid (C_{16}) and stearic acid (C_{18})), with different lengths of carbon chains, influenced the physicochemical properties of SLNs, where stearic acid-SLNs registered a larger particle size, PdI value and higher zeta potential as compared to the other two fatty acids (Xie *et al.*, 2011a).

We have shown that using structurally different lipids, namely tripalmitin (triglyceride) and palmitic acid (fatty acid), influenced the particle size diameters and PdI values of the SLNs (Fig. 3.5). Formulation Fa1, which contained 100 mg tripalmitin, registered a z-average and PdI value of 293.3 ± 5.2 nm and 0.30 ± 0.03 respectively (Table 3.2), both being the lowest amongst the formulations studied. As mentioned above, increasing the ratio of palmitic acid led to a significantly higher z-average (p<0.05). This trend was not surprising as it was observed in Fa5 that when palmitic acid was used as the sole lipid core, the particles registered a significantly higher z-average (699.0 ± 6.5 nm) when compared to tripalmitin as the sole lipid core (Fa1) (p<0.05) (Table 3.2). The PdI values between Fa1 (0.30 ± 0.03) and Fa5 (0.33 ± 0.03) were found to be not statistically significant (p>0.05), where the low PdI values indicate good sample homogeneity for both these formulations. For the structurally different tristearin-SLNs and stearic acid-SLNs, different z-average values were also reported for both these SLNs, with the former being slightly larger (Paliwal *et al.*, 2009).

The inclusion of palmitic acid in the formulations (Fa2 – Fa5) produced larger-sized particles and more polydispersed samples. This interesting observation has not been reported elsewhere in the literature, though the use of palmitic

acid as the lipid matrix in itraconazole-loaded SLNs resulted in the production of nanoparticles with a wide particle size distribution, demonstrated by a high PdI value of more than 0.6 (Mukherjee *et al.*, 2009a). There seems to be a synergistic effect when these two structurally different lipids (tripalmitin and palmitic acid) are present as it was observed that the z-average values increased significantly beyond the values obtained when palmitic acid was the sole lipid, from Fa2 through Fa4 (p<0.05) (Fig. 3.5). Therefore, this increase can be attributed mostly to the presence of palmitic acid. A possible explanation is that palmitic acid chain is able to form weak dynamic interactions via hydrogen bonding with tripalmitin as postulated in Figure 3.3. Thus, this generates more spatial freedom in the lipid matrix and consequently higher z-average will be obtained for these formulations (Fa2 – Fa4). As such, the increase seen was closely related to the amount of palmitic acid incorporated into the formulations (Table 3.2). The PdI values for these formulations (Fa2 – Fa4) were all significantly higher than the formulations containing sole lipids (Fa1 and Fa5) (p<0.05), although no significant differences were noted between the values for Fa2 and Fa3. This indicates that the co-presence of two structurally different lipids resulted in the production of nanoparticles with a wider particle size distribution, due to a possible explanation similar to that of the z-average as discussed.

The zeta potentials for all formulations investigated indicate that they are within the acceptable range for electrostatic stability (Table 3.2). It is currently accepted that zeta potentials above |30 mV| are needed for full electrostatic stabilisation, thus particle aggregation is rather unlikely to occur due to electric repulsion caused by the surface charges (Heurtault *et al.*, 2003).

Based on Table 3.2, there were no significant differences observed between the zeta potential values for formulations Fa1, Fa2 and Fa3 (p>0.05), which indicates that varying the tripalmitin content from 50 % to 100 % of the formulation had not significantly impacted the zeta potentials of these formulations. However, the zeta potential of formulation Fa5 containing solely palmitic acid was -50.6 ± 1.6 mV, being significantly higher than the value (-39.9 ± 1.3 mV) recorded for formulation Fa1 (p<0.05). The negative value of zeta potential is due to the presence of a carboxyl group –COOH at one end of the single chain palmitic acid, which is capable of forming a negatively charged carboxylate ion (COO^-) when deprotonated. These values are also in concert with those reported for stearic acid-SLNs and tristearin-SLNs, where stearic acid-SLNs recorded a more negative value of zeta potential attributable to the highly negative charge distributed at the surface of the fatty acid SLNs (Paliwal *et al.*, 2009).

Similarly to the increase in z-average due to palmitic acid content, there was an increase in zeta potential values for formulations Fa2 through to Fa4 (Table 3.2). Though an increasing trend, the zeta potential values for Fa2 (-39.6 ± 1.7 mV), Fa3 (-40.0 ± 1.2 mV) and Fa4 (-44.0 ± 1.3 mV) were all significantly lower than that of formulation Fa5 (-50.6 ± 1.6 mV), which consists of solely palmitic acid (p<0.05). This indicates that the zeta potential of the nanoparticles can be significantly affected when palmitic acid was used in combination with tripalmitin. It is also interesting to note that the presence of tripalmitin, however, tended to counterbalance the negative charge effects due to palmitic acid (Fa2 – Fa4). This is likely to be due to the interaction between the two types of lipids at the carboxylic acid moieties which are capable of participating in hydrogen bonding (Fig. 3.3).

Table 3.3 Z-average(nm), polydispersity index and zeta potential (mV) for formulations Fa1-ins to Fa5-ins (insulin-loaded SLNs) (*n=3*).

Formulation	**Z-average (nm)** [mean ± SD]	**PdI** [mean ± SD]	**Zeta potential (mV)** [mean ± SD]
Fa1-ins	185.0 ± 6.8	0.21 ± 0.04	-36.9 ± 1.3
Fa2-ins	345.4 ± 7.2	0.59 ± 0.03	-40.4 ± 1.4
Fa3-ins	440.4 ± 9.8	0.54 ± 0.05	-43.7 ± 1.5
Fa4-ins	559.1 ± 8.5	0.50 ± 0.08	-47.5 ± 1.5
Fa5-ins	658.8 ± 8.7	0.41 ± 0.05	-45.8 ± 1.7

Insulin-loaded SLNs formulations were prepared as described previously, labelled as Fa1-ins to Fa5-ins. Table 3.3 shows the z-average, PdI and zeta potential values recorded for these insulin-loaded nanoparticles. Interestingly, with insulin incorporated into the nanoparticles, it was observed that the particle size recorded for all the 5 formulations were generally smaller than their corresponding insulin-free SLNs counterparts. The difference in z-average between the insulin-free SLNs and insulin-SLNs counterparts were statistically significant for all formulations ($p<0.05$). This suggests that incorporation of insulin into the formulations led to the production of nanoparticles which were more compact in size as opposed to without insulin. A similar trend was also observed here for insulin-loaded SLNs, where an increase in z-average values was noted when the palmitic acid content was high. This corresponds to the findings obtained from the insulin-free SLNs, which further ascertain that the particle size increase was solely attributed to the presence of palmitic acid.

SLNs can form an architectural arrangement where a polar core with the polar heads of the triglycerides are oriented towards the aqueous phase, much like chylomicrons. This chylomicron-like behaviour can be potentially achieved for SLNs with particle sizes that are similar (Paliwal *et al.*, 2009). Therefore, insulin incorporated into such SLNs can potentially associate with the polar region of the lipid nanoparticles. The size decrease observed for all insulin-SLNs versus the insulin-free counterparts can be attributed to the insulin being held closely to the polar regions of the nanoparticles, where positively charged insulin interacts with the negatively charged SLNs resulting in a more compact, and hence smaller particle sizes. Insulin has an isoelectric point of 5.3 (Park, 1999). Having been dissolved in an acidic environment (~ pH 2), insulin therefore carries a net positive charge.

In terms of particle size distribution, the PdI values did not exhibit any statistical significance between the respective counterparts of insulin-free SLNs and insulin-loaded SLNs for all formulations studied ($p>0.05$). This suggests that incorporation of insulin into the SLNs did not affect the sample homogeneity of the formulations. Instead, the differences seen in PdI values between each formulation were predominantly influenced by the lipids used to prepare the SLNs.

The insulin-loaded formulations (Fa1-ins and Fa5-ins), which consists of sole lipid in the formulation, registered significantly lower zeta potentials compared to corresponding insulin-free SLNs formulations ($p<0.05$) (Table 3.3). Incorporation of insulin into the formulation resulted in the decrease in zeta potential possibly due to the modification of the surface charge by the positively charged insulin. However, the zeta potential values for formulations with combination of lipids (Fa2-ins, Fa3-ins and Fa4-ins) were generally higher than

their insulin-free SLNs counterparts. The increase in the zeta potential values were significantly higher for Fa3-ins vs Fa3 and Fa4-ins vs Fa4 (p<0.05), although there was no significant difference in the values recorded for formulation Fa2-ins vs Fa2 (p>0.05). This increase is possibly attributable to the spatial freedom generated between the hydrophobic chains, as proposed in Figure 3.3, where insulin is able to fit into the spaces between, and as a result the surface charges of these formulations (Fa2-ins, Fa3-ins and Fa4-ins) were not counterbalanced by the incorporation of insulin into the formulation.

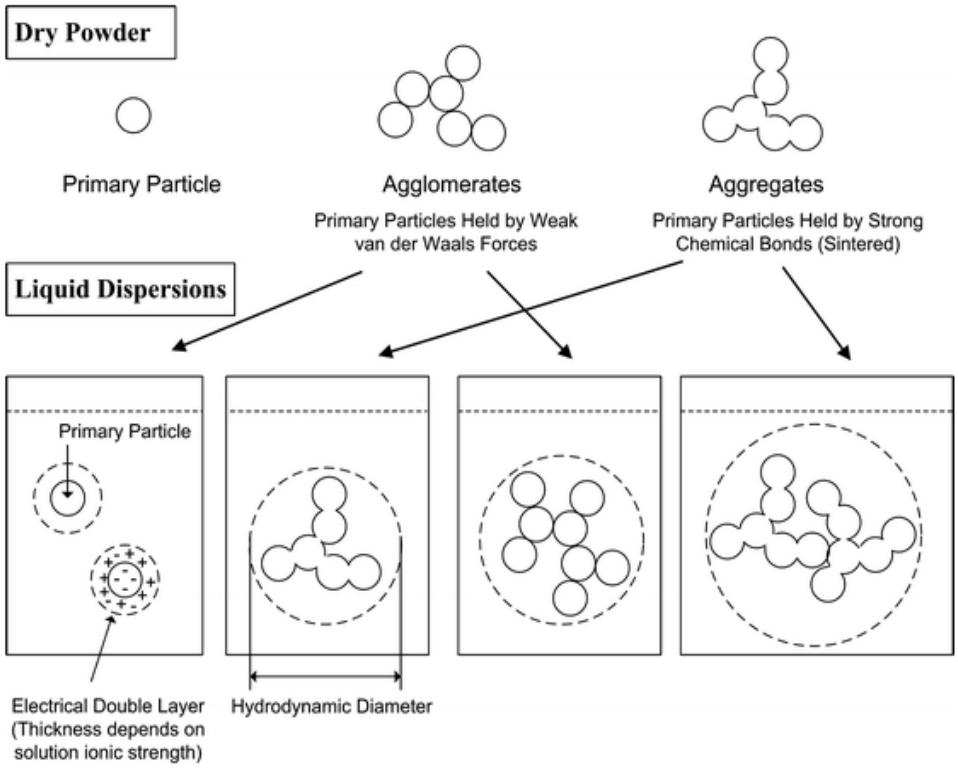

Figure 3.6 Various states and configurations of nanoparticles in dry state and when dispersed in liquids.
[Adapted and modified from (Jiang *et al.*, 2008)]

In terms of physical stability, all these prepared SLNs formulations may be deemed to be stable and free from particle aggregation based on the zeta potential measurements. However, the zeta potential of nanoparticle dispersions depends on other factors such as the ionic strength and the solution pH both of which can influence the stability and agglomeration behaviour of the nanoparticles (Jiang *et al.*, 2008). The surface characteristics can affect the particles ability to agglomerate or aggregate as illustrated in Figure 3.6 (Jiang *et al.*, 2008), which can in turn influence the uptake and translocation of nanoparticles by the cells (Hoshino *et al.*, 2004). It has also been shown that by using unstable and agglomerated nanoparticle dispersions in an *in vitro* and *in vivo* experiment could lead to significant implications in the assessment of nanoparticle toxicity (Warheit *et al.*, 2004). Therefore, it is crucial to address the issue of particle agglomeration or aggregation during the SLNs formulation stage.

Visual observation of the SLNs formulations is vital in investigating the physical stability of formulations by means of agglomerates or aggregates formation during storage. The images of formulations (Fa1 – Fa5) are illustrated in Figure 3.7. Seven days after production, Fa1 (Fig. 3.7(a)) appeared homogenous and did not exhibit any aggregated particles and the consistency remained the same for 45 days.

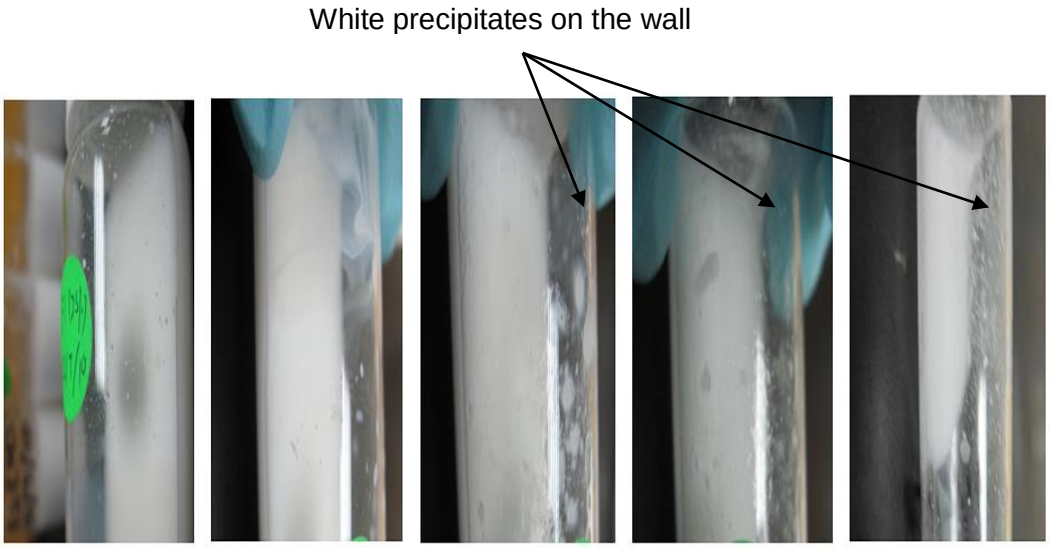

Figure 3.7 Visual observation of formulations Fa1 – Fa5 (insulin-free SLNs) on day 7 of production.
[(a) = Fa1; (b) = Fa2; (c) = Fa3; (d) = Fa4; (e) = Fa5]

Conversely, for Fa5, large aggregates were formed at the time of production which correlated with the high PdI and z-average values (Table 3.2). Furthermore, within 7 days of storage, white precipitates were seen on the walls of the vial which could not be redispersed upon vigorous shaking or sonication in water bath (Fig. 3.7(b)). This demonstrates physical instability despite zeta potential value of -50.6 ± 1.6 mV, which indicated good electrostatic stability. In addition, formulations Fa2, Fa3 and Fa4 which comprised of increasing amounts of palmitic acid respectively, also showed signs of physical instability during storage at ambient temperature for 7 days, where sediments and large aggregated particles were formed (Fig. 3.7 (b), (c) and (d) respectively). These aggregates also did not redisperse on shaking or bath sonication.

Therefore, contributing factors other than electrostatic stability clearly have a role in the tendency of the SLNs to agglomerate or aggregate. The stability of

nanosuspensions strongly depend on the thermodynamics of the dispersed system which can be termed as metastable and therefore has the tendency to coalesce eventually in order to reduce the excess surface free energy (Kipp, 2004). Instability of nanosuspensions may be due to a shift in particle size distribution from smaller to larger sizes (Ostwald ripening), irreversible agglomeration or aggregation (Kipp, 2004). In the event where interparticle repulsive forces due to electrostatic barriers cannot overcome the inertia of particle collision, formation of heavy aggregates will result in rapid sedimentation (Kipp, 2004).

Figure 3.8 shows the images of the insulin-loaded SLNs formulations (Fa1-ins to Fa5-ins) after 7 days of storage. In this study, Fa1-ins seemed to be the formulation which exhibited considerable physical stability.

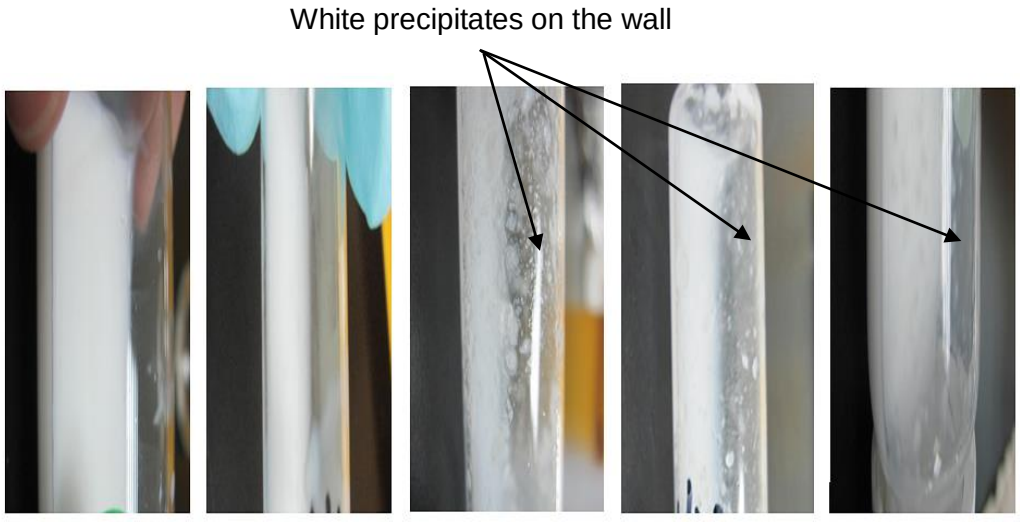

Figure 3.8 Visual observation of formulations Fa1-ins – Fa5-ins (insulin-loaded SLNs) on day 7 of production.
[(a) = Fa1-ins; (b) = Fa2-ins; (c) = Fa3-ins; (d) = Fa4-ins; (e) = Fa5-ins]

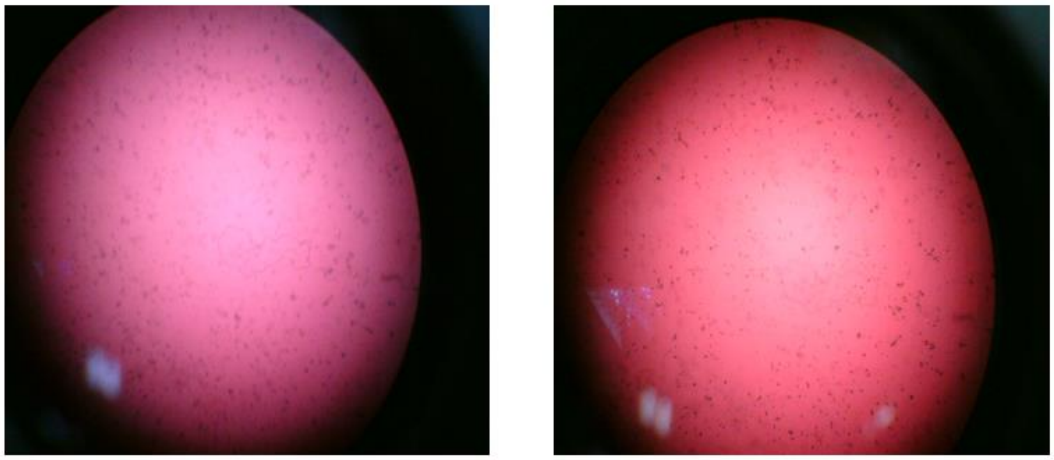

Figure 3.9 Polarised light microscopy analysis of SLNs formulation Fa1 (left) and Fa1-ins (right) viewed at 100x magnification.

Formulation Fa1 (insulin-free SLNs) and Fa1-ins (insulin-loaded SLNs) when viewed under polarised light microscopy, demonstrated a relatively homogenous matrix, with no phase separation observed (Fig. 3.9). No obvious particle aggregation was detected in both insulin-free and insulin-loaded SLNs formulations containing solely tripalmitin (Fig. 3.9).

3.4.1.2 Influence of sample dilution factor

The nanoparticle dispersions prepared according to the method described above appeared milky-white and were concentrated. In order to perform particle size analysis on the Zetasizer Nano-ZS® (Malvern Instruments Ltd., UK), the sample had to be diluted to allow the laser beam to penetrate the dispersion.

Therefore, an optimal sample dilution factor was sought, in order to standardise the dilution for all samples prior to measuring the z-average, polydispersity index and zeta potential of subsequent formulations. Formulation Fa1 containing 50 mg (0.5 %w/w) lecithin, used as the model formulation, was diluted with deionised water by various dilution factors, ie. 0.1, 0.04, 0.02, 0.0125 and 0.01.

Figure 3.10 shows the z-average and PdI of formulation Fa1 at the respective dilution factors. It can be seen that the diluted and undiluted samples gave contrasting z-average and the polydispersity index of the formulation. Undiluted formulations registered a higher z-average value since the nanoparticles in the lipid dispersion were very much crowded and have the tendency to agglomerate. Similarly, the PdI indicated that the sample had low homogeneity due to the close proximity of the individual nanoparticles.

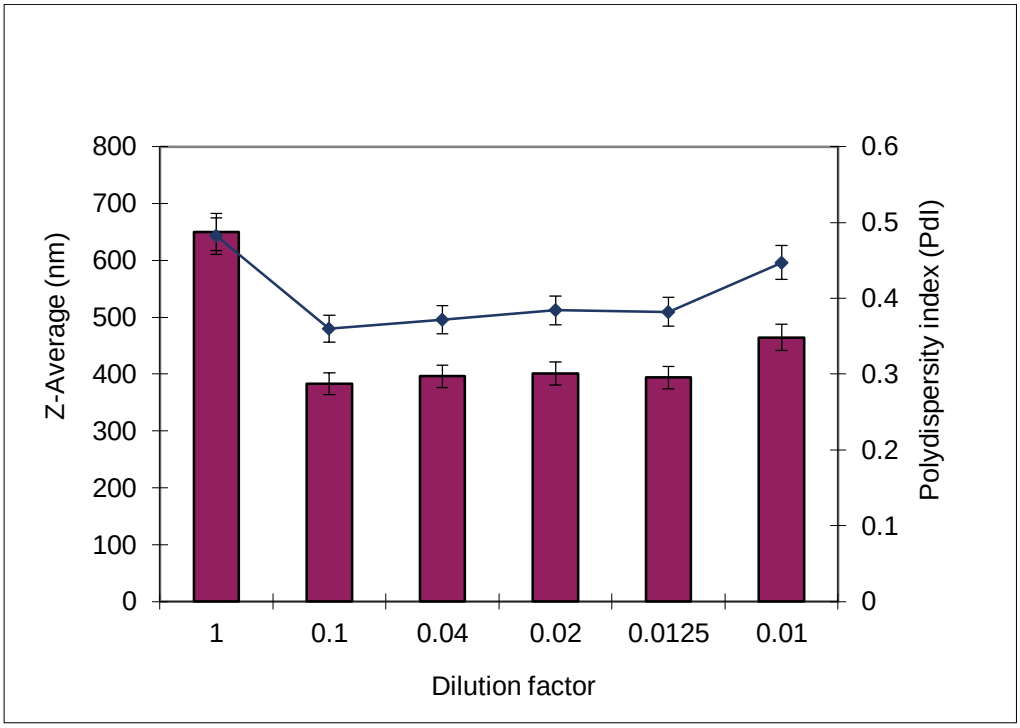

Figure 3.10 Z-average (bars) and polydispersity index (line) of formulation Fa1 at various dilution factors 0.01 - 1 of the lipid dispersion.

Conversely, samples being diluted registered significantly lower z-average and PdI values (Fig. 3.10). Furthermore, the results of the z-average and PdI were more consistent for diluted samples in contrast to the more concentrated ones as seen in Figure 3.10. Diluted samples appeared as pale white and translucent in contrast to undiluted samples that appeared milky-white (Fig. 3.11).

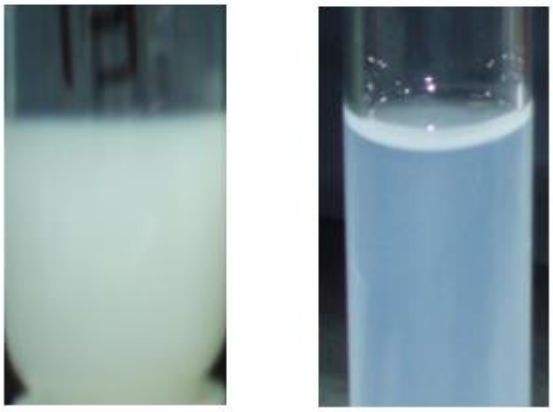

(a) (b)

Figure 3.11 Appearance of an (a) undiluted and (b) diluted of formulation Fa1.

No significant differences in the z-average particle size was observed between dilution factors of 0.1 to 0.0125 (p>0.05). Therefore, a dilution of 1 in 10 (factor of 0.1) was considered optimal and was used for subsequent sample dilutions in the PCS analysis. However, at excessively high dilution factor (0.01), a slight rise in z-average and PdI was observed, possibly due to the concentration of the stabiliser added to the formulation being excessively diluted. A stabiliser is added to the formulation in order to stabilise the emulsion formed during nanoparticle production. Since it adsorbs at the boundary layer between the water phase and the organic phase during particle formation (Cassidy *et al.*, 1999), a change in the stabiliser concentration may cause an increase in the particle size (Vandervoort and Ludwig, 2002). In this instance, at high dilution factor, the solubilisation phenomenon of poloxamers included in the formulation was disrupted which promoted the separation of the stabiliser into the continuous phase and leading to a less stable nanosuspension with larger particle size and PdI (Binks, 2002).

3.4.1.3 Influence of lipid compositions on thermal behaviour

Differential scanning calorimetry is a useful analytical tool used to evaluate the physical state of materials. It has been used to study the physicochemical properties and thermodynamic stability of SLNs dispersions (Souto and Müller, 2006). In the present study, we aimed to investigate whether composites of structurally different solid lipids, ie. tripalmitin and palmitic acid, could be utilised to create mutual disorder within the solidified matrix by way of evaluating the changes in entropy of fusion of the system. Entropy of fusion (ΔS_{fusion}) was calculated according to the Second Law of Thermodynamics as described in Equation 3.3 (Folmer and Franzen, 2003). The magnitude of ΔS_{fusion} gives an indication of the disruptive index, being higher for more orderly structures (York and Grant, 1985). Conversely, a lower disruptive index represents a more disordered structure.

Figure 3.12 displays the typical DSC thermograms, indicating the melting endothermic peaks, as measured for these formulations. Individual DSC thermograms for bulk tripalmitin and insulin-free tripalmitin SLNs (formulation Fa1) are shown in Figure 3.13. Melting events were observed in all formulations, confirming the crystalline attributes of these formulations. A single distinctive endothermic peak for bulk tripalmitin recorded at 63.6 °C seen in Figure 3.13(a) indicates the tripalmitin melting peaks observed in both insulin-free formulation Fa1 (Fig. 3.13(b)) and insulin-containing formulation Fa1-ins (Fig. 3.12). The melting temperatures palmitic acid were recorded as 58.5 °C (Fig. 3.12). These values are in good agreement with previous studies on: tripalmitin (65.53 °C) (Garcia-Fuentes *et al.*, 2005a) and palmitic acid (64.5 °C) (Cedeno *et al.*, 2001).

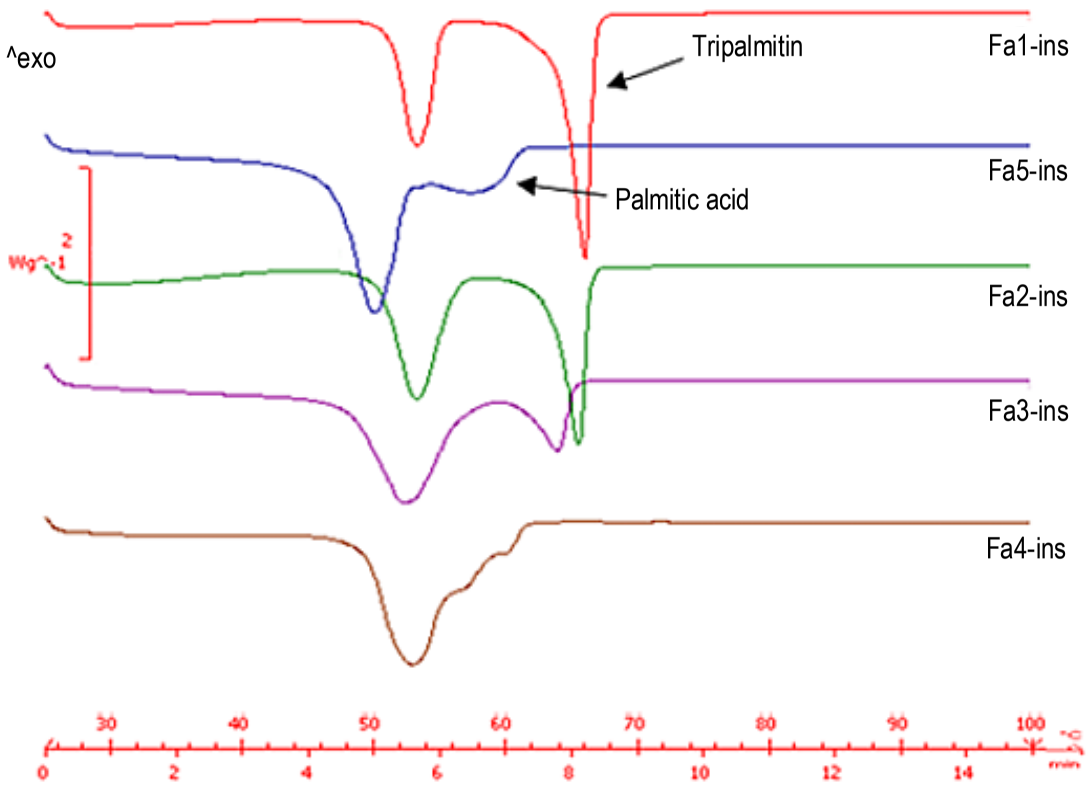

Figure 3.12 DSC thermograms for SLNs formulations Fa1-ins through to Fa5-ins (*n=3*).

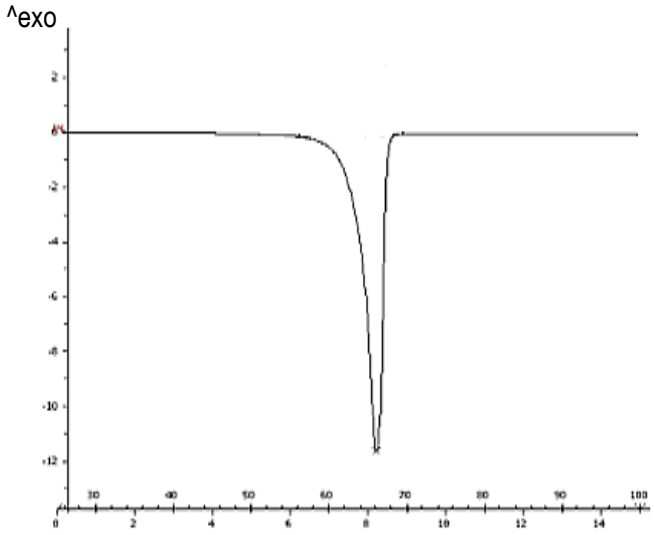

(a) bulk tripalmitin

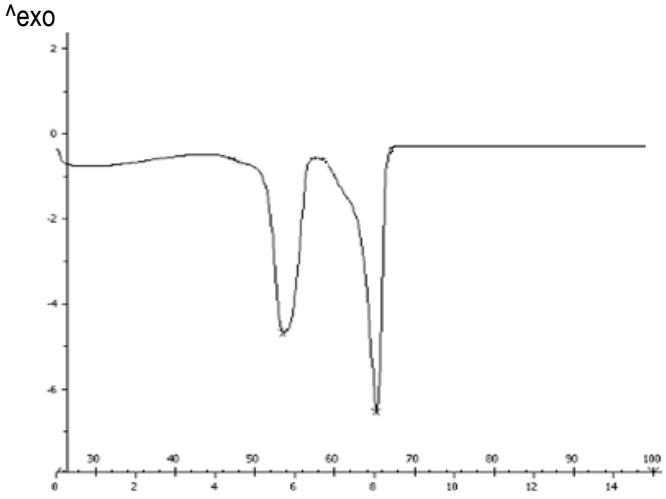

(b) formulation Fa1

Figure 3.13 DSC thermograms for (a) bulk tripalmitin and (b) formulation Fa1

Accordingly, there was another melting endotherm observed in all insulin-containing formulations at approximately 50-52 °C (Fig. 3.12), which was also present in insulin-free formulation Fa1 (Fig. 3.13(b)). This peak can be attributed to the melting temperature of the excipient Poloxamer 188 which corresponds with that previously reported in the literature at 50.9 °C (Passerini *et al.*, 2002).

Interestingly, with reduced tripalmitin content, the intensity of the melting peak described above decreased in Fa2-ins and was almost completely absent in Fa4-ins (Fig. 3.12). There was also a reduction in melting temperatures for lipid formulations Fa2-ins to Fa4-ins, with decreased tripalmitin content. Tripalmitin has a slightly higher melting point compared to the single-chained palmitic acid and therefore, the reduction in melting temperatures and peak intensity observed in Fa2-ins to Fa4-ins is due to the decline in tripalmitin content. This could be attributed to the composite of lipids used which led to the formation of imperfect crystals. Mixtures of mono-, di- and triglycerides and also fatty acids of different chain length have been reported to form less perfect crystal structure with many imperfections when used in combination (Müller *et al.*, 2000). Furthermore, the lipid mixtures are potentially associated via weak dynamic interactions between tripalmitin and palmitic acid chains, as suggested in Figure 3.3. As a result of the spatial freedom having been formed into a less densely packed structure, reduced melting point is manifested (Israelachvili, 2011). In addition, these intermolecular forces of attraction are relatively weak and do not pose structural constraints during heating and therefore will naturally contribute to a decrease in the melting point of these formulations.

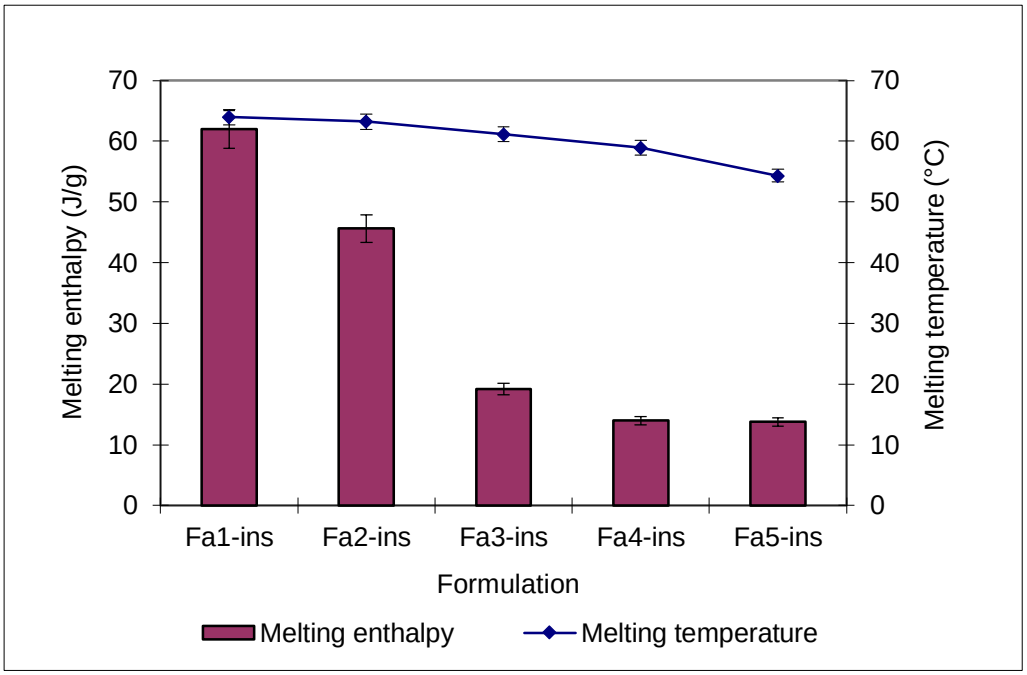

Figure 3.14 Melting enthalpy (endothermic) and melting temperature for SLNs formulations.

Figure 3.14 shows the enthalpy of fusion (endothermic) and temperature at melt for the insulin containing SLNs formulations. Formulation Fa1-ins (sole tripalmitin) recorded the highest melting enthalpy (62.0 ± 2.2 J/g) and melting temperature (64.0 ± 2.9 °C) amongst the formulations studied. In contrary, the melting enthalpy for Fa5-ins containing palmitic acid was the lowest recorded (13.8 ± 0.9 J/g), and likewise for the melting temperature (54.3 ± 2.5 °C). When both lipids are present at different ratio within the formulations, a significant decrease in melting enthalpy (p<0.05) was observed with increasing palmitic acid content (Fa2-ins to Fa4-ins). The melting temperatures for the same series of formulations (Fa2-ins to Fa4-ins) showed no significant differences (p>0.05), despite a shift of T_m towards lower temperatures when palmitic acid content is increased. The decreasing trend seen in the melting temperatures was clearly

noted in formulation Fa5-ins, containing solely palmitic acid in the absence of tripalmitin within the formulation. This clearly indicates that the inclusion of another structurally different solid lipid into the formulation can influence the melting enthalpy and temperature of the lipid nanoparticles, as a result of changes in the structural packing, as explained earlier.

Table 3.4 Change in entropy of the respective insulin-SLNs formulations (*n=3*).

Formulation	**ΔS_{fusion} ($-Jg^{-1}{}^{o}C^{-1}$)** [mean ± SD]
Fa1-ins	0.97 ± 0.04
Fa2-ins	0.72 ± 0.05
Fa3-ins	0.31 ± 0.04
Fa4-ins	0.24 ± 0.02
Fa5-ins	0.25 ± 0.03

Based on the above findings shown in Table 3.4, as palmitic acid content is increased, the ΔS_{fusion} decreases, in the direction of a less ordered structure. The inclusion of palmitic acid into the tripalmitin lipid nanoparticles (Fa1-ins) significantly reduced the entropies of formulations Fa2-ins to Fa4-ins ($p<0.05$), which suggests that palmitic acid interrupts the structural orderliness within the particles of Fa1-ins. Conversely, ΔS_{fusion} increases with the increase in tripalmitin which indicates a less disrupted or a more crystalline structure. This further shows that the type of lipids used, whether alone or in combination, has

a direct influence on the disorderliness of the packing structures of the nanoparticles.

Comparing the entropies between the insulin-free SLNs and insulin-SLNs, the ΔS_{fusion} for Fa1 (insulin-free SLNs) and Fa1-ins (insulin-SLNs) were found to be -0.77 ± 0.02 $Jg^{-1}°C^{-1}$ and -0.97 ± 0.04 $Jg^{-1}°C^{-1}$ respectively. This indicates that the incorporation of insulin into tripalmitin lipid nanoparticles does make the SLNs more crystalline. Fa1 (insulin-free SLNs) which is composed of tripalmitin as sole lipid matrix instead exhibited a less orderly and more amorphous nature, in comparison to Fa1-ins (insulin-SLNs). However, this was not the case for palmitic acid nanoparticles, where ΔS_{fusion} for both Fa5 and Fa5-ins were found to be similar, 0.25 ± 0.02 $Jg^{-1}°C^{-1}$ and 0.25 ± 0.03 $Jg^{-1}°C^{-1}$ respectively. Hence, we observed that type of lipids used can also influence the effect insulin has on the entropy changes of the nanoparticles. Fangueiro *et al.* (2013) reported that there was a difference in the melting endotherm for Softisan®100 insulin-free SLNs and insulin-SLNs, with the insulin-free SLNs showing a higher melting endotherm at 14.3 J/g, thus demonstrating that the incorporation of insulin can indeed influence the thermal behaviour of SLNs. In the present study, we recorded a higher melting endotherm for Fa1 (insulin-free SLNs) at 48.47 J/g, as opposed to Softisan®100 insulin-free SLNs reported by Fangueiro *et al.* (2013), where both these formulations were composed of different types of lipids.

Another interesting observation noted was that for all formulations, the decrease in z-average due to increase in tripalmitin content as shown in Table 3.3 were found to be in contrast to the values of ΔS_{fusion} (Table 3.4). SLNs formulation with smaller particle size was found to display a larger ΔS_{fusion}, which indicates a more orderly and closely packed structure within the particles.

Formulation containing solely tripalmitin (Fa1-ins) had the largest ΔS_{fusion} (Table 3.4). This can be explained by the tendency of SLNs composed of a monoacid triglyceride to form highly crystalline structure with a perfect lattice due to its chemical nature (Müller *et al.*, 2000). Therefore, the decrease in ΔS_{fusion} of formulations Fa2-ins to Fa4-ins with the incorporation of palmitic acid into the lipid mixture, further supports the proposed association model (Figure 3.3), where the generation of spatial freedom between the chains of the lipid disrupts the orderliness of the structural arrangement of the lattice.

3.4.1.4 Influence of lipid compositions on encapsulation efficiency

The encapsulation efficiency (%) of insulin within the SLNs formulations are listed in Table 3.5.

Table 3.5 Encapsulation efficiency (%) of respective formulations (*n=3*).

Formulation	**Encapsulation Efficiency (%)** [mean ± SD]
Fa1-ins	38.1 ± 1.2
Fa2-ins	40.6 ± 0.8
Fa3-ins	41.3 ± 1.5
Fa4-ins	34.7 ± 1.3
Fa5-ins	44.7 ± 0.9

The drug encapsulation efficiency does not appear to correlate with the state of disorder of the lipid nanoparticles, based on the data from the ΔS_{fusion} described in section 3.4.1.3. It was previously reported that mixture of chemically diverse lipids showed better drug incorporation capacities owing to the formation of imperfect crystals lattices that offer more space to accommodate the drugs (Müller *et al.*, 2000). We found that encapsulation efficiency of insulin was not necessarily dependent on the state of disorderliness of the crystal lattice within the SLNs. Drug encapsulation efficiency in nanoparticles is also influenced by the lipophilicity of the incorporated drugs (Barichello *et al.*, 1999), production technique (Almeida and Souto, 2007) as well as the temperature condition of the dispersed aqueous phase (F.Q. Hu *et al.*, 2004).

Generally, as shown in Table 3.5, the encapsulation efficiencies derived from the formulations studied were not particularly high, but these are acceptable values in view of the drug being a hydrophilic protein being incorporated into a lipophilic matrix. Barichello *et al.* (1999) achieved an encapsulation efficiency of 7-12 % for insulin-loaded PLGA nanoparticles, which was much lower than that obtained in this study, although it must be noted that the nanoparticles were made from PLGA polymer. The stability and the encapsulation efficiency of the loaded protein/peptide are the key concerns faced in the preparation of micro- and nanoparticulate formulations (Xu and Zhang, 2007). Lower encapsulation efficiency observed is attributable to the hydrophilicity of the proteins, which tends to be expelled out from the hydrophobic nanoparticle (Mundargi *et al.*, 2008). Other studies on encapsulation efficiencies of insulin in SLNs have also been reported to be relatively low with a maximum at approximately 58 % (Xue *et al.*, 2013; Zhang *et al.*, 2009), also attributable to drug expulsion.

3.4.2 Influence of emulsifier (lecithin) content

Soy lecithin in SLNs has been shown to be useful as an emulsifier which ensures the production of stable nanoparticle dispersions (Hatziantoniou *et al.*, 2007; Schubert and Müller-Goymann, 2005). It has been reported in the literature that at least 10 %w/w lecithin is necessary in the lipid matrix, as the colloidal dispersion would not be stable below this lecithin concentration. Lecithin is commonly used as an emulsifier due to its reported safety and tolerability in humans, apart from being able to delay the transitions of lipids from the less stable α-form to the stable β-polymorphs (Bunjes and Koch, 2005; Schubert and Müller-Goymann, 2005). It has been postulated that lecithin tends to form a monolayer core surrounding the triglyceride core of the nanoparticles (Bunjes and Koch, 2005). At optimal lecithin concentrations, lecithin appeared strongly bound to the nanoparticle surface and thus by having limited mobility, particle agglomeration was less likely to occur. On the other hand, excessive lecithin concentration has been found to destabilise SLNs dispersion in terms of agglomeration and particle growth due to possible accumulation of lecithin multilayers on the particles' surface or formation of liposomes within the aqueous phase (Schubert and Müller-Goymann, 2005).

Therefore a series of formulations comprising of varying amounts of lecithin were formulated in order to study the effect of lecithin content (Table 3.6) on the stability of the SLNs. These formulations are subsequently labelled as Fb1 – Fb5. The amount of lecithin in each formulation was varied from 25, 50 and 100 mg.

Table 3.6 Varying amount of lecithin content in formulations Fb1 to Fb5.

Formulation	Lipids (mg)		Surfactant (oily) (mg)
	Tripalmitin	Palmitic acid	Lecithin
Fb1	100	0	25 / 50 / 100
Fb2	75	25	25 / 50 / 100
Fb3	50	50	25 / 50 / 100
Fb4	25	75	25 / 50 / 100
Fb5	0	100	25 / 50 / 100

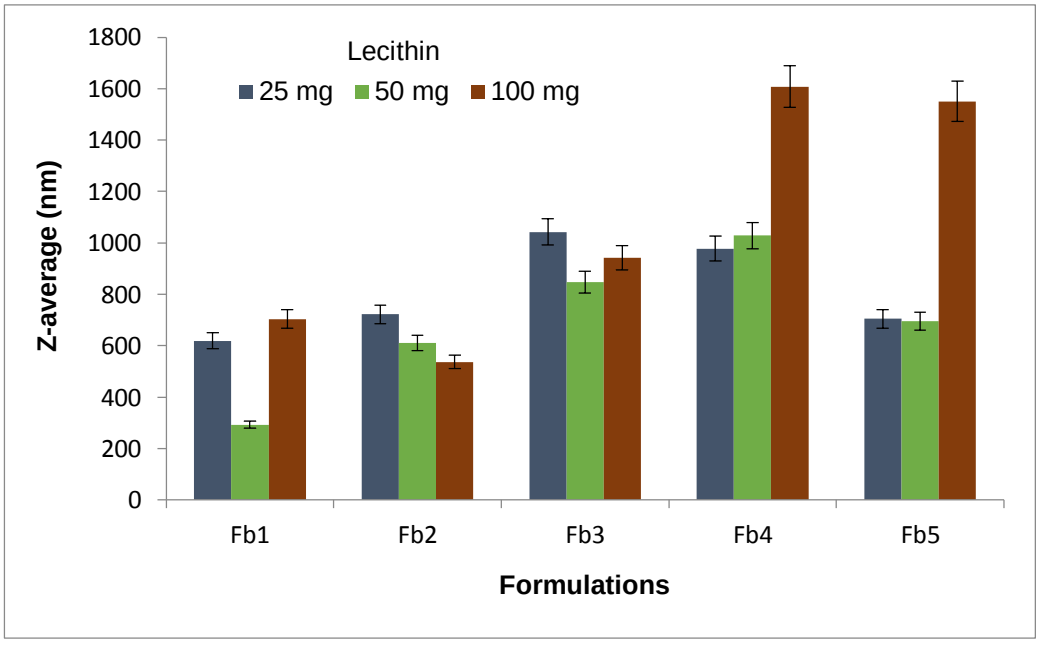

Figure 3.15 Z-average (nm) of the lipid nanoparticles for formulations Fb1 – Fb5 with varying amounts of lecithin (*n=3*).

Figure 3.15 illustrates the z-average values for formulations Fb1 to Fb5 with varying amounts of lecithin. Formulation Fb1, containing solely tripalmitin, recorded a significantly higher z-average value for lecithin content 25 mg and 100 mg, in comparison to 50 mg of lecithin (p<0.05). Fb5 (palmitic acid only) also recorded a trend similar to that of Fb1, but there were no significant differences in the z-average values for lecithin content 25 mg and 50 mg (p>0.05). As observed in section 3.4.1.1, an increase in palmitic acid content in these series of formulations (combination of tripalmitin and palmitic acid) also led to an increase in the z-average of formulations Fb2 to Fb4. These formulations containing 25 mg lecithin saw an increasing trend in z-average, but the increase was insignificant between formulations Fb3 and Fb4. On the other hand, a significant increase in z-average was observed in all three formulations with increasing palmitic acid content (Fb2 to Fb 4) for lecithin content of 50 mg and 100 mg respectively (p<0.05). Interestingly, this increase in z-average was most apparent in formulation containing 100 mg of lecithin as emulsifier.

At 25 mg lecithin, there was possibly insufficient coverage over the crystallised nanoparticles. This sets the stage for agglomeration of smaller size nanoparticles into larger ones due to Ostwald ripening. On the other hand, when the amount of lecithin was high (100 mg), there was a saturation of emulsifier over the surface of the formed nanoparticle, thus increasing the Helmholtz layer and consequently the z-average. In these circumstances, the mobility of lecithin increases with increasing lecithin concentrations resulting in multi-layered SLNs and formation of liposomal structures around the particles due to constant Brownian motion. Fusion of the lecithin bilayers as well as particles

agglomeration are likely to occur, which would increase the z-average size of the SLNs (Schubert and Müller-Goymann, 2005).

There were no visually aggregated particles for formulation Fb1 containing 50 mg lecithin, however aggregated particles were formed in formulation Fb2 and Fb5 containing 50 mg lecithin. Formulations Fb1, Fb2 and Fb5 containing 25 mg and 100 mg lecithin had aggregated particles which were not redispersible upon shaking, indicating that the amount of lecithin was not optimal. Fb3 and Fb4 showed comparatively larger z-average values with corresponding amounts of lecithin incorporated. This showed that the average particle sizes for Fb3 and Fb4 were possibly more influenced by the type of lipids used instead of the amount of lecithin.

It was also observed that the extent of aggregation depended on the amount of lecithin, such that formulations containing 50 mg lecithin had smaller and less aggregated particles. On the other hand, formulations containing 25 mg and 100 mg lecithin had relatively large aggregates, which is consistent with the z-average data shown in Figure 3.15. 50 mg lecithin (50 %w/w) was found to be an optimal amount to be incorporated into the formulations in view of lower z-average values (Fig. 3.15).

Based on the above, formulation Fb1 containing 50 mg lecithin was subsequently selected for further evaluation.

Table 3.7 Zeta potential of formulation Fb1 at different ratio of tripalmitin:lecithin (*n=3*).

Ratio of tripalmitin:lecithin	**Zeta potential (- mV)** [mean ± SD]
1 : 0.25	35.3 ± 1.2
1 : 0.5	54.2 ± 1.5
1 : 0.75	48.3 ± 1.1
1 : 1	53.9 ± 1.2

A further variation in the lecithin content of formulation Fb1 was evaluated and the zeta potential as well as the ratio of tripalmitin:lecithin varied are shown in Table 3.7. The zeta potentials of all these formulations can be considered to be physically stable (above |30| mV), in terms of the electrostatic repulsion (Heurtault *et al.*, 2003). The zeta potential measured for the formulation Fb1 containing lecithin at the ratio of 1:0.5 (50 mg lecithin) was -54.2 ± 1.5 mV, which was predicted to be the most stable formulation. Formulation Fb1 containing lecithin at the ratio of 1:1 (tripalmitin:lecithin) was not selected despite recording an electrostatically stable zeta potential value of -53.9 ± 1.2 mV, as the high lecithin content (100 mg) led to an increase in the z-average size of the SLNs (Fig. 3.15).

Based on the data from this part of formulation study, formulation Fa1 containing 100 mg tripalmitin and Fb1 containing 50 mg lecithin as emulsifier was selected for further work.

3.4.3 Influence of other processing variables on physical properties of the SLNs

Ultrasonication energy is a common dispersion technique used to produce solid lipid nanoparticles (Sharma *et al.*, 2009; Xie *et al.*, 2011b; Zhang *et al.*, 2009). The principle is based on dissipation of energy in the form of cavitation generated within the dispersion due to ultrasonic energy (Parhi and Suresh, 2010). In this study, probe sonication technique was utilised which is capable of producing a powerful 20 kHz ultrasound radiation during the formation of the particles. This sonochemical reaction can rupture chemical bonds by means of the creation, growth and collapse of a bubble that is formed in the liquid (Gedanken, 2004). Ultrasonication method is reported to produce a more uniform particle size distribution of nanoparticles (Awati *et al.*, 2003) and yield smaller particles (Yin *et al.*, 2002). It has been reported that particle uptake is very much dependent on the size of the particles, with larger-sized particles found to be taken up at a slower rate and retained for longer periods of time in Peyer's patches compared to smaller sized particles (Jani *et al.*, 1989). The selected formulation Fa1 was prepared according to the double emulsion technique. The two-step emulsification process involved the use of a probe sonicator to mix the immiscible water and oil phases. This technique is mainly useful for encapsulation of hydrophilic drugs such as peptides, as it avoids any heating processes.

Referring to the schematic diagram in Figure 3.16, the method involves two emulsification steps. The first step is to obtain a water-in-oil (W/O) primary emulsion, which consists of the lipid, an oily surfactant and the drug that is dissolved in the aqueous phase. This freshly prepared W/O primary emulsion is then re-emulsified in the second step with an excess of hydrophilic surfactant to obtain the final W/O/W emulsion.

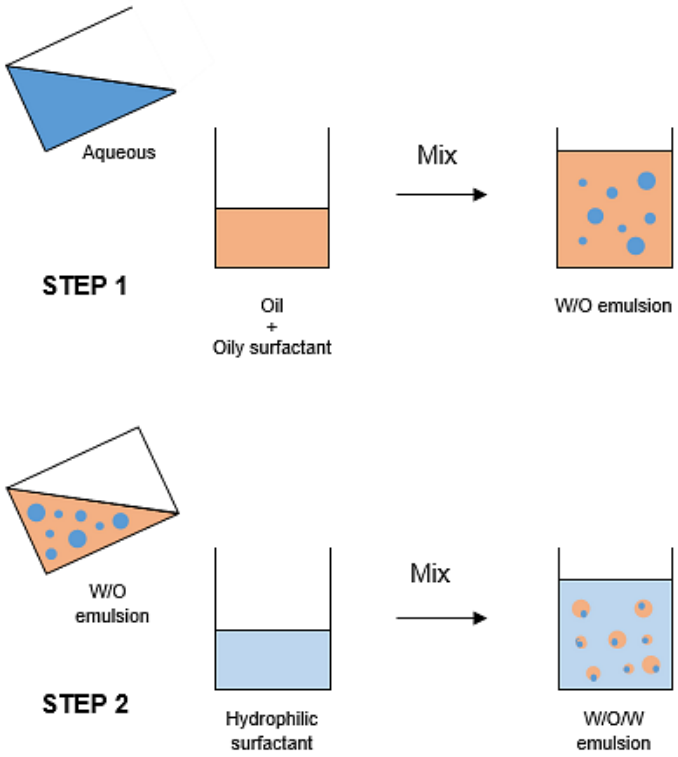

Figure 3.16 Schematic diagram of two-steps emulsification method to produce W/O/W double emulsion.

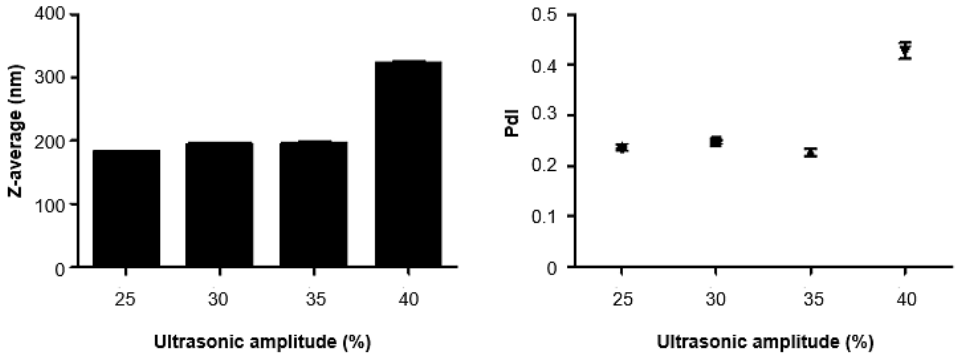

(a) (b)

Figure 3.17 (a) z-average and (b) PdI values for the primary emulsion of Fa1 prepared at different ultrasonic amplitude (*n=3*).

The aim here was to optimise the ultrasonic processing variables in order to obtain nanosize range particles with desirable physical characteristics. We also aimed to establish a method that was reproducible. Consequently, the dispersion was subjected to ultrasonication at various amplitudes 25 %, 30 %, 35 % and 40 % during formulation of the primary (W/O) emulsion. Ultrasonication amplitude can be translated into specific energy input, which is a parameter combining both power and time, both of which are vital in deagglomeration of particles (Sauter *et al.*, 2008). From Figure 3.17, it was observed that at the ultrasonication amplitude of 25 %, SLNs with a smaller z-average (180.9 nm) and polydispersity value (0.24) were produced. However, instability of the primary emulsion post-sonication was observed where phase separation of the primary emulsion occurred with the formation of two distinct layers (Fig. 3.18 (a)). Furthermore, when this formulation was viewed under the SEM, isolated nanoparticles were not seen (Fig. 3.17). Instead, oily droplets were observed in Figure 3.18(a), indicating that SLNs did not formed. This observation can be explained taking into account the fact that the ultrasonic amplitude of 25 % was insufficient in generating requisite sonic energy necessary in the formation of the SLNs. A previous study outlined the importance of primary emulsion stability, as a prerequisite for a successful stabilisation of a multiple emulsion as well as for drug loading (Nihant *et al.*, 1994). These observations are in concert with those of Nihant *et al.* (1994), where an unstable primary emulsion that exhibited phase separation post-sonication subsequently led to the formation of SLNs with undesirable physical properties.

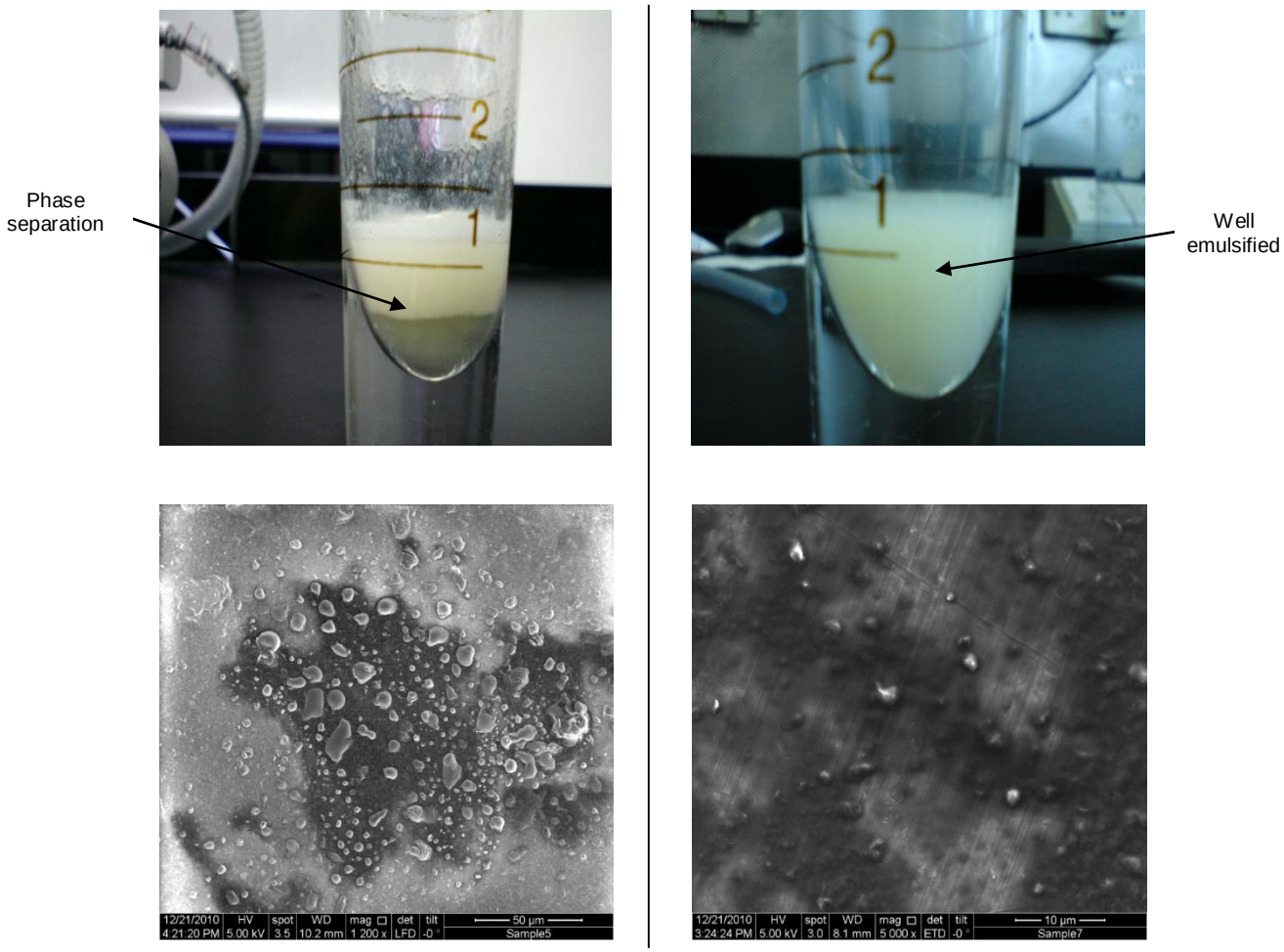

(a) Amplitude 25 %

(b) Amplitude 30 %

Figure 3.18 Primary (W/O) emulsion and SEM micrograph of formulation Fa1 prepared by ultrasonication at (a) Amplitude 25 % and (b) Amplitude 30 %.

The z-average values at amplitudes 30 % and 35 % were recorded as 194.5 nm and 196.0 nm respectively. For the same amplitudes, the PdI values were registered as 0.25 and 0.23 respectively (Fig. 3.17). There was no phase separation observed when the formulation was ultrasonicated at amplitude 30 %, and the SLNs were successfully formed as observed under SEM (Fig. 3.18(b)). At a higher amplitude of 40 %, it was expected that the z-average

would be smaller since the power and energy input into the system was higher, however the z-average and PdI values increased in proportion (Fig. 3.17). This can be explained by the fact that when the vibration amplitude increases, the cavitation created grows too large to the extent that the time available in the adjacent rarefaction cycle is not sufficient for them to collapse (Sauter *et al.*, 2008). Therefore, there will actually be less energy generated in the system due to the collapse of the bubble. Clearly then, a higher ultrasonication amplitude at 40 % was not desirable in the deagglomeration of nanoparticles. Based on these findings, ultrasonication amplitude of 30 % was selected for further optimisation.

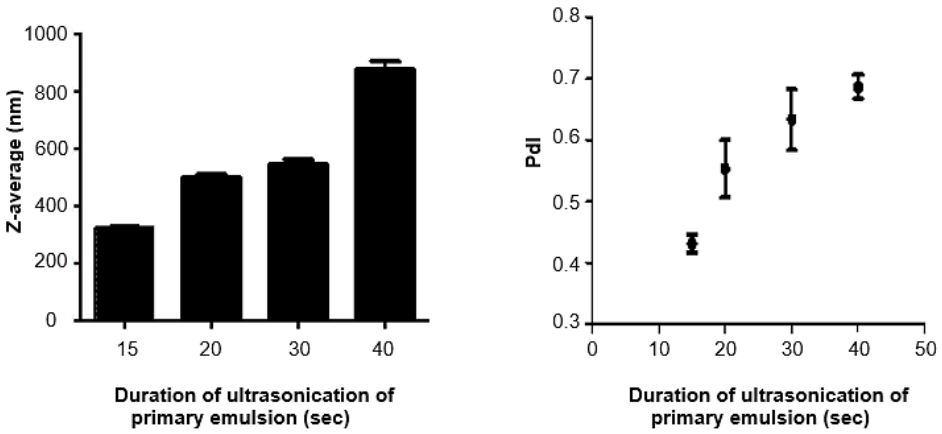

(a) (b)

Figure 3.19 (a) z-average and (b) PdI values for formulation Fa1 prepared at varying duration of ultrasonication of the primary (W/O) emulsion (*n=3*).

The duration of ultrasonication can also directly influence the specific energy input into the system. An increase in the duration of ultrasonication is expected

to increase the amount of specific energy within the system and therefore cause the droplets to be broken down more readily due to the increased shear stress generated which results in particle size reduction (Budhian *et al.*, 2007). It has been previously reported that by increasing the power and/or the duration of sonication, the mean diameter of PLGA polymeric nanoparticles was reduced and the particle size distribution was altered from bimodal to unimodal (Budhian *et al.*, 2007; Mainardes and Evangelista, 2005). Contrary to this, the findings in the present study showed a rising trend in z-average and polydispersity as the duration of ultrasonication of the primary (W/O) emulsion was extended from 15 seconds to 40 seconds (Fig. 3.19). When the primary emulsion was subjected to 15 seconds of ultrasonication, the z-average and PdI value was 324.1 nm and 0.43 respectively. At 20 seconds of ultrasonication, the z-average and PdI was recorded as 500.4 nm and 0.55 respectively. Here we observed that an additional 5 seconds of ultrasonication resulted in a significant increase in both these parameters. For 30 and 40 seconds of ultrasonication time, the recorded z-average were 545.5 nm and 876.9 nm respectively. PdI values were registered at 0.63 and 0.69 for the respective durations of 30 and 40 seconds. This increase in the particle size diameter and the polydispersity of the distribution can be explained based on the collisions that occur when there is an increase in the energy being imparted into the system. Some of such collisions are likely to result in agglomeration of the particles and subsequently an increase in z-average. Since this phenomenon is selective (ie. not all particles necessarily particulate), there is thus a differential of particles-type which is what accounts for the rise in PdI as well.

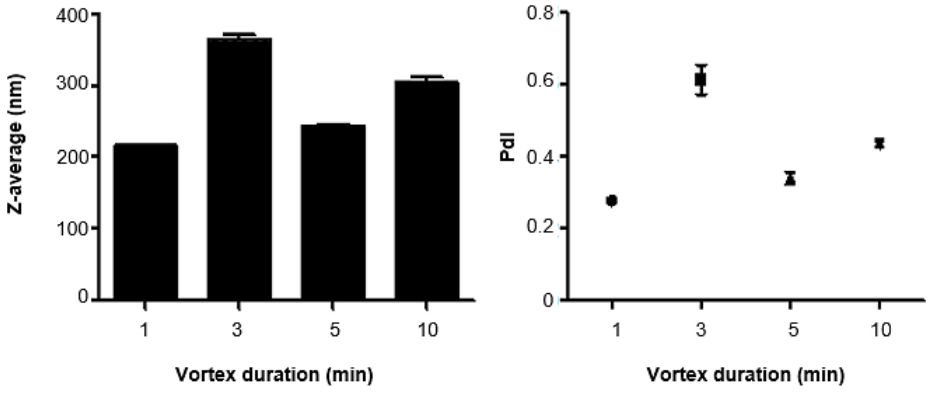

(a) (b)

Figure 3.20 (a) z-average and (b) PdI values for formulation Fa1 prepared at varying vortex mixing duration prior to ultrasonication of the primary (w/o) emulsion (*n=3*).

We aimed to investigate the effect of vortex-mixing, in addition to ultrasonication, prior to the first emulsification step to prepare the primary (W/O) emulsion on the physical properties of the SLNs. Some studies have utilised vortex-mixing during the initial emulsification step to successfully prepare nanoparticles (Bilati *et al.*, 2005b; Laroui *et al.*, 2007; Zambaux *et al.*, 1999). Optimisation of this parameter involved the introduction of vortex-mixing step for 1, 3, 5 and 10 minutes prior to emulsification using ultrasonicator. There was no apparent trend observed when the duration of vortex-mixing was increased (Fig. 3.20). However, when the mixture was vortex-mixed for 1 and 3 minutes, an instantaneous phase separation of the primary emulsion was observed. The instability of the primary emulsion seen in this case due to the additional energy input from the vortex-mixing, has shown that the stability of the formulation was compromised and thus not as conducive in the successful formation of SLNs. The importance of the stability of primary emulsion has been outlined previously.

It was also observed that the z-average and PdI values of nanoparticles subjected to 3 minutes of vortex-mixing was the highest recorded (364.5 nm and 0.61 respectively), as compared to the other durations. The process of emulsification operated by vortex-mixing is less stable than by ultrasonication (Zambaux *et al.*, 1999). Therefore, ultrasonication of nanoparticles is necessary in conjunction with vortex-mixing in order to improve stability of the SLNs. However, when there is additional input of energy imparted into the system by means of vortex mixing, there is also an increased tendency of particles to agglomerate as a result of high collision rates between rapidly moving particles. This could possibly be the reason for the significant increase in z-average and PdI when the primary emulsion was vortex-mixed for 3 minutes (Fig. 3.20). Unexpectedly, when the duration of vortex mixing of the primary emulsion was extended to 5 minutes, the z-average and PdI reduced to 242.9 nm and 0.34 respectively. This observation can be attributed to the presence of high shear stress being contributed by the prolonged vortex mixing leading to deagglomeration of any previously agglomerated particles and hence a reduction in z-average.

In summary, 5 minutes of vortex mixing of the primary emulsion prior to 15 seconds of ultrasonication at 30 % amplitude was favourable in the preparation of optimal SLNs.

3.4.4 Microscopy imaging

3.4.4.1 FE-SEM Imaging

The initial stages of the preformulation work indicated that scanning electron microscopic (SEM) imaging of the lipid nanoparticles needed some optimisation. The sample preparation method as well as the intrinsic properties (eg. melting point) of the lipids present researchers with challenges in order to obtain satisfactory SEM images of SLNs. Therefore, much work has been done during the preformulation in order to optimise the method for sample preparation as well as the parameters used for imaging.

SEM images of insulin-free and insulin-loaded SLNs of formulation Fa1 (containing 100 mg tripalmitin) are shown below in Figure 3.21. The particles were freeze-dried directly from colloidal lipid dispersion prior to imaging. The freeze-dried particles were then placed on a carbon sticky tape which was secured on an aluminium stub. The sample was gold-sputter coated before imaging.

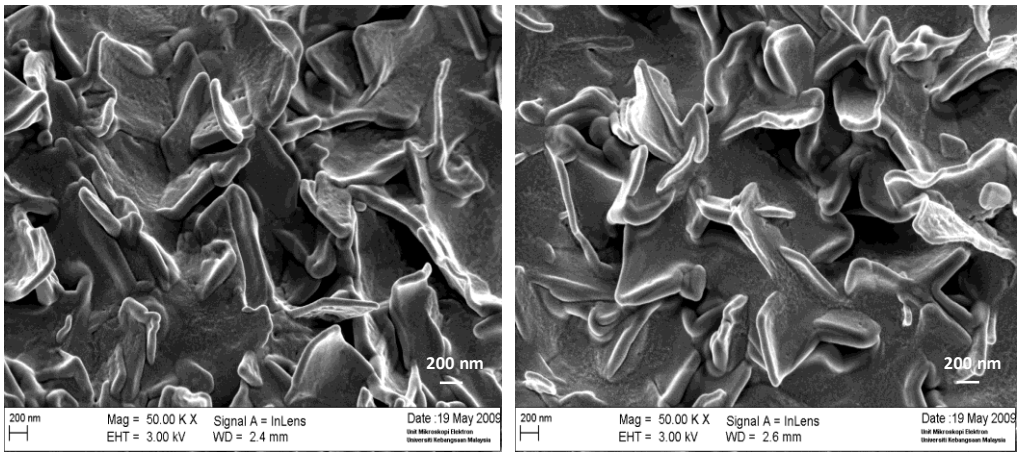

(a) (b)

Figure 3.21 SEM images of solid lipid nanoparticles (a) insulin-free SLNs and (b) insulin-SLNs. (Scale bar of 200 nm)

Referring to Figure 3.21, the shape and morphology of the lipid nanoparticles were observed to be flat, flaky and of amorphous nature and not the spherically-shaped particles commonly seen in SEM images of the SLNs (Hatziantoniou *et al.*, 2007; Liu *et al.*, 2007; Mukherjee *et al.*, 2009b). Furthermore, the particles appeared agglomerated.

Due to the particles being non-spherical in shape, the size of the particles would not be representative. It was theorised that the change in shape and morphology was due to the freeze-drying process which exerted stress on the nanoparticles during abstraction of water, causing the particles to flatten out. A similar observation has been described by Jores *et al.* (2003) who showed flat needle structures from the side view of the particles in a TEM picture, calling those as “spoon structure” or “nanospoon”. The authors suggested that the structures seen were due to the lipid hydrophobic tail of tripalmitin sticking out on the SLNs surface. On another note, suspensions of platelet-like shaped tripalmitin nanocrystals stabilised by the pure lecithin dilauroyl phosphatidylcholine (DLPC) and the lecithin blend S100 have also recently been studied as potential drug delivery systems, exploiting the large surface area available for drug incorporation (Schmiele *et al.*, 2014).

A close examination of the SEM images in Figure 3.21 shows a sticky matrix adjoining the particles. This is likely to be due to the presence of high concentration of Poloxamer 188, which was imposed by the freeze-drying process. Poloxamers are water-miscible polymeric surfactants with high viscosities (Karmarkar *et al.*, 2008), and thus it is possible for a sticky matrix to be formed during drying of the sample which appeared as a network of trapped nanoparticles.

In order to further optimise the sample preparation method for the SEM imaging, the nanoparticle formulations were viewed without freeze-drying and were diluted to low concentration (1 in 5 dilution). As opposed to 1 in 10 dilution used in particle size analysis, a dilution factor of 1 in 5 was selected for SEM sample preparation in order to view a reasonable number of nanoparticles in the samples. At the same time, freeze-dried particles were also viewed as an experimental control. Instead of viewing the freeze-dried particles directly as previously done, these particles were suspended in 50 ml purified water and then sonicated for 30 minutes in an ultrasonic bath.

Figure 3.22 displays SEM image of diluted (1 in 5 dilution) lipid nanodispersion, where it can be observed that spherical nanoparticles had been formed for the sample derived directly from the diluted colloidal lipid dispersion. However, it seemed that these existed as large agglomerates of smaller nanoparticles.

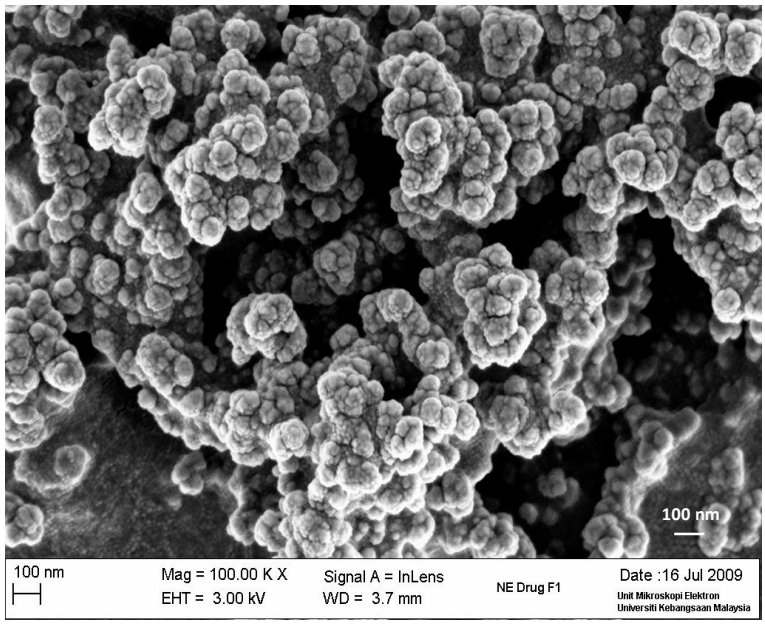

Figure 3.22 SEM image of diluted formulation Fa1. (Scale bar of 100 nm)

SEM images of freeze-dried nanoparticles (insulin-free and insulin-loaded) which were suspended in water and sonicated prior to viewing are shown in Figure 3.23. For the freeze-dried SLNs suspended in water and sonicated thereafter, the insulin-free nanoparticles (Fig. 3.23(a)) looked similar to the nanoparticles seen in Figure 3.21(a), but agglomerated. Interestingly, the insulin-loaded freeze-dried nanoparticles were observed to be completely different from the other freeze-dried counterparts (Fig. 3.23(b)). The image resembled the nanoparticles from the diluted fresh colloidal lipid dispersion (Fig. 3.22).

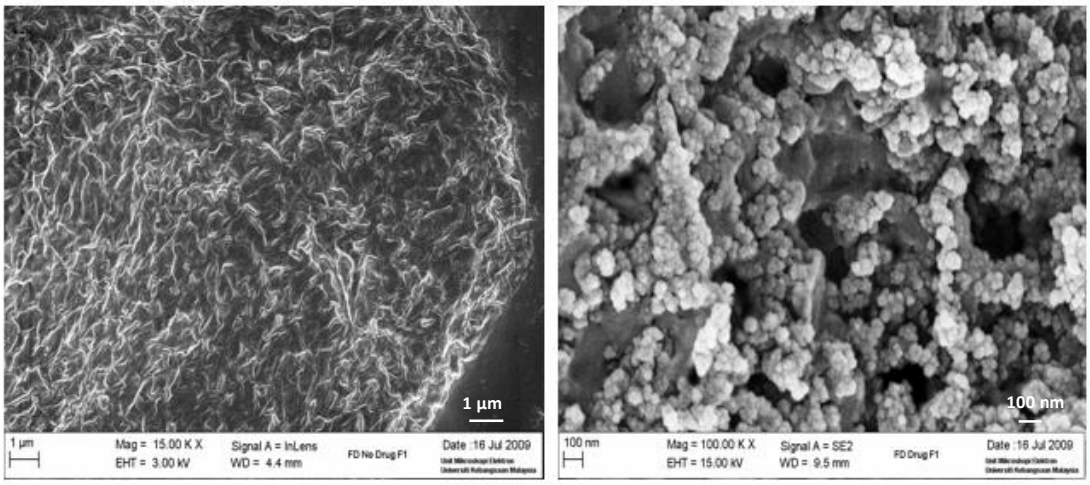

(a) (b)

Figure 3.23 SEM micrographs of freeze-dried nanoparticles
(a) insulin-free and (b) insulin-loaded (post-sonication).

These findings indicate that the presence of insulin in the formulation appear to negate the effects of the freeze-drying process. It has been reported in the literature that entrapped drug in nanoparticles may in certain cases influence the freeze-drying of nanoparticles in a positive or negative manner when water is being abstracted during the freeze-drying process (Abdelwahed *et al.*, 2006).

In this case, we observed a positive effect of freeze-drying on drug-loaded SLNs containing insulin, in which the quality of reconstituted nanoparticles had been retained.

Being lipidic in nature with low melting points, samples were found to be extremely sensitive to the electron beam, resulting in the location of interest being damaged by the electron beam focused on that area. Beam damage on lipid substance is common since high-energy electron beam causes local heating of the area, thus altering the surface structure (Aguilera and Stanley, 1999). Therefore, the accelerating voltage of the electron beam was decreased to below 5 kV.

Routinely, samples are coated with gold prior to viewing under the SEM. However, gold coating procedure has its own drawback as the gold layer may mask the true surface morphology of the nanoparticles and obscure fine details. The particles could also be entirely buried underneath the coat if the right parameters are not sought (Aguilera and Stanley, 1999). If the lipid nanoparticles were not gold-coated, there was another problem faced due to the similarities seen between the lipid nanoparticles (Fig. 3.24(a)) and the carbon nanoparticles of the carbon sticky tape used in SEM imaging (Fig. 3.24(b)). The carbon sticky tape was used as the substrate to secure the sample on the aluminium stub. However, without gold-coating, the carbon nanoparticles from the carbon sticky tape would be imaged on the SEM as seen in Figure 3.24(b). This posed a problem as it was necessary to clearly differentiate the solid lipid nanoparticles from those due to the carbon sticky tape.

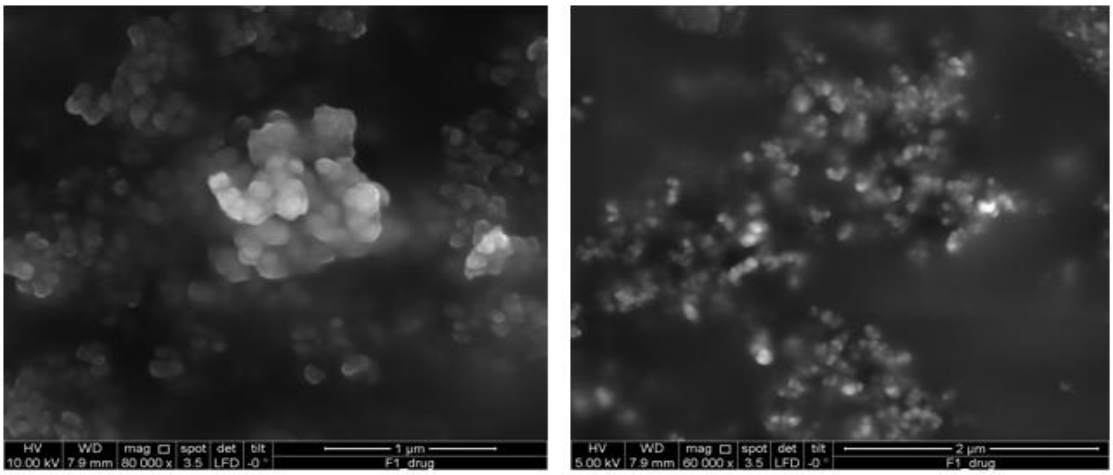

(a) (b)

Figure 3.24 SEM image of (a) lipid nanoparticles (uncoated with gold) and (b) blank carbon sticky tape used as sample substrate.

In order to further optimise the sample preparation method, the lipid droplet was placed directly onto an aluminium stub, instead of on the carbon sticky tape as before and the nanoparticles were not coated. Figure 3.25 shows the optimised SEM image of the uncoated lipid nanoparticles, although the nanoparticles were largely agglomerated.

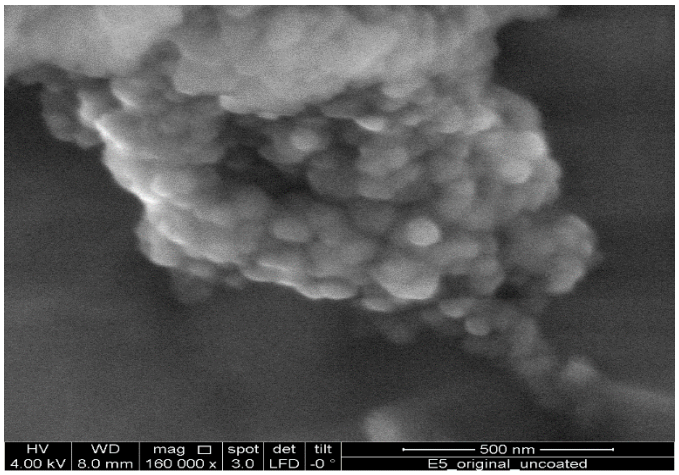

Figure 3.25 SEM image showing a bunch of agglomerated nanoparticles.

In order to address the issue of agglomeration, the lipid dispersion was sonicated in a sonic bath for 30 minutes. The resulting SEM image shows isolated spherical lipid nanoparticles, with central indentation in some of the particles (Fig. 3.26). The average size diameter of the isolated nanoparticles was approximated at 250 nm, which corroborated with the z-average data measured using the Zetasizer.

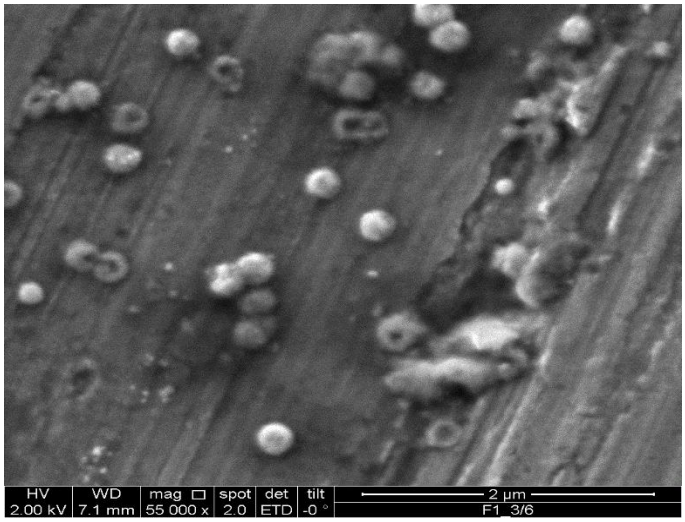

Figure 3.26 SEM image showing isolated lipid nanoparticles.

3.4.4.2 TEM Imaging

Numerous studies on solid lipid nanoparticles use TEM to characterise the morphology and internal structure of their formulations (Bayat *et al.*, 2008; Garcıa-Fuentes *et al.*, 2003; Sarmento *et al.*, 2007a). As described, optimisation of SEM imaging was found to be challenging. In order to improve and complement the images obtained from SEM, TEM imaging was also pursued to shed some additional insights on the morphology and investigate the internal structure of the lipid nanoparticles.

The lipid samples were negatively stained using osmium tetraoxide 0.1 M to enhance the image of the sample. The images obtained were not particularly satisfactory although it was possible to demonstrate that the size was approximately 250 nm and the spherical/ellipsoidal shape of the nanoparticles (Fig. 3.27) was consistent with the particle size obtained from SEM image in Figure 3.26.

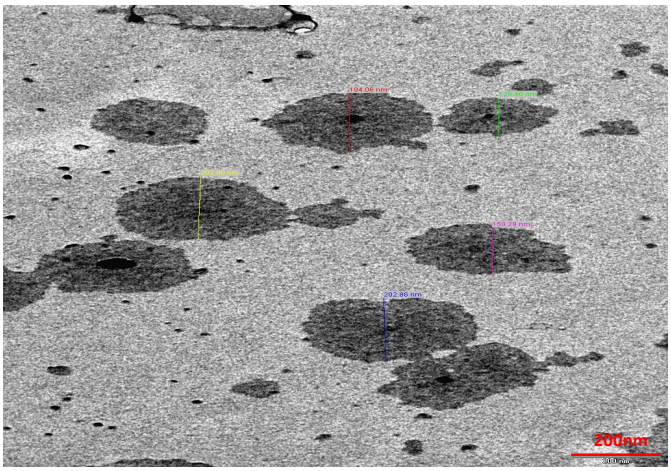

Figure 3.27 TEM micrograph of lipid nanoparticles. (Scale bar of 200 nm)

3.5 Concluding remarks

Insulin-containing solid lipid nanoparticles, comprising of palm oil lipids, have been successfully fabricated using W/O/W double emulsion solvent evaporation technique.

Production and processing parameters were optimised to obtain desirable particle size range, polydispersity index and zeta potential as well as physical properties of the formulation. Based on the findings here, the most desirable formulation to be pursued further was that containing 100 mg tripalmitin as lipid and 50mg lecithin as emulsifier.

Sample preparation method for SEM and TEM had been optimised to obtain clear images of isolated nanoparticles in the micrographs. The shape and morphology of the nanoparticles were ascertained, with the particle size measured from the microscopy images corroborated with that determined using Zetasizer, hence being valuable complementary characterisation tools in the present work.

CHAPTER 4

Identification of Insulin Localisation Model within the Optimised SLNs

4.1 Introduction

4.1.1 Drug Localisation Models

Many studies have explored the possibility of incorporating drugs into SLNs in a bid to improve the loading capacities within the SLNs. However, limited information is available about the drug release from these SLNs, particularly the release mechanisms involved (Cavalli *et al.*, 1999; Mühlen and Mehnert, 1998; Yang *et al.*, 1999). Drug release profiles are influenced by the particle size and the nature of lipid matrix (Mühlen and Mehnert, 1998). The drug release profiles from SLNs can be modulated to achieve a prolonged release with or without an initial burst release (Müller *et al.*, 2000). As a result of the variations obtained in drug release profiles, three different drug incorporation models (Fig. 1.8) have been proposed (Müller *et al.*, 2000). Based on these models, the solid solution model (Fig. 1.8A), in which the drug is molecularly dispersed in the lipid matrix, is often produced by cold homogenisation technique, in the absence of surfactant or drug-solubilising surfactant. The drug-enriched shell model (Fig. 1.8B) in which the drug is released from the particle surface and hence often manifest as a burst release. For the drug-enriched core model (Fig. 1.8C), where the drug is located in the inner core shielded by the lipid shell, the drug is released in a prolonged manner and based on diffusion through the matrix. Müller and his co-workers proposed the drug incorporation models (Fig. 1.8) for lipophilic drugs, which are soluble in the lipid matrix of the SLNs systems.

The production of protein-loaded SLNs formulations, eg. insulin (Xie *et al.*, 2008; Yang *et al.*, 2011) and salmon calcitonin (Garcia-Fuentes *et al.*, 2005c; Martins *et al.*, 2009), have been designed in order to achieve a sustained drug release profile with minimal burst release. Whilst sustained protein release has been

achieved in the preceding cases, there has been no attempt to establish the possible location of the hydrophilic drugs (eg. peptides, like insulin) within the formulated SLNs to our knowledge, unlike for lipophilic drugs. The drug localisation models, apart from helping to decipher the possible release mechanisms of the hydrophilic payload from the SLNs, also sheds some light on the propensity of the SLNs to be taken up within the gastrointestinal tract.

4.1.2 Aims and Objectives

The main aim of this part of study was to fabricate insulin-containing SLNs, in order to achieve the three hypothetical drug incorporation models as illustrated in Figure 1.8. Following the fabrication, suitable techniques will be employed to distinguish the different types of drug localisation models achieved.

4.2 Materials

Pure crystalline recombinant human insulin (lyophilised powder) was manufactured by EMD Biosciences (San Diego, USA) and purchased from Merck. Solid lipid tripalmitin (99 % purity) was purchased from Acros Organics (Geel, Belgium). L-α-phosphatidyl choline (soy lecithin) and poloxamer 188 were purchased from Fluka (Australia) and BASF (Germany) respectively were used as surfactants. Dichloromethane, hydrochloric acid, sodium chloride and disodium hydrogen phosphate and potassium dihydrogen phosphate were supplied by R&M Chemicals. Trifluoroacetic acid (TFA) and acetonitrile (both HPLC grades) were purchased from Fisher Scientific (Loughborough, UK). All the other solvents used were of analytical grade and the materials were used as received.

4.3 Methods

4.3.1 Preparation of insulin-containing SLNs

The formulations were prepared using solvent-evaporation emulsification technique, adapted from (Garcıa-Fuentes *et al.*, 2003). The SLNs (Model A) was prepared based on the optimised method outlined in Chapter 3. Briefly, solid lipid tripalmitin and soy lecithin were dissolved in dichloromethane (DCM), forming the oily phase. 1 mg of human recombinant insulin (Calbiochem, USA) was dissolved in 100 µL of 0.1 % trifluoroacetic acid and added to the oily phase. The emulsion was first mixed with a vortex mixer for 5 minutes, then subsequently dispersed with an ultrasonicator probe (750 W VCX Series, Sonics Inc., USA) for 15 seconds to produce a primary W/O emulsion. A 2 % Poloxamer 188 solution in distilled water was added subsequently, followed by ultrasonication to form a W/O/W double emulsion. The resultant double emulsion was made up to a final volume of 10 ml with 1 % Poloxamer 188 and the solvent was evaporated off. For the insulin-loaded SLNs (Model A), insulin solution was incorporated in the suspension prior to ultrasonication. For the physically-adsorbed insulin formulation (Model B), the insulin solution was added to the unloaded SLNs dispersion after the solvent was evaporated off. The drug-enriched core model (Model C) was not studied due to the formulation constraints of the ingredients used that did not permit formation of this model. It is not possible to achieve all three incorporation models at once using the same ingredients without introducing additional variables into the system.

4.3.2 Zeta potential measurements

The zeta potential of the SLNs formulations were measured using Zetasizer Nano-ZS (Malvern Instruments Ltd., U.K.). Samples were loaded in a clear disposable zeta cell (DTS 1060C) for measurement at 25 °C, performed in triplicates. The zeta potential values were calculated based on Smolochowski equations (Eq. 3.2) using Malvern Zetasizer Software 6.01®, as determined by the electrophoretic mobility of the samples.

4.3.3 *In vitro* drug release studies

In vitro insulin release studies were evaluated in phosphate-buffered saline (PBS) buffer (pH 7.4), maintained at 37 °C under stirring at 50 rpm. Samples were removed at pre-determined time intervals over 1 hour for both formulations, followed by quantification using high pressure liquid chromatography (HPLC) as well as zeta potential measurements.

4.3.4 Scanning Transmission Electron Microscopy (STEM) Imaging

Sample nanoparticles were placed on Formvar-film copper grids and stained using 1 % phosphotungstic acid (PTA) solution. Formulations were subsequently viewed using STEM detector (FEI Quanta 400F, U.S.).

4.4 Results and Discussion

4.4.1 Preparation of insulin-containing SLNs

Some modifications had to be made to the formulation procedure for insulin-containing SLNs as indicated in Figure 4.1 in order to achieve the different drug incorporation models (Fig. 1.8). The procedure used to prepare insulin-containing SLNs using method 1 (Fig. 4.1) is described in Section 3.4. For method 2 (Fig 4.1), a slight modification was made to the addition step of insulin solution. The insulin solution was added into the w/o/w emulsion of the SLNs formulation, instead of being added at the initial step to form the primary w/o emulsion.

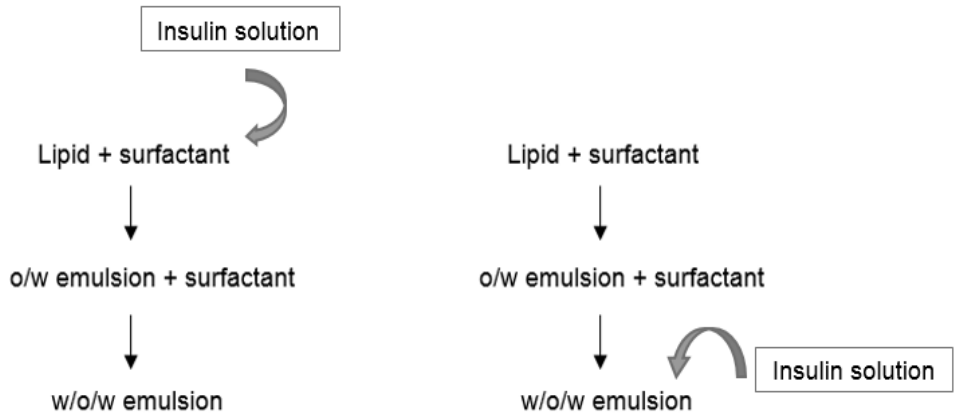

Method (1) Method (2)

Figure 4.1 Methods (1) and (2) to prepare insulin-containing SLNs, with modification steps, to achieve different drug incorporation models.

This loading technique via adsorption of proteinaceous drug onto preformed system has been widely utilised in polymeric nanoparticulate carriers (Almeida and Souto, 2007; Couvreur *et al.*, 1979; Soppimath *et al.*, 2001). It is desirable in the present context due to the availability of a large surface area offered by nanoparticles for protein adsorption (Almeida and Souto, 2007). Furthermore, proteins such as bovine serum albumin (Gualbert *et al.*, 2003) and calcitonin (Garcia-Fuentes *et al.*, 2005b) have been loaded onto preformed SLNs surface by means of this physical adsorption technique. Surface chemistry of the solid surfaces can influence its interaction with the protein molecules. For example, it was suggested that albumin, which undergoes adsorption via a single step process of protein-surface interactions, exhibits a stronger affinity towards $–CH_3$ hydrophobic surface compared to the –OH terminated hydrophilic surface (Roach *et al.*, 2005). Surface modification of SLNs using amphiphilic lipid lecithin and non-ionic emulsifier has been used to improve loading capacities of the protein bovine serum albumin (Schubert and Müller-Goymann, 2005).

In this regard, each tripalmitin molecule, which consists of three long aliphatic chains (C_{16}), is capable of interacting with the proteins. These long aliphatic chains of the SLNs can contribute to the adsorption of protein onto the $–CH_3$ hydrophobic surface via weak attractive Van der Waals interactions, though not particularly favourable due to the susceptibility of surface-induced structural alteration (Lee *et al.*, 2011). The inclusion of surfactants in the formulation offers protein-stabilising effect against adsorption loss by reducing the surface activity of the lipid nanoparticles. The hydrophobic tail of lecithin has a strong affinity towards the long aliphatic chains of tripalmitin, which enables the lecithin to bind preferentially to the lipids at interfaces. The ionised phosphate hydrophilic groups present in lecithin can contribute negative charges (PO_4^-) to the lipid

nanoparticles. Therefore, the positively charged insulin molecules are electrostatically attracted to the SLNs. Furthermore, the presence of –OH group in Poloxamer 188 can also participate in the formation of hydrogen bonds with the insulin at the interface of these SLNs where the proteins adsorbed. This procedure of surface adsorption of proteins on SLNs is particularly advantageous as it offers a promising alternative which can minimise the exposure of proteins to harsh processing conditions during SLNs production (Almeida and Souto, 2007; Schubert and Müller-Goymann, 2005).

Here, we have successfully prepared insulin-containing SLNs formulations conforming to two of the three types of proposed drug incorporation models as described earlier in Section 4.1.1. It was not possible to achieve the drug-enriched core model (Model C) without significantly modifying the protocol which would have made the comparing between them difficult. As mentioned earlier, formulation constraints of the ingredients used did not permit this model from being materialised. In the following section, both of these formulations which conform to the localisation models (Model A and B) will be characterised accordingly in order to ascertain the insulin localisation models.

4.4.2 Ascertaining the Location of Insulin within SLNs

Following the production of the two types of the SLNs with different localisation of insulin, the next crucial step was to confirm the insulin localisation models (Model A and B). It is indeed challenging to determine the drug location within a nanoparticle in view of its small size (Benita, 2005); thus our approach was based on indirect means such as spectroscopy, fluorescence imaging and zeta potential measurements.

4.4.2.1 Energy Dispersive X-Ray (EDX) spectroscopy

Energy Dispersive X-ray spectroscopy (EDX) is a powerful technique used for elemental analyses as well as mapping of distribution of elements. Fernandez-Hervas *et al.* (1998) and Edge *et al.* (1999) had previously applied this technique to identify and map the distribution of elements present in their formulations. This technique was utilised on the basis of identifying elements solely present in insulin and mapping of these elements across the surface and inner regions of the nanoparticles in order to establish the location of insulin within the fabricated nanoparticles.

The analysis and mapping of elements were carried out using an FE-SEM, equipped with EDX functionality. The element of interest potentially detectable in pure insulin is sulphur, which is found in cysteine amino acid residues. Sulphur is absent from the lipid matrix of the SLNs, therefore eliminating any possibility of interference due to the lipid materials during analysis.

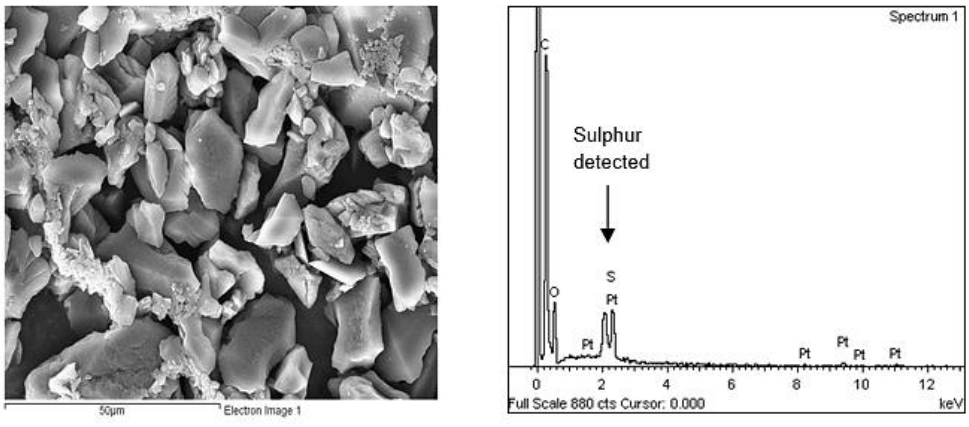

(a) (b)

Figure 4.2 Pure insulin (a) SEM image and (b) EDX spectrum (Pt represents platinum-coated)

Pure recombinant human insulin displayed crystalline structures when viewed under FE-SEM (Fig. 4.2(a)). Figure 4.2(b) shows the EDX spectrum for pure recombinant human insulin which confirmed the presence of sulphur in the sample. Therefore, the element sulphur which was exclusive to insulin, was utilised as a means of indirectly identifying insulin in the sample.

Figure 4.3 and 4.4 illustrate the EDX spectra for insulin-free and insulin containing lipid nanoparticles respectively. Despite the high intensity for sulphur in the pure insulin sample (Fig. 4.2), sulphur was not detected within the insulin-containing SLNs. This could possibly be due to the amount of sulphur in the SLNs being below the threshold of sensitivity for the equipment. The concentration of insulin present in the formulation was 100 µg/ml and only a drop of the dispersion was used for EDX sampling, hence the level was too low for detection. Typical theoretical detection limits in SEM-EDX measurements are accepted as approximately 0.08 wt.% (Kuisma-Kursula, 2000). Another explanation could possibly be due to insulin being already encapsulated within the nanoparticles, resulting in low available sulphur concentration on the surface of the nanoparticles. Due to the constraint mentioned above, mapping of sulphur for the purpose of detecting the localisation of insulin within the SLNs could not be performed across the surface and inner region of the nanoparticles. Therefore, the EDX analysis was not used for further analysis.

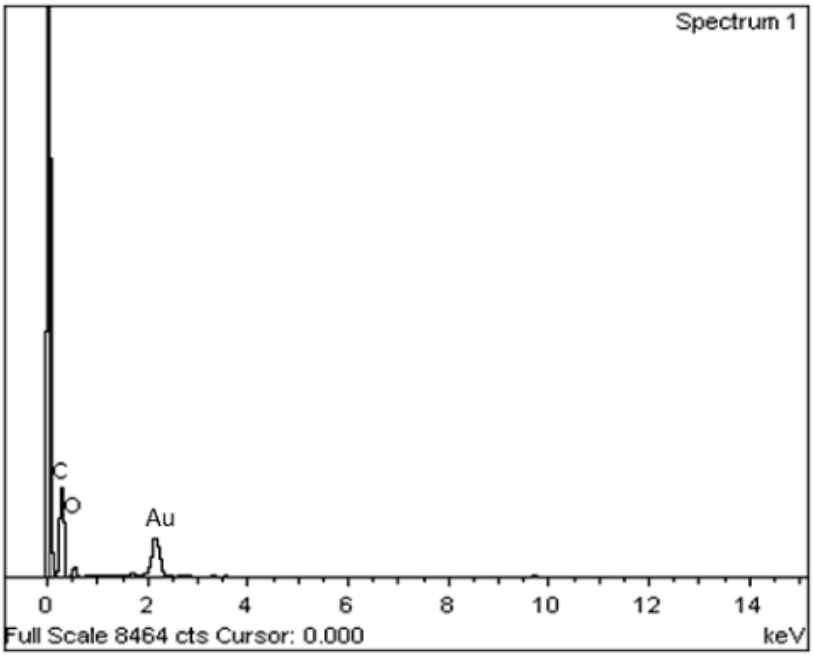

Figure 4.3 EDX spectrum for insulin-free lipid nanoparticles. (Au represents gold-coat)

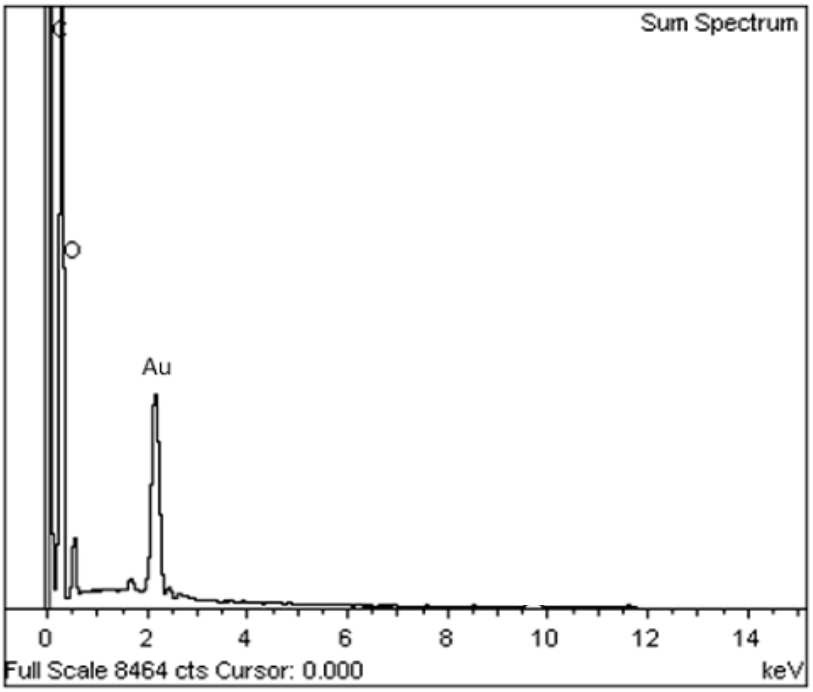

Figure 4.4 EDX spectrum for insulin-containing lipid nanoparticles. (Au represents gold-coat)

4.4.2.2 Fluorescence spectroscopy

The presence of aromatic amino acid tyrosine in the insulin molecule contribute to its fluorescence characteristics. Aqueous insulin solution has been reported to emit the highest fluorescence intensity at band maxima λ_{max} 304 nm wavelength, consistent with other tyrosine-containing proteins such as ribonuclease, prolamine and ovomucoid (Teale, 1960). Therefore, we theorised that this intrinsic fluorescence attribute of insulin can be exploited in order to predict its location within the SLNs. This approach has previously been adopted to study the structural, physicochemical and functional properties of proteins (Permyakov *et al.*, 1982). Although insulin solution is capable of autofluorescing (Bekard and Dunstan, 2009), it typically displays low intrinsic emission at $\lambda_{ex}/\lambda_{em}$ = 276/300 nm (Gök and Olgaz, 2004). Ideally, insulin is routinely tagged with a fluorophore, such as fluorescein isothyocianate (FITC), by binding to the amine groups of the protein molecules to probe their extrinsic emission for *in vivo* studies (Gök and Olgaz, 2004; Trotta *et al.*, 2011). However, tagging of payload can significantly alter the physicochemical properties of the SLNs.

In our attempt to establish the location of drug within the SLNs, we anticipated that the fluorescence intensity would vary between the two different models as shown in Figure 4.5 so that a qualitative comparison of relative fluorescence intensities can be used as an inference.

Figure 4.6 shows the emission spectra of insulin for insulin solution, insulin-free SLNs and insulin-containing SLNs excited at λ_{ex}= 255 nm. Excitation wavelength was fixed at 255 nm to minimise interference from solvents. All three emission spectra displayed a unique λ_{em} = 293 nm either in the presence or absence of insulin in the samples. Accurate measurement or detection of

insulin fluorescence intensity can be hindered due to the presence of background fluorescence at wavelength 293 nm. Contributing factors such as autofluorescence or spectral overlap can lead to the occurrence of background fluorescence (Hulspas *et al.*, 2009). Therefore, this technique of comparing relative fluorescent intensities was found to be inconclusive.

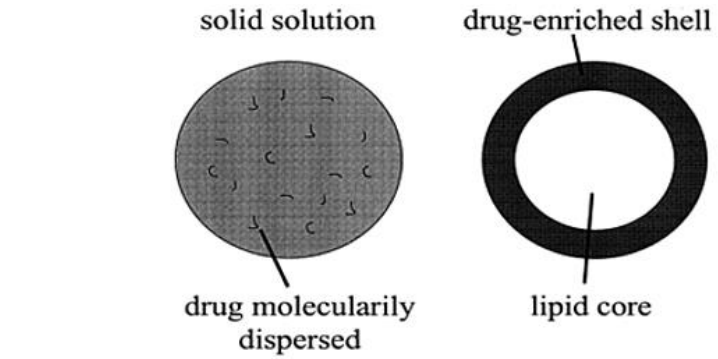

Figure 4.5 Prediction of tyrosine fluorescence intensity of insulin through relative comparison for drug localisation models A and B (+ indicates low intensity; ++ indicates high intensity)

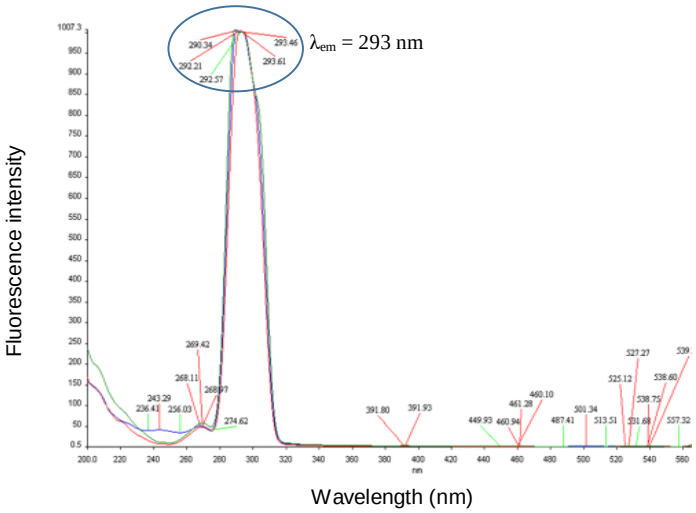

(i) Insulin solution

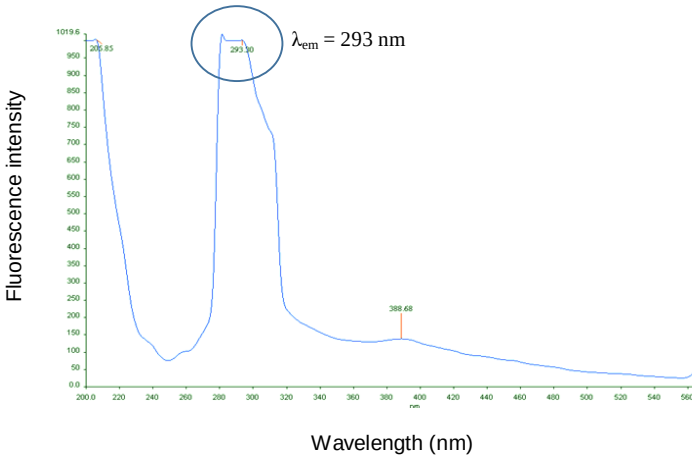

(ii) Insulin-free SLNs

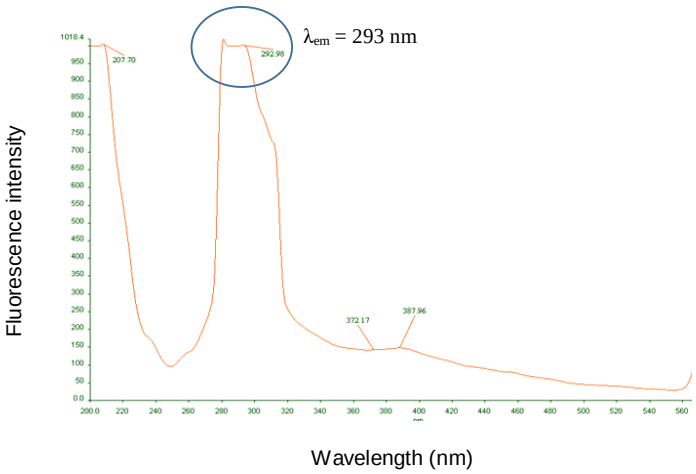

(iii) Insulin-containing SLNs

Figure 4.6 Fluorescence emission spectra of insulin at λ_{ex}= 255 nm for (i) insulin solution, (ii) insulin-free SLNs and (iii) insulin-containing SLNs

4.4.2.3 Confocal Laser Scanning Microscopy (CLSM)

Confocal laser scanning microscopy (CLSM) (Olympus FV1000 Fluoview) has the ability to image nanoparticles under microscopy and simultaneously provide information on the fluorescence intensity of the SLNs particles upon laser stimulation. CLSM imaging of the nanoparticles was based on insulin's autofluorescence ability due to the presence of tyrosine residues (Figure 4.5) as well as based on fluorescent lipid probe Nile Red incorporated within the lipid tripalmitin in SLNs. Erni *et al.* (2002) labelled lipid tripalmitin at 0.1 %w/w Nile Red fluorescent dye with respect to the mass of tripalmitin to evaluate the potential of cationic solid lipid microparticles as an efficient carrier system in the delivery of therapeutic macromolecules to phagocytic cells. The qualitative comparison of fluorescence intensity as expected for insulin is shown in Figure 4.5, while for Nile Red-labelled SLNs the intensity prediction is as shown in Figure 4.7. Figure 4.7 indicates that the fluorescence intensities are predicted to be higher for the solid solution model (Model A) as compared to the drug-enriched shell model (Model B) which was expected to display the least brightness.

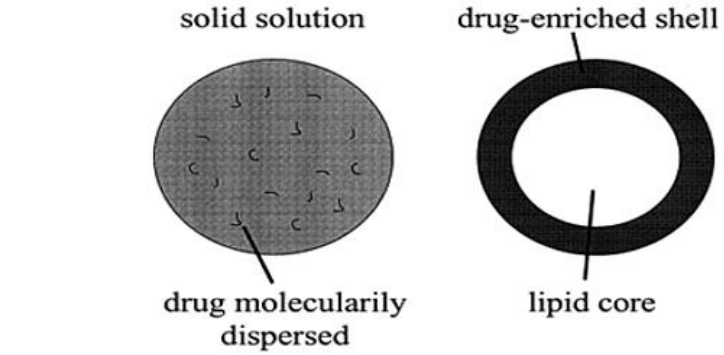

Figure 4.7 Prediction of fluorescence intensity of Nile Red-labelled lipid through relative comparison for each drug localisation models (+ indicates low intensity; ++ indicates high intensity)

As shown in Figure 4.8, the CLSM images of both insulin-containing SLNs and insulin-free SLNs displayed fluorescence emission upon laser stimulation. This interesting observation was not expected as insulin-free SLNs also fluoresced in the same manner as insulin solution, therefore it would be impossible to differentiate the fluorescence intensities when both particles and drug of interest fluoresces intensely at any wavelengths of laser stimulation. Dissolving the fluorophore Nile Red in lipid tripalmitin also did not yield any differences (Fig. 4.9). These findings using CLSM did not appear conclusive.

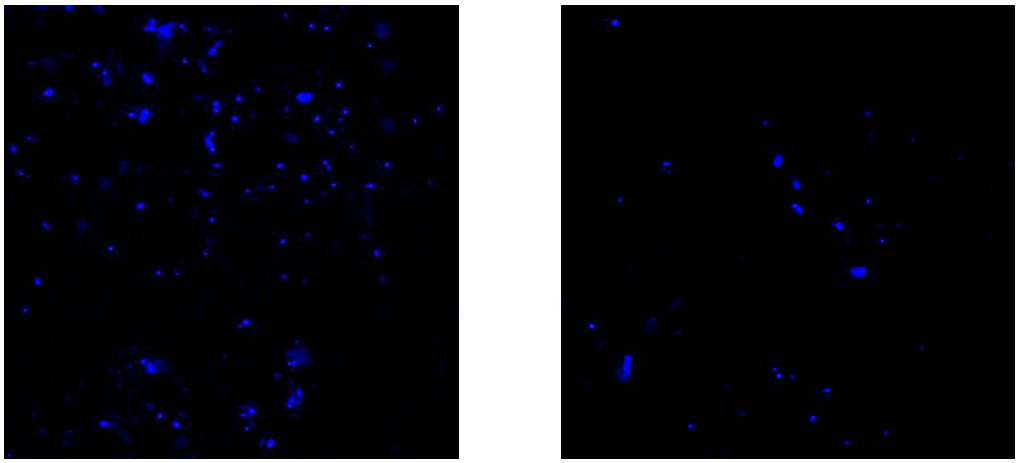

(a) (b)

Figure 4.8 Image acquired from CLSM imaging of (a) insulin-containing SLNs and (b) insulin-free SLNs

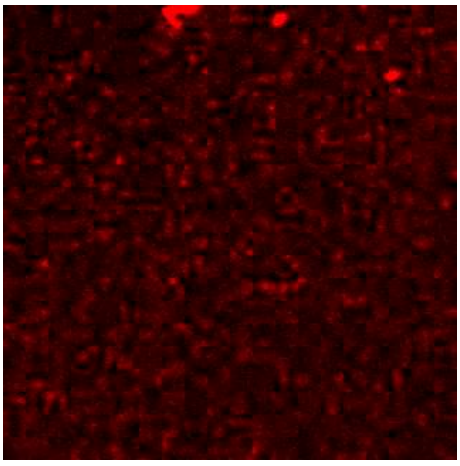

Figure 4.9 Image acquired from CLSM imaging of insulin-containing SLNs tagged with lipid fluorescent dye Nile Red at $\lambda_{ex}/\lambda_{em}$ = 530/590 nm

4.4.3 Zeta Potential Measurements

Zeta potential measurement was used as a further means to help in indirectly deciphering the different location of insulin within the SLNs. A study by Aboubakar *et al.* (1999b) adopted the zeta potential measurements in order to predict the location of drug within colloidal particles, by means of a differential gradient in zeta potential values. The measurements were carried out to determine whether insulin was completely encapsulated within the core of the nanocapsules or that it was simply adsorbed onto the surface of the nanocapsules. This novel use of zeta potential measurements suggested that it is indeed possible to determine the insulin location within poly(isobutylcyanoacrylate) polymeric nanocapsules prepared by interfacial polymerisation method, since surface-adsorbed insulin caused a decrease in zeta potential value (Aboubakar *et al.*, 1999b). In their work, the formulated insulin-loaded nanocapsules recorded an almost identical zeta potential value of -19 mV as the unloaded nanocapsules. Thus, it was hypothesised that the insulin was completely encapsulated within the core of the nanocapsules with respect to the identical zeta potential values (Aboubakar *et al.*, 1999a, 1999b).

This thus formed the basis for the use of zeta potential measurements in the present study as a potential indirect indicator of the location of insulin within the SLNs. The SLNs formulations prepared here fitted just two of the three hypothesised drug incorporation models (Fig. 1.8), as it was impractical to achieve all three possibilities due to formulation constraints, as explained earlier.

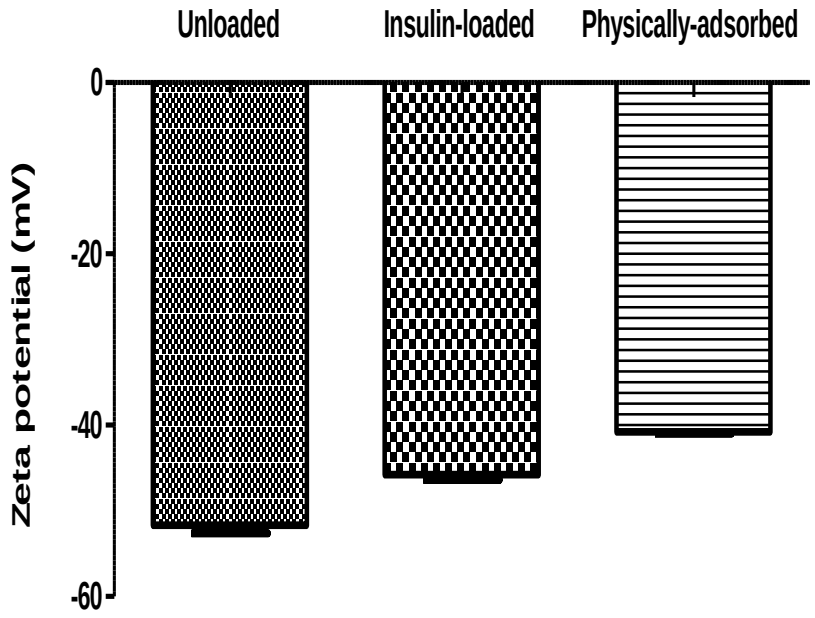

Figure 4.10 Zeta potential values of unloaded, insulin-loaded and physically-adsorbed insulin SLNs formulations (*n*=3).

The mean zeta potential value of insulin-free SLNs was found to be -51.7 ± 1 mV. The insulin-loaded SLNs formulation and the physically-adsorbed insulin SLNs were -45.8 ± 1 mV and -40.8 ± 1 mV respectively (Fig. 4.10).

In the absence of insulin within the SLNs formulation, the zeta potential of the unloaded SLNs was the highest in magnitude and negative (-51.7 ± 1 mV). This negative magnitude in zeta potential is ascribable to lecithin (emulsifier), which contains two alkyl chains and an ionised phosphate hydrophilic group, which bears a net negative charge (Kunitake and Okahata, 1978).

Zeta potential is influenced by small changes within the electrical properties of the particle surface, due to the adsorption of peptides, proteins, or any other polyelectrolytes at the surface of the colloidal particles (Aboubakar *et al.*,

1999a). With the incorporation of insulin within the SLNs formulations (insulin-loaded SLNs), there was a significant decrease in mean zeta potential value to -45.8 ± 1mV (p<0.05). The physically-adsorbed insulin SLNs showed further decrease in zeta potential value (-40.8 ± 1 mV) as compared to the unloaded SLNs (p<0.05). This most certainly is due to the positive charge contribution by insulin that neutralises the negative charge induced by lecithin and indicates that most of the insulin is surface-based. Insulin carry a net positive charge when their pH is below the isoelectric point, and vice versa. The isoelectric point for insulin is 5.3 (Park, 1999), therefore when dissolved in an acidic environment (~ pH 2), it carries a net positive charge. This finding is consistent with that reported by Aboubakar *et al.* (1999b) who described the presence of surface-adsorbed insulin could induce variation in zeta potential to the more positive range in a concentration-dependent manner. The decrease in zeta potential value of SLNs due to physically-adsorbed insulin can be attributed to the neutralisation of the negative charge on insulin-free nanoparticle as a result of insulin molecules adsorbing on the surface of the SLNs. The adsorption occurs in the Stern layer of the colloidal particle, where the net electrical charge of the surface becomes less negative as reflected from the zeta potential measurements. The decrease in the zeta potential value therefore appeared to be more prominent in the physically-adsorbed insulin SLNs formulations. This further suggests that the protein-surface interaction is governed by electrostatic attraction of the insulin and the lipid nanoparticles.

4.4.4 *In vitro* drug release studies

In vitro drug release studies can be used to reflect the accessibility of the drug to the dissolution medium (Mühlen *et al.*, 1998), as mentioned in Section 4.1.1. This section describes results on the two insulin-containing SLNs formulations (Section 4.4.1) in order to further support the observations made in Section 4.4.3.

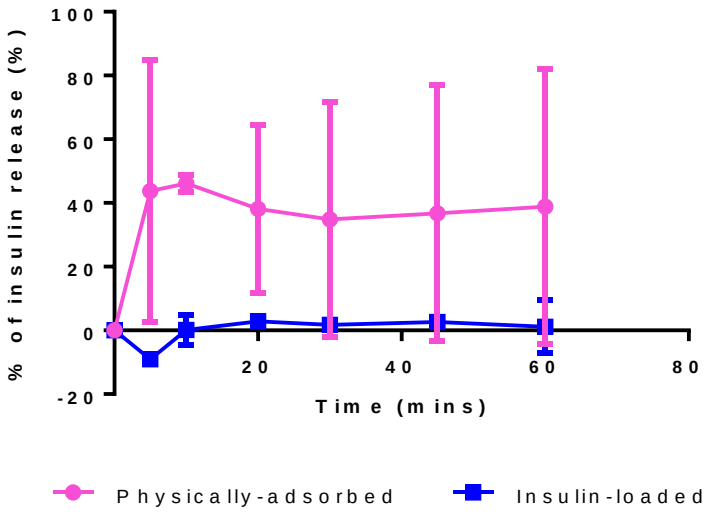

Figure 4.11 Insulin release profile over 1 hour of *in vitro* drug release studies for both SLNs formulations (*n=3*).

Here, the *in vitro* insulin release studies for both SLNs formulations were evaluated using two different methods, namely HPLC analysis and zeta potential measurements. For HPLC analysis, release of insulin from the SLNs formulations was quantified and subsequently presented as percentage (%) of insulin release over a study period of 1 hour (Fig. 4.11). It was, however, observed here that no significant differences were demonstrated in the insulin

release profiles for both insulin-loaded SLNs formulations and physically-adsorbed insulin SLNs (p>0.05) (Fig.4.11). The amount of insulin released from the respective SLNs formulations were comparable in this instance and therefore, it was not possible to differentiate the release profiles between both these formulations and to deduce information accordingly. Here, the findings from HPLC analysis did not appear to be conclusive, as the small quantity of released insulin from both SLNs formulations displayed differences which were deemed insignificant.

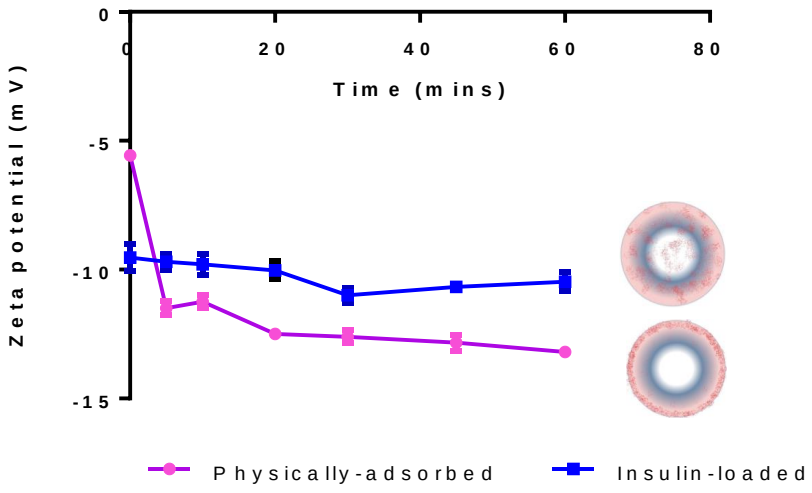

Figure 4.12 Zeta potential measurements over 1 hour of *in vitro* drug release studies for both SLNs formulations (n=3).

Apart from evaluating the release of insulin using HPLC analysis, zeta potential measurements were also performed on both SLNs formulations over the same study duration. Zeta potential values reflect the surface charges on the lipid nanoparticles, as described earlier. Any changes in the zeta potential values suggest that the nanoparticles surface charges have been modified, and that

these changes correspond to the rate of insulin released from the nanoparticles. The figure shows an increase in zeta potential values as a function of insulin release from both types of nanoparticles (Fig. 4.12). As described previously, the presence of insulin on the surface of the nanoparticle contributes to a positive magnitude in zeta potential values. Therefore, the reverse is true when insulin is released from the nanoparticle surface.

Interestingly, both insulin-containing SLNs formulations exhibited distinctively different release profiles when evaluated using zeta potential measurements (p<0.05) (Fig. 4.12), despite that being not evident in the profiles shown in Figure 4.11. Based on Figure 4.12, the changes seen in the zeta potential values clearly indicate that there were indeed changes in the surface charges of the nanoparticles over the study duration of 1 hour as a result of insulin being released from the SLNs. This is a particularly interesting finding where a small amount of insulin released from the different SLNs formulations can be reflected as distinctive differences in the zeta potential values, otherwise not demonstrated when using HPLC analysis in this instance.

Insulin-loaded SLNs formulation (Model A) displayed a release trend consistent with controlled release behaviour over a drug release period of 1 hour. In contrast, the physically-adsorbed insulin SLNs formulation had an initial burst release for the first 10 minutes of study, then gradually decreased and adopted a release profile similar to a sustained-release mechanism (Fig. 4.12).

The release profile of insulin-loaded SLNs formulation demonstrates that insulin was molecularly dispersed within the matrix of the SLNs. A gradual increase in zeta potential from –9.2 mV to –10.8 mV over an hour duration was recorded (Fig. 4.12). No distinctive burst release was observed in this instance, but a

slow and sustained insulin release (Fig. 4.12). This prolonged release profile is indicative of a longer path length that insulin diffuses through before reaching the dissolution medium and confirms that this formulation has an architectural arrangement that conforms to the solid solution model (Model A) illustrated in Figure 1.8. Unless the zeta potential of the insulin-loaded SLNs is recorded to be almost similar to that of unloaded SLNs due to complete encapsulation of insulin within the core of the nanoparticles, the model is ascribable to the solid solution model. Mühlen *et al.* (1998) also reported a similar controlled release profile where slow diffusion of the drug out from the lipid matrix was consistent in SLNs formulation that fits the homogenous solid solution model.

On the other hand, for the physically-adsorbed insulin-SLNs, the zeta potential value increased rapidly from –5.75 mV to –11.5 mV within 10 minutes of drug release studies, reflecting the initial burst release of insulin observed in Figure 4.12. Insulin physically-adsorbed on the SLNs permitted ease of insulin release into the aqueous phase, hence the initial burst release. The occurrence of initial burst release is that the adsorbed insulin is released unimpeded when the SLNs come into immediate contact with the dissolution media, thus confirming that insulin is present on the surface of the SLNs, forming a drug-rich outer shell (Model B) as illustrated in Figure 1.8.

Based on the results from the *in vitro* drug release studies by means of zeta potential measurements, we can conclude that the two types of drug incorporation models (Fig. 1.8), namely the solid solution model (Model A) and the drug-enriched shell core-shell model (Model B), have been successfully formulated.

4.4.5 STEM imaging

The STEM images of unloaded SLNs as well as insulin-loaded SLNs and physically-adsorbed SLNs are presented in Figure 4.13, 4.14(A) and 4.15(A) respectively, showing the rounded morphology of the SLNs. Prior to the insulin release studies, insulin-loaded SLNs (Fig. 4.14(A)) and insulin physically-adsorbed SLNs (Fig. 4.15(A)) appeared morphologically similar to those with unloaded SLNs (Fig. 4.13). However, it was observed that after these SLNs were subjected to 60 minutes of *in vitro* drug release studies, the physically-adsorbed insulin SLNs displayed a different morphology with a rough surface (Fig. 4.15(B)). The insulin-loaded SLNs post insulin release (Fig. 4.14(B)), however, seemed to have retained its shape.

Generally, drug release process from nanoparticles is governed by the (1) drug desorption of surface bound/adsorbed drug, (2) drug diffusion through the nanoparticle matrix or (3) nanoparticle matrix erosion/degradation (Dinda *et al.*, 2013; Mudshinge *et al.*, 2011). The external morphology of nanoparticles are subject to changes as a result of drug release from the nanoparticles. A spontaneous modification of the external morphology of the octreotide acetate-loaded PLGA polymeric microspheres was observed during the release of the peptide, where a porous appearance on the microsphere surface was apparent (Wang *et al.*, 2002). Degradation of the PLGA microspheres during the release of bovine serum albumin resulted in external morphological changes of the microspheres with the surfaces becoming wrinkled with several pores (Yang *et al.*, 2000).

The burst release of insulin from the physically-adsorbed SLNs is due to desorption of the surface bound insulin from the nanoparticles within a short

duration. This also indicates the presence of a weak interaction between the insulin and the lipid nanoparticle which allows easy dissociation of insulin. It has been reported that drug release can also be affected by the ionic interaction between the drug as well as the auxiliary ingredients in the formulations (Mudshinge *et al.*, 2011). Both tripalmitin and lecithin have the ability to form hydrogen bonding due to the presence of hydrophilic –OH functional groups and the polar head group of the lecithin, which contributes to the formation of weak hydrogen bonds between insulin molecule and the components of the SLNs. It is also possible for insulin to be electrostatically attracted to the negatively charged SLNs due to the opposing surface charges (Aboubakar *et al.*, 1999b), which formed the basis of the zeta potential measurements as described in section 4.4.3. This is because insulin carries a net positive charge below its isoelectric point of 5.3 (Park, 1999). The nature of these attractive forces are relatively weak and therefore allows easy dissociation of insulin from the SLNs, reflected as the burst release effect.

Desorption of insulin from the nanoparticle surface of physically-adsorbed insulin-SLNs will destabilise the charge on the SLNs. The modified surface morphology, with rough surfaces and porous edges seen on the surface of the physically-adsorbed insulin SLNs after 60 minutes of incubation in the release medium (Fig. 4.15(B)), is a result of surface erosion due to the inability of the lipid matrix to retain its integrity. At a faster drug release rate, there is a greater tendency of lipid Gelucire 50/13 matrix erosion taking place via surface disintegration due to the flexibility of the surface during swelling (Khan and Craig, 2003).

Conversely, the insulin-loaded SLNs did not exhibit surface erosion (Figure 4.14(B)) as compared to the physically-adsorbed insulin-SLNs. Insulin released

from the insulin-loaded SLNs is governed by diffusion through the nanoparticle matrix which is consistent with the controlled release profile of a solid solution drug incorporation model. Such a system only displays the erosion characteristics when the diffusion of the drug is faster than the matrix erosion, and therefore diffusion largely controls the mechanism of drug release (Aguilar, 2013). The surface erosion of the nanoparticles was not apparent in the absence of insulin burst release (Fig. 4.14(B)). It can therefore be attributed to the rapid release of insulin from the nanoparticle surface which had compromised the lipid matrix integrity, causing external morphological changes of the nanoparticles such as surface erosion.

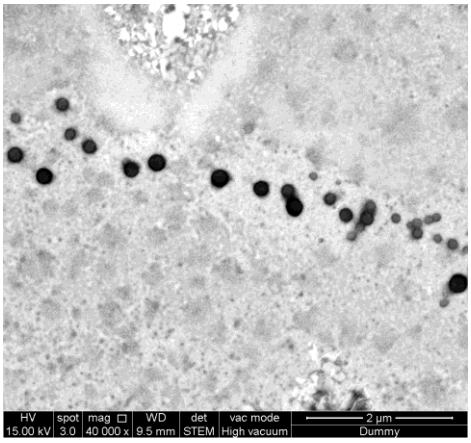

Figure 4.13 STEM image of unloaded SLNs

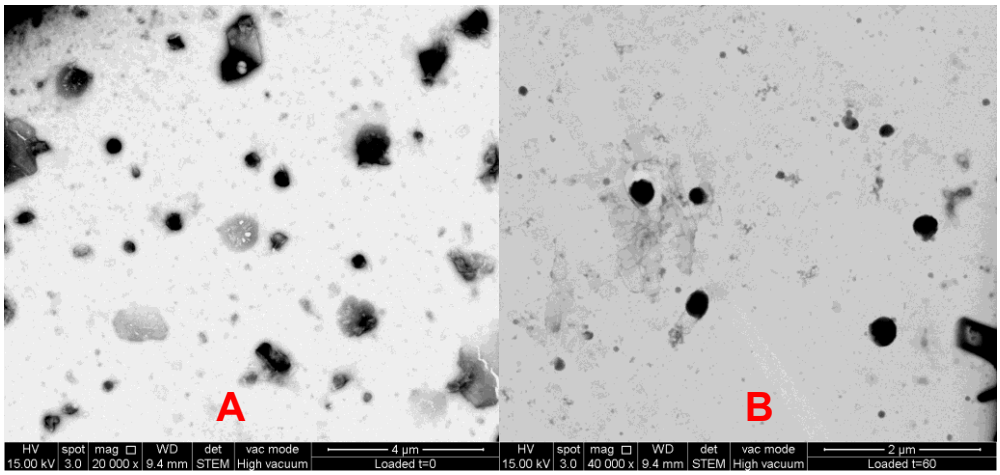

Figure 4.14 STEM images of insulin-loaded SLNs over release duration of (A) 0 minute and (B) 60 minutes.

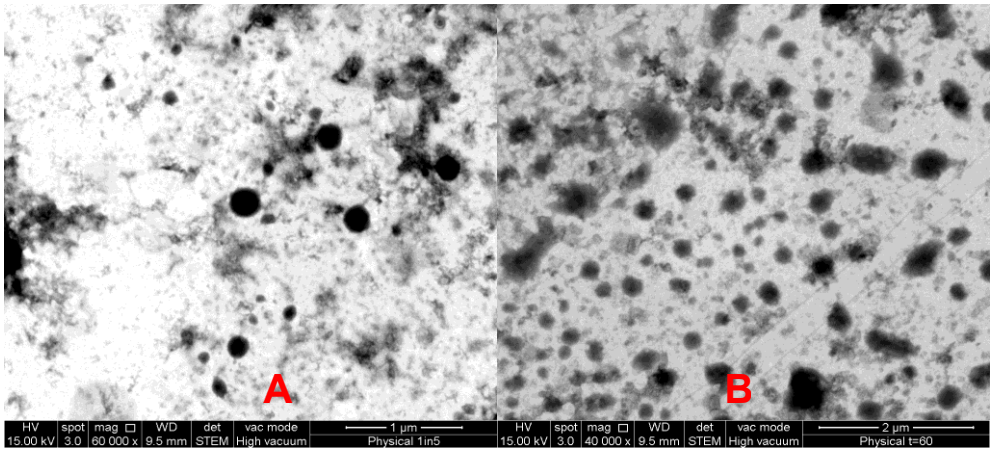

Figure 4.15 STEM images of physically-adsorbed SLNs over release duration of (A) 0 minute and (B) 60 minutes.

4.5 Concluding remarks

It is shown here that two of the three hypothetical drug incorporation models have been achieved and successfully prepared. Following the fabrication of the insulin-containing SLNs, a simple and reliable method to investigate the location of insulin within the SLNs lipid matrix was developed as it is indeed crucial for this study. Zeta potential measurements have been shown to be a potential indicator here, which is able to fairly suggest the location of insulin within the solid lipid nanoparticles. In addition, these findings have been further supported by *in vitro* drug release studies and STEM imaging.

In summary, the drug incorporation models that are possibly adopted by the fabricated SLNs formulations in this study are illustrated in Figure 4.16.

(A) Solid solution model

(B) Core-shell model with drug-enriched shell

Figure 4.16 Possible drug incorporation models adopted by (A) insulin-loaded SLNs and (B) insulin physically-adsorbed SLNs.

CHAPTER 5

Cellular uptake studies of Different Insulin-SLNs Localisation Models

5.1 Introduction

5.1.1 Cellular uptake of drug-loaded nanoparticles

Improved bioavailability is one of the main key goals in the development of a successful oral delivery system. For an orally administered system, the bioavailability is strongly influenced by the physicochemical properties of the nanocarriers and the drug uptake process across the gastrointestinal epithelium. Several methods have been explored in an attempt to improve the bioavailability of proteins following oral administration, such as the use of mucoadhesives, penetration enhancers, protease inhibitors and encapsulation of the payload in nanoparticles (Carino and Mathiowitz, 1999). Nanoparticles can offer protection to the incorporated insulin from the harsh environment of the gastrointestinal tract and also at the same time facilitate permeation across the epithelial barrier (Damgé *et al.*, 2007; Sarmento *et al.*, 2007a, 2007b).

Recent studies have emphasised the importance of understanding drug uptake process and the fate of nanoparticles after oral administration in order to develop more efficient oral nanocarriers (Plapied *et al.*, 2011). It is also vital to understand how these nanoparticles behave within the harsh environment of the gastrointestinal tract during the drug uptake (Deli, 2009). Once the mucosal layer is traversed, the drug-loaded nanoparticles have to be transported across the intestinal epithelium mainly via the paracellular and transcellular pathway, endocytosis and/or receptor-mediated endocytosis via either the enterocytes or M cells, before the drug is free to enter the systemic circulation. The drugs may appear as free or encapsulated in the systemic circulation post-absorption, and will therefore influence the pharmacokinetics as well as their biodistribution in the body (Plapied *et al.*, 2011).

Possible mechanisms of drug uptake across the intestinal epithelium are illustrated in Figure 5.1 (Shah *et al.*, 2006).

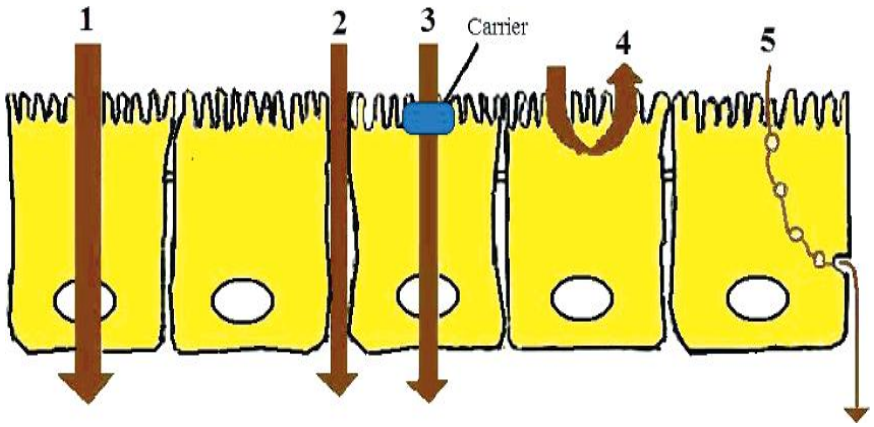

Figure 5.1 Schematic illustration of mechanisms of drug uptake across the intestinal epithelium: (1) passive transcellular route, (2) passive paracellular route, (3) carrier-mediated transport, (4) carrier-mediated efflux, and (5) vesicular transport.
(Adapted from Shah *et al.*, 2006).

The transport of therapeutic proteins across the enterocytes can occur via several pathways, primarily through the cell membrane of the enterocytes (transcellular) or via the tight junctions between the cells (paracellular), although uptake by this route is relatively small (Balimane *et al.*, 2000; Kavimandan and Peppas, 2008). Passive transcellular pathway is favoured for non-polar and lipophilic drugs. However, insulin, a hydrophilic peptide, has a low octanol-water partition coefficient of approximately 0.0215 (Lee, 1987). Therefore, passive transcellular transport of insulin across the hydrophobic cell membrane is not favourable. Instead, the preferred route is the transcellular pathway which involves the binding of proteins to specific receptors, known as receptor

mediated endocytosis (Morishita *et al.*, 2002). Aqueous paracellular pathway is another possible alternative route for insulin transport across the intestinal epithelium (Kavimandan and Peppas, 2008). However, as mentioned earlier, insulin is highly susceptible to enzymatic degradation and any possible uptake by carrier proteins may be negated by the degradation.

A study has suggested that the delivery of insulin using poly (methacrylic acid-g-ethylene glycol) [P(MAA-g-EG)] polymeric microparticles facilitated the transport of insulin across epithelium via the paracellular route (Kavimandan *et al.*, 2003). The drug uptake was governed by the physicochemical properties of the nanoparticles once the drug is encapsulated within the nanoparticles. Nanoparticles can be used to improve the transport of the encapsulated drugs across the epithelium, owing to various mechanisms such as mucoadhesion to mucosa, nanoparticle internalisation in enterocytes and permeation enhancing effects (Sarmento *et al.*, 2007a). Nanoparticles can be transported via the transcellular route, either through the M-cells of the Peyer's patches in the gut-associated lymphoid tissue (GALT) or through enterocytes via receptor-mediated endocytosis (Clark *et al.*, 2001; Hussain *et al.*, 2001; Sarmento *et al.*, 2007a). The pathway taken by the drug-loaded nanoparticles for internalisation into the cells depends largely on the physicochemical characteristics of the nanoparticles as well as the type of cells, for example M cells of the Peyer's patches are more likely to take up larger nanoparticles (>100 nm) (des Rieux *et al.*, 2007; Hillaireau and Couvreur, 2009). It has been reported that the fate of the nanoparticles is also influenced by the composition of the nanoparticles, whether the nanoparticles will remain intact after traversing the cells (Plapied *et al.*, 2011).

5.1.2 Caco-2 cell line

The development of *in vitro* models such as cell culture has opened up vast opportunities to researchers to better understand and predict how particles are taken up by intestinal cells, since it is not always feasible to conduct *in vivo* studies. Cell culture studies have proven to be a useful alternative tool as the data from cell culture studies have been validated by the findings from published *in vivo* studies (Delie, 1998).

Caco-2 cell line is a continuous line of heterogeneous human epithelial colorectal adenocarcinoma cells originally obtained from a 72-year adult Caucasian male. It is one of the collection of one hundred and twenty seven cell lines first established from gastrointestinal tumours in the 1970s for the purpose of performing studies to understand cancers and the related cytotoxic drugs (Fogh *et al.*, 1977). The human intestinal Caco-2 cell line has been widely studied over the last thirty years as a model intestinal barrier, owing to the capability of this cell line to undergo spontaneous differentiation in long-term culture to achieve a cell monolayer that expresses resemblance to the mature enterocytes in terms of the morphological and functional characteristics (Hidalgo *et al.*, 1989; Pinto *et al.*, 1983; Sambuy *et al.*, 2005). The differentiated cells form a monolayer that exhibits a cylindrical polarised morphology, with microvilli and tight junctions as well as uptake transporters and several intestinal enzymes (eg. peptidases, esterases) (Sambuy *et al.*, 2005). Hence, it is suitable to use this cell line as an intestinal membrane model for this present study.

5.1.3 Aims and Objectives

Insulin-containing SLNs of the solid-solution model and the core-shell model with a drug-enriched shell, were successfully prepared and the location of insulin within the SLNs were ascertained as described in Chapter 4. In this chapter, the propensity of these SLNs to be taken up by Caco-2 cell line was investigated. To our knowledge, no literature has so far correlated the location of drug payload within a nanoparticle with the mechanism of uptake across the intestinal epithelium, and this is the first report on such a study. As mentioned in previous chapters, the propensity of SLNs to be taken up in the gastrointestinal tract depends largely on its physicochemical properties. We believe that possible interactions occur between the SLNs and the epithelia prior to uptake and that the localisation of insulin within the SLNs might point to such possible interactions.

5.2 Materials

Caco-2 cells (ATCC® designated No: HTB-37™) were obtained from the American Type Culture Collection (ATCC, Manassas, Virginia, U.S.A). Culture medium consists of Minimum Essential Media (MEM) with L-glutamine and Phenol Red (Gibco® BRL Life Technologies, New York, U.S.A.), standard Fetal Bovine Serum (FBS) (Cellgro® by Mediatech, Inc., U.S.A.) and Penicillin-Streptomycin (Pen-Strep) liquid (100X) (Gibco® BRL Life Technologies, New York, U.S.A.). Other supplements included in the culture medium were Sodium Pyruvate (100 mM) and MEM Non-Essential Amino Acids (NEAA) Solution (100X) (Gibco® BRL Life Technologies, New York, U.S.A.). 0.25 % Trypsin in ethylenediaminetetraacetic acid disodium salt (EDTA) (Cellgro® by Mediatech,

Inc., U.S.A.) was used as the trypsinising solution for cell detachment. For the purpose of washing the cell lines, Calcium (Ca^{2+}) and Magnesium (Mg^{2+}) free Phosphate-Buffered Saline (PBS) at pH 7.4 was obtained from (Cellgro® by Mediatech, Inc., U.S.A.). Both trypan blue and dimethyl sulfoxide (DMSO) were obtained from Sigma Aldrich, U.S.A.). Insulin-free SLNs and insulin-containing SLNs were prepared as described in Chapter 3 and 4.

5.3 Methods

5.3.1 Cell culture protocols

Cell culture protocol for Caco-2 cell line was adapted and modified from ATCC. The human colorectal adenocarcinoma Caco-2 cell line was grown under standard culture conditions of 37 °C, 70 % humidity and 5 % CO_2, in a culture medium of MEM, supplemented with 20 % FBS, 1.0 mM sodium pyruvate, 1 % non-essential amino acids and 1 % Pen-Strep antibiotic solution.

For thawing of cryopreserved cells, the cell culture medium was firstly pre-warmed to 37 °C in a water bath for 30 minutes prior to use. The frozen Caco-2 cell line contained in a cryovial was removed from the liquid nitrogen vessel and placed in the water bath at 37 °C until the content was completely thawed. The contents were then transferred to a 25 cm^2 cell culture flask (Nunc™, U.S.A.) with 5 ml of pre-warmed cell culture medium. The cell culture flask was subsequently placed in an incubator at 37 °C, 70 % humidity and 5 % CO_2. The cell culture medium was changed 24 hours after seeding.

The cultured cells proliferated until the cells occupied all the available spaces on the substrate, known as reaching confluency (Freshney, 2000). At this point,

subculturing or passaging of these confluent cells was necessary to provide more room for continued growth, avoiding senescence from occurring as a result of prolonged high cell density. The cell culture medium and trypsin as well as PBS were warmed to 37 °C in a water bath prior to use. The medium was aspirated from the culture flask using a sterile serological pipette and the adherent cells were gently rinsed with Ca^{2+} and Mg^{2+} free PBS to remove traces of the medium. 0.25 % trypsin-EDTA (1 ml for 25 cm^2 cell culture flask; 3 ml for 75 cm^2 cell culture flask) was added into the flask and then incubated at 37 °C for 5 minutes to detach the cells. The flask was then gently swayed and tapped to aid cell detachment. Next, the cells were viewed under an inverted microscope (Nikon Eclipse TS100, Japan) to ensure the cells were fully detached from the bottom of the flask. Fresh culture medium (5 ml for 25 cm^2 cell culture flask; 15 ml for 75 cm^2 cell culture flask) was added into the culture flask and the re-suspended cells were centrifuged for 5 minutes at 1500 rpm at 4 °C (Universal 320R, Hettich Centrifuge, Germany). Thereafter, the supernatant was discarded and the soft cell pellet was re-suspended in fresh culture medium. The single cell suspension was then diluted and split into different flasks. A change of culture medium was carried out every 48 hours to ensure a conducive environment for the cells, until the cells achieve confluence and ready to be subcultured.

The concentration of cells in the culture was estimated by performing a cell counting procedure on the cell suspension, calculated using the following equation (Eq. 5.1):-

$$C = \frac{n}{v} \times d$$

(Eq. 5.1)

where C = concentrations of cells (cells / ml); n = average number of cells (cells / mm^2 area); v = volume counted (10^{-4}); d = dilution factor due to trypan blue solution.

5.3.2 Cellular uptake

The Caco-2 cells grown to confluency on T25 flask were harvested. The cells were seeded in a 12-well sterile tissue cell culture plate with flat bottom (BD Falcon®, U.S.A.) at the seeding concentration of 1 x 10^5 cells/3.8 cm^2 well and incubated at standard culture conditions (37 °C, 70 % humidity, 5 % CO_2). After 24 hours, the old cell culture medium was aspirated and was replaced with fresh culture medium into each well. 400 µl of treatment solutions, representing physically-adsorbed insulin-SLNs and insulin-loaded SLNs formulation, were pipetted into each of the wells in triplicates (*n=3*). Untreated cells and cells treated with insulin-free SLNs were used as controls. For blank, the experiment was carried out using culture medium only, in the absence of cells. The plate was incubated again (37 °C, 70 % humidity, 5 % CO_2) and removed at time intervals of 30, 60 and 90 minutes for viewing under the inverted microscope (Nikon Eclipse TS100, Japan) to examine and distinguish the differences in the Caco-2 cells upon treatments with insulin-containing solid lipid nanoparticles.

5.4 Results and Discussion

5.4.1 Maintenance of Caco-2 cell line

Caco-2 cell line was maintained at standard cell culture conditions as detailed in Section 5.3.1. The cells were grown in 25 cm^2 (T25) tissue culture flask with a vented cap (Orange Scientific, Belgium). Daily culture check was performed, including examining the media colour and media clarity. A microscopic check on the cell confluence, morphology and contamination was also necessary by viewing the Caco-2 cells under an inverted microscope which was equipped with a camera (Nikon Eclipse TS100, Japan) (Fig. 5.2 and Fig. 5.3). The cells were passaged according to the subculturing protocol in Section 5.3.1, 72 to 96 hours after seeding when the cells achieved confluence.

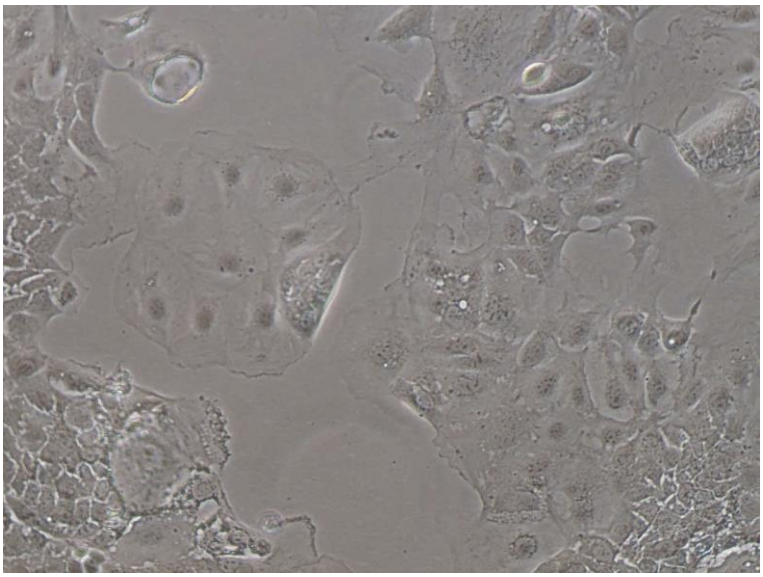

Figure 5.2 Caco-2 cells 24 hours post seeding. (100x magnification)

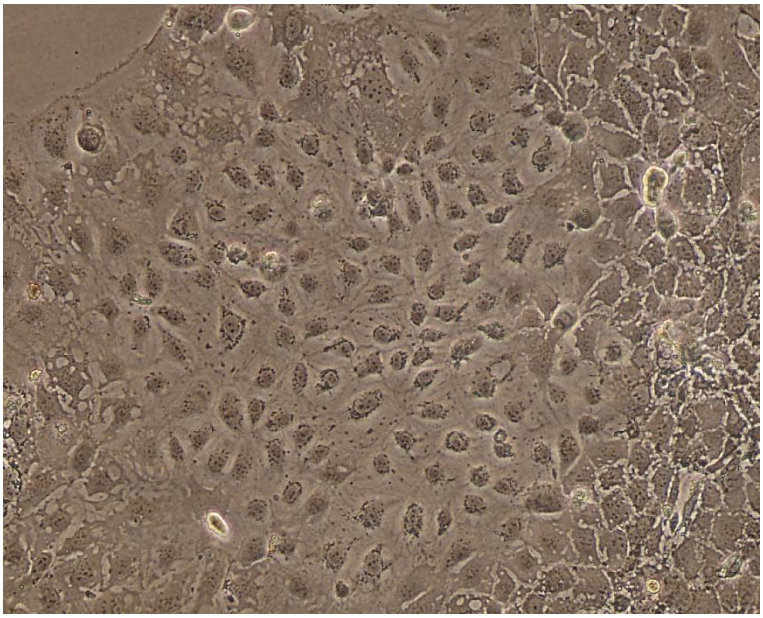

(a)

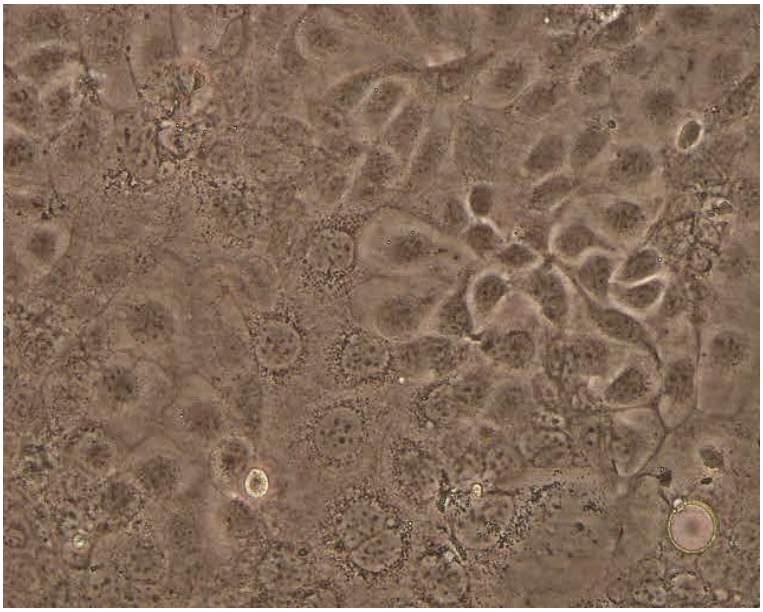

(b)

Figure 5.3 Confluent Caco-2 cells 96 hours post seeding, viewed under an inverted microscope at (a) 100x magnification and (b) 200x magnification.

5.4.2 Cellular uptake

Cellular uptake of insulin-containing SLNs across Caco-2 cells were studied over a duration of 90 minutes. The Caco-2 cells were initially seeded on a 12-well tissue cell culture plate (BD Falcon®). The plate was incubated for 24 hours to allow the cells in each individual well to achieve confluence. Figure 5.4 shows the microscopy image of confluent Caco-2 cells prior to treatment, which depicts healthy cells. The cells were thereafter treated with insulin-loaded SLNs and physically-adsorbed insulin SLNs, while the controls were untreated cells, insulin-free SLNs as well as free insulin solution. These treated cells were incubated for a total study duration of 90 minutes. During the treatment period, microscopy images were taken at a half hourly interval. The photomicrographs of Caco-2 cells which represents the cellular uptake of these nanoparticles based on the respective treatments that were carried out on the cells, were taken at regular time intervals of 30, 60 and 90 minutes (Fig. 5.5).

Figure 5.4 Photomicrograph of Caco-2 cells seeded on a 12-well cell culture plate prior to treatment. (100x magnification)

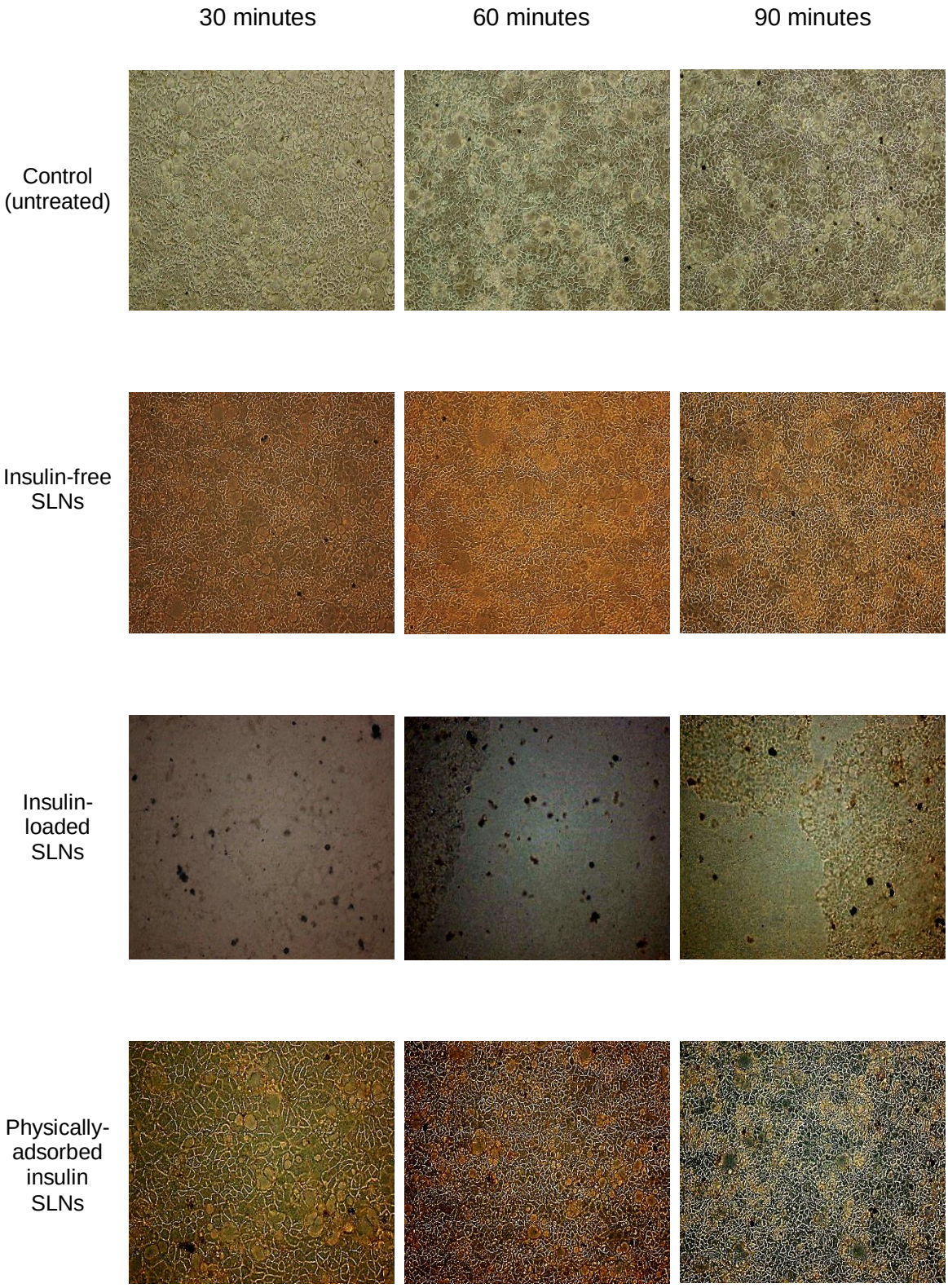

Figure 5.5 Photomicrographs of Caco-2 cells from the cellular uptake studies taken at 30 minutes, 60 minutes and 90 minutes after treatment. (100x magnification)

Based on the images in Figure 5.5, we can say that the untreated Caco-2 cells (control) remained healthy and confluent throughout the study duration. When the Caco-2 cells were exposed to insulin-free SLNs, the cells appeared to be confluent and morphologically similar to those seen in the untreated group even after 90 minutes of incubation period. Interestingly, the Caco-2 cells that were exposed to the insulin-loaded SLNs and the physically-adsorbed insulin SLNs, displayed contrasting observations in terms of the appearance of the Caco-2 cells. Here, we observed that by exposing the Caco-2 cells to the insulin-loaded SLNs, cell death had occurred as early as 30 minutes of treatment. The images showed cell shrinkage and subsequently cell detachment from the substrate, leaving traces of dead cells in the individual wells. In contrary, this occurrence was not apparent in the treatment group of physically-adsorbed insulin SLNs. Over the incubation period of 90 minutes, the Caco-2 cells remained confluent with minimal cell death. The cell morphology here also appeared similar to those cells exposed to insulin-free SLNs.

It is important to note that these observations were made based on viewing the cells under the inverted microscope to determine any differences in the appearance of the Caco-2 cells upon exposure to different SLNs formulations. Cellular uptake of the nanoparticles by the absorptive cells was not evident in this case (Fig. 5.5). Nevertheless, the differences in the cell appearance may allow us to predict possible differences in the uptake of SLNs by the cells, though further investigation such as fluorescence imaging of the cells was certainly required to confirm such findings.

The insulin-free SLNs prepared as described in Chapter 3, was composed of tripalmitin as the core lipid material. Tripalmitin has often been used in pharmaceutical preparations for its biodegradability and safety benefits, where

it is of the generally regarded as safe (GRAS) status. Several studies have addressed the safety issues and the *in vitro* toxicity and tolerability of SLNs (Doktorovova *et al.*, 2014; Petersen *et al.*, 2011; Severino *et al.*, 2014). It has been reported that SLNs and NLCs usually show better *in vitro* tolerability as compared to their polymeric counterparts (Doktorovova *et al.*, 2014). In order to prove that the lipid nanoparticulate carrier itself was non-toxic to the cells investigated, blank SLNs were included as a control in a study. It was, therefore, shown here that the tripalmitin SLNs formulation displayed good *in vitro* tolerability and was non-toxic to the Caco-2 cells. The influence of SLNs particle size on cell viability *in vitro* has been reviewed by Doktorovova *et al.* (2014) and it was reported that the highest cell viability was observed within the range of 100 to 300 nm (z-average). The reported z-average values were in good agreement with that of our SLNs formulations. On this basis, insulin-free SLNs have shown to be non-toxic to the Caco-2 cells being investigated (Fig. 5.5).

It can be recalled that insulin-loaded SLNs had caused cell death as early as 30 minutes of exposure. In contrary, physically-adsorbed insulin SLNs did not exhibit cell death over the duration of study which was similar to that seen in insulin-free SLNs. The contrasting observations were particularly notable for these two different types of insulin-containing SLNs formulations despite both having z-average values which were within the range of 100 – 300 nm, reportedly being optimal for cell viability (Doktorovova *et al.*, 2014). The extent of uptake and translocation of nanoparticles after oral administration is dependent on factors such as particle diameter, surface charge, surface ligands, shape and elasticity as well as their colloidal stability (Florence, 2005). Generally, absorption increases with decreasing particle diameter for nanoparticles with diameter below 1 µm. For particle diameters exceeding 1 µm,

particle uptake by the M-cells of Peyer's patches have been mainly implicated (Florence, 2005). Considering that the particle diameters for both these prepared SLNs formulations were of nano-sized range, the uptake of these SLNs was deemed to be efficient. Therefore, the different effects seen between both the insulin-containing formulations on the Caco-2 cells could potentially be directly related to the variances in the rate and the extent of SLNs uptake.

Lecithin has been reported to promote oral absorption of drug by favouring the passage of the SLNs through the intestinal wall (Bargoni *et al.*, 1998). Orally administered cyclosporine formulation containing lecithin permitted 45 times more cyclosporine to be taken up by cells than when excluded (Yanagawa *et al.*, 1989). In this instance, both of these SLNs also contained lecithin in their formulations which favours the uptake of nanoparticles. Cellular uptake and translocation of nanoparticles have also been reported to be influenced by surface charges of the nanoparticles (Florence, 2005; Hoshino *et al.*, 2004; Jiang *et al.*, 2008). Surface charges can affect the uptake of nanoparticles through surface charge-specific interactions. It was reported that for polymeric nanoparticles, the positively charged polymeric nanoparticles were found to interact mostly with clathrin on cell membranes, whilst the negatively charged polymeric nanoparticles were mainly internalised by lysosomal endocytosis (Bhattacharjee *et al.*, 2013). However, internalisation mechanisms for SLNs have been proven to be predominantly active transport, via both clathrin- and caveolae-mediated endocytosis, but not through macropinocytosis (Fan *et al.*, 2014; Martins *et al.*, 2012). Neutral and negatively charged nanoparticles were reported to have lower affinity of interaction with the negatively charged cell-membrane surface, hence lower levels of internalisation as compared to the positively charged nanoparticles (Verma and Stellacci, 2010). However,

another study found that the negative charges on the surface of SLNs does not appear to affect the uptake of the nanoparticles to the extent that results in a reduced uptake as observed for polymeric nanoparticles with negative surface charges (Bargoni *et al.*, 1998). Although the zeta potential values for insulin-loaded SLNs (-45.8 ± 1 mV) were higher in magnitude than that for physically-adsorbed insulin SLNs (-40.8 ± 1 mV), both SLNs have negative surface charges and therefore uptake via interaction with clathrin or caveolin would involve similar uptake mechanisms. Since the hydrodynamic size and surface charges of nanoparticles can influence the way cells respond to the SLNs, the contrasting behaviours observed between both types of insulin-containing SLNs is attributable to other possible contributing factors outlined below.

As observed, the two insulin-containing SLNs formulations caused cell death to different extents and they can be distinguished by the rate of death of the cells. We have observed a shorter time to cell death with the insulin-loaded SLNs. In contrast, the physically-adsorbed insulin SLNs when incubated with Caco-2 cells did not reveal widespread cell death, but minimal cell death. For insulin-loaded SLNs, insulin is molecularly dispersed within the lipid matrix and therefore the components of the lipid matrix exposed on the surface of the SLNs are recognisable as hydrophobic surfaces by the enterocytes. On the other hand, physically-adsorbed insulin SLNs were predicted to have a drug-enriched shell where insulin was mostly found adsorbed on the surface of the SLNs by electrostatic attractive forces. Hydrophobic surfaces of nanoparticles are believed to favour cell-nanoparticle interactions that can result in better uptake of nanoparticles by the intestinal epithelium, as compared to those with hydrophilic surfaces (Eldridge *et al.*, 1990). Thus, the differences seen in the effects of these insulin-containing SLNs on the Caco-2 cells (Fig. 5.5) could be

influenced by the surface hydrophobicity of the SLNs as a result of different localisation of insulin within the SLNs.

From the observations made, although not conclusive, we cannot discount the possibility of these observations being correlated to the cellular uptake of the SLNs. Since our findings suggested a distinctive differences in the appearance of the Caco-2 cells, it is indeed justifiable to further investigate the cellular uptake of the SLNs which has adopted different insulin localisation models by means of performing fluorescence imaging on the Caco-2 cells. This finding is therefore crucial as this key parameter can potentially influence the cell uptake of SLNs, which have not been discussed before.

5.5 Concluding remarks

Despite three different drug incorporation models being proposed by Müller *et al.* (2000) (Fig. 1.8), these models were suited to the incorporation of lipid soluble drugs. Having incorporated a hydrophilic drug in the lipid matrix, there was certainly a constraint in getting all three hypothesised localisation models. In this study, we have thus successfully fabricated insulin-containing SLNs which fitted the two different types of insulin localisation models, namely the solid-solution model (insulin-loaded SLNs) and the core-shell model with a drug-enriched shell (physically-adsorbed insulin SLNs). Furthermore, we found that these two different insulin localisation models demonstrated distinctive differences in the appearance of the Caco-2 cells upon exposure to these SLNs. It is important to note that it is not reasonable to accept these observations as the cellular uptake of the SLNs into the Caco-2 cells. However, the findings here potentially indicate that the cellular uptake can indeed be different for both of these SLNs, subject to further investigation by performing cellular uptake studies to confirm these findings. We have also shown that the insulin-free SLNs produced were non-toxic to the Caco-2 cells.

CHAPTER 6

Conclusion And Future Work

6.1 Conclusion

Diabetes is a progressive, chronic metabolic disease which remains as one of the leading causes of mortality worldwide. The major concern in this mortality data lies in the alarming increase in global prevalence with almost half still undiagnosed. Unfortunately, there is no cure for diabetes. Insulin is the mainstay of treatment for diabetics when other oral hypoglycaemic agents fail to achieve optimal blood glucose levels. Insulin, a polypeptide hormone, functions as the body's blood glucose regulator. Recent advances in biotechnology have brought vast opportunities to the medical sector by increasing the production of biopharmaceuticals, giving rise to the availability of insulin for therapeutic use. However, delivery of insulin to patients is indeed a real challenge. Being a protein, insulin is susceptible to enzymatic degradation along the gastrointestinal tract. Thus, insulin is currently administered via multiple subcutaneous injections albeit less well-received by the patients. There is a need for a desperate search of feasible alternative approaches, especially the more practical and acceptable oral route. Colloidal nanoparticulate delivery systems have been widely explored in recent years due to their ability to encapsulate, protect and deliver biopharmaceuticals via the oral route (Bilati *et al.*, 2005a; Vonarbourg *et al.*, 2006). In fact, solid lipid nanoparticles are favoured over other colloidal carriers especially for its lack of toxicity of physiological lipids as compared to polymeric nanoparticles.

In this study, we aimed to develop an insulin-containing colloidal nanoparticulate delivery systems based on solid lipid nanoparticles as a potential oral insulin delivery carrier. By utilising natural non-toxic constituents to formulate the SLNs, it was hoped that this potential carrier would offer the benefit of non-toxicity. Within this context, we aimed to establish whether the

localisation of insulin within the SLNs influenced the uptake of the nanoparticles by absorptive cells. To realise this objective, the insulin-containing SLNs are firstly formulated and characterised to optimise the nanoparticles. Following the fabrication, formulation and processing parameters were manipulated in order to achieve different insulin localisation models. Thereafter, we attempted to identify the location of insulin within the SLNs matrix by exploring viable methods to distinguish the different types of insulin localisation models that have been achieved. In order to investigate the influence of different insulin localisation models on the uptake of nanoparticles, *in vitro* cell culture studies were employed to distinguish the differences, if any, on the uptake of such lipid nanoparticles by absorptive cells.

As part of preformulation studies, a simple and reproducible HPLC method for insulin analysis was developed and validated with respect to linearity, precision and accuracy, followed by stability-indicating studies on insulin using HPLC and DLS technique to ascertain optimal storage and working conditions.

The solid lipid nanoparticles, comprising of palm oil lipids, were successfully fabricated using W/O/W double emulsion solvent evaporation technique. Production and processing parameters were optimised in order to attain desirable parameters, such as z-average, PdI, zeta potential and other physical properties. Selection of suitable lipid core compositions was investigated by employing either tripalmitin or palmitic acid, as the sole lipid or a combination of both, based on their unique feature that contain identical C_{16} saturated fatty acid chains. The optimised SLNs formulation consist of solely tripalmitin as lipid matrix and lecithin as emulsifier. The optimised SLNs has a mean size of 293.3 ± 5.2 nm and zeta potential of about -39.9 ± 1.3 mV. The size and zeta potential of the SLNs indicated a suitable and stable lipid nanoparticulate delivery system

to potentially deliver insulin. The SEM and TEM images verified that the lipid nanoparticles were spherical in shape with an approximate size diameter measured at 250 nm, which corresponded with the z-average value obtained from dynamic light scattering. No obvious particle aggregation of the SLNs formulation was detected when viewed under polarised light microscope, an indication of physical stability of the formulation, which was in good agreement with the zeta potential measurements obtained from DLS.

Using similar compositions, insulin-containing SLNs with two different localisation models were successfully achieved by means of carrying out modifications to the production parameters. In this study, it is indeed crucial to develop a simple and reliable method in order to ascertain the localisation of insulin within the SLNs lipid matrix. Zeta potential measurements have been shown to be able to suggest the location of insulin within the SLNs. To further complement the findings, drug release studies and STEM imaging were performed on both types of insulin-containing SLNs. This method which utilises DLS technique to measure zeta potential of the SLNs and applied in conjunction with drug release studies is certainly considered a milestone as it confirms its potential ability to serve as a useful indirect indicator of the drug location within the nanoparticles. The two possible drug incorporation models adopted by the insulin-containing SLNs formulations are the solid solution model (insulin-loaded SLNs) and the drug-enriched core-shell model (physically-adsorbed insulin SLNs).

From the *in vitro* cellular studies, we found that both these formulations with different insulin localisation models demonstrated distinctive differences when these nanoparticles were exposed to the Caco-2 cells. Our insulin-free tripalmitin SLNs was also found to be non-toxic to the Caco-2 cells, hence

potentially safe for oral delivery. The localisation of insulin was believed to be the reason behind the differences seen in the appearance of the Caco-2 cells. It is important to note that the contrasting observations made here potentially indicate that the cellular uptake can indeed be different for both of these SLNs, although further investigation is necessary to establish the cellular uptake of the fluorescent tagged insulin into the Caco-2 cells as part of future studies. However, this finding by itself is particularly significant as it highlights the importance of characterising drug localisation in nanoparticles, which has not been previously discussed, since it can potentially determine the cellular uptake of the insulin-containing SLNs and hence ultimately impact the drug bioavailability. For that reason, due emphasis should be given to the characterisation of drug location within the SLNs as one of the key parameters to be characterised during the formulation optimisation phase.

In conclusion, much interest has been focused on developing nanocarrier drug delivery system to deliver insulin orally in recent years and if found successful, it is expected to make a breakthrough in diabetes management. In this study, successful fabrication of insulin-containing SLNs with different localisation models has shown significant differences in cellular uptake of the nanoparticles. Characterisation of such parameter, which had not been addressed before, ought to be carried out in the development stages of SLNs formulation, in a bid to predict the efficiency of cellular uptake and ultimately the drug bioavailability in advance. Therefore, localisation of insulin within the SLNs is one of the significant contributing factors to the successful development of a promising oral insulin delivery in the future.

6.2 Suggestions for Future Work

Recent advances in the field of nanotechnology and biotechnology have brought vast opportunities to the development of nanoparticulate drug delivery systems that are safe and effective to deliver protein and peptide therapeutics. However, much research is required to deliver these nanoformulations orally as it still remains a challenge to ultimately achieve the clinical stage. Having successfully fabricated the two different types of insulin SLNs formulations (insulin-loaded SLNs and physically-adsorbed insulin SLNs), ongoing research will be focused on the gastrointestinal absorption aspect of the orally administered insulin-containing SLNs formulations in order to evaluate their gastrointestinal transit as well as the bioavailability of insulin. Here, we discuss some suggestions for future work as a further extension to the present one.

Insulin adsorption studies on the physically-adsorbed insulin SLNs (core-shell model with a drug-enriched shell) can be performed to evaluate whether the adsorbed insulin tends to form monolayers or multilayers, according to the Langmuir or Freundlich isotherms respectively. Moreover, it can provide better understanding of the nanoparticulate system in terms of its ability to associate with the drug, either governed by the incorporation approach (physical entrapment) or by means of great affinity of the peptide for the lipids (physicochemical association), as well as the drug release from the surface-associated nanoparticles (Garcia-Fuentes *et al.*, 2005b). In terms of evaluating the long-term stability of these nanoparticle formulations, an accelerated stability study can be performed using a stability separation analyser (LUMiFuge) by studying the real-time separation behaviour of the samples (Vitorino *et al.*, 2011).

Further evaluation in terms of the *in vitro* cellular studies of the current SLNs formulations is important as part of this work extension to develop a safe and efficacious oral insulin formulation. A cell viability study can be performed using diphenyltetrazolium bromide (MTT) assay to determine the effects of the insulin-containing SLNs formulations on the Caco-2 cell growth. Subsequently, performing a Caco-2 cell permeability assay is crucial to evaluate the response of the Caco-2 cell monolayer to the fabricated SLNs formulations as well as to assess the drug absorption process across the monolayer (Ma and Lim, 2003). When cultured as a monolayer, Caco-2 cells are able to differentiate to form tight junctions and expresses proteins and enzymes which mimics the human intestinal epithelium (van Breemen and Li, 2005). As an extension work from Section 5.4.2 to further improve the data and to evaluate the uptake mechanisms of the insulin-containing SLNs formulations, insulin is labelled with FITC which is a fluorescence tag. The Caco-2 cell monolayers treated with FITC-insulin SLNs will be examined under a confocal microscopy and the fluorescence-labelled insulin can be detected through green fluorescence (Yin *et al.*, 2009).

In vivo studies are useful as a proof of concept for the developed insulin-containing SLNs formulations. The bioavailability of the orally administered insulin is very much influenced by their transit rate in the gastrointestinal tract which is indeed a critical factor to determine the drug absorption (Kimura and Higaki, 2002). In order to study the biological efficacy of these SLNs formulations, they can be evaluated by means of sampling blood glucose levels as well as performing biopsies on the intestinal epithelium, ie. the follicular mucosa (Peyer's patches) and the non-follicular mucosa (Damgé *et al.*, 2007). The formulation will be administered orally to overnight fasted diabetic rats and

the plasma glucose levels of the rats can be determined by measuring the blood sampled from the tail vein of the rats at regular time intervals. Investigations on possible insulin absorption mechanisms and intestinal uptake can be examined by administering FITC-labelled insulin SLNs via intra-luminal injections in an *in situ* isolated intestinal loop (Damgé *et al.*, 2007; Sarmento *et al.*, 2007b). The biopsies of the intestinal epithelium sections can then be observed through confocal microscopy to detect the appearance fluorescent points representing the fluorescence-labelled insulin inside the structures.

It has been suggested that the main SLNs uptake pathway may be via the M-cells overlying the lymphoid follicles as well as the Peyer's patches and non-patches (Bargoni *et al.*, 1998). These formulations can be evaluated in terms of the extent of lymphatic uptake by administering radiolabelled SLNs formulations into the duodenum of the anaesthetised rats. Two catheters separating the lymph and the jugular vein allow simultaneous collection of each lymph and blood samples respectively (Bargoni *et al.*, 1998). The radioactivity found in both lymph and blood samples can be detected by gamma-counting which can provide insights on the extent of lymphatic uptake of the SLNs formulations.

Gastrointestinal transit rate of the orally administered drug has a significant influence on the drug absorption as it also determines the residence time of the drug in the absorption site which is particularly important since there is site-difference in drug absorbability (Kimura and Higaki, 2002). It is possible to analyse and estimate the drug absorption kinetics and the bioavailability of the orally-administered insulin SLNs formulations by applying the GI-Transit-Absorption Model, developed by Kimura and Higaki (2002), which takes into account site differences by dividing the GI tract into eight segments (stomach, duodenum, upper jejunum, lower jejunum, upper ileum, lower ileum, cecum and

large intestine). This can potentially provide additional information on the contribution of absorption in each different segments to determine the substantial absorption site of the formulation *in vivo*.

REFERENCES

A.D.A.M. Inc. "Lower digestive tract". Available at http://www.adamimages.com/Lower-digestive-anatomy-Illustration/PI1806/F4 (Accessed on 30th July 2014).

Abdelwahed, W., Degobert, G., Stainmesse, S., Fessi, H., 2006. Freeze-drying of nanoparticles: formulation, process and storage considerations. *Adv. Drug Deliv. Rev.*, 58, 1688–1713.

Aboubakar, M., Puisieux, F., Couvreur, P., Deyme, M., Vauthier, C., 1999a. Study of the mechanism of insulin encapsulation in poly (isobutylcyanoacrylate) nanocapsules obtained by interfacial polymerization. *J. Biomed. Mater. Res.*, 47, 568–576.

Aboubakar, M., Puisieux, F., Couvreur, P., Vauthier, C., 1999b. Physico-chemical characterization of insulin-loaded poly(isobutylcyanoacrylate) nanocapsules obtained by interfacial polymerization. *Int. J. Pharm.*, 183(1), 63-66.

Aguilar, M.I., 2004. *HPLC of Peptides and Proteins, Methods and Protocols.* Humana Press, Totowa, NJ.

Aguilar, Z., 2013. *Nanomaterials for medical applications*. Elsevier, Waltham, MA.

Aguilera, J.M. and Stanley, D.W., 1999. *Microstructural principles of food processing and engineering*. 2nd ed., Aspen Publ., Gaithersburg, MD.

Ahmad, A., Othman, I., Zaini, A., Chowdhury, E.H., 2012. Oral nano-insulin therapy: Current progress on nanoparticle-based devices for intestinal epithelium-targeted insulin delivery. *J. Nanomed. Nanotechnol.,* s4(007), 1-10.

Al-Haj, N. and Rasedee, A., 2009. Solid lipid nanoparticles preparation and characterization. *Int. J. Pharmacol.*, 5, 90–93.

Allémanna, E., Gurny, R., Doelker, E., 1993. Drug-loaded nanoparticles - Preparation methods and drug targeting issues. *Eur. J. Pharm. Biopharm.*, 39, 173–191.

Allémanna, E., Leroux, J.-C., Gurnya, R., 1998. Polymeric nano- and microparticles for the oral delivery of peptides and peptidomimetics. *Adv. Drug Deliv. Rev.*, 34, 171–189.

Almeida, A.J. and Souto, E., 2007. Solid lipid nanoparticles as a drug delivery system for peptides and proteins. *Adv. Drug Deliv. Rev.*, 59, 478–490.

Arbit, E. and Kidron, M., 2009. Oral insulin: the rationale for this approach and current developments. *J. Diabetes Sci. Technol.*, 3, 562–567.

Arbit, E., Majuru, S., Gomez-Orellana, I., 2008. Oral Delivery of Biopharmaceuticals Using the Eligen® Technology. *Drugs Pharm. Sci.*, 175, 285.

Association, A.D., 2010. Diagnosis and classification of diabetes mellitus. *Diabetes Care*, 33, S62–S69.

Awati, P.S., Awate, S. V., Shah, P.P., Ramaswamy, V., 2003. Photocatalytic decomposition of methylene blue using nanocrystalline anatase titania prepared by ultrasonic technique. *Catal. Commun.*, 4, 393–400.

Balimane, P. V, Chong, S., Morrison, R.A., 2000. Current methodologies used for evaluation of intestinal permeability and absorption. *J. Pharmacol. Toxicol. Methods*, 44, 301–312.

Bargoni, A., Cavalli, R., Caputo, O., Fundarò, A., Gasco, M.R., Zara, G.P., 1998. Solid lipid nanoparticles in lymph and plasma after duodenal administration to rats. *Pharm. Res.*, 15, 745–750.

Bargoni, A., Cavalli, R., Zara, G.P., Fundarò, A., Caputo, O., Gasco, M.R., 2001. Transmucosal transport of tobramycin incorporated in solid lipid nanoparticles (SLN) after duodenal administration to rats. Part II—tissue distribution. *Pharmacol. Res.*, 43, 497–502.

Barichello, J.M., Morishita, M., Takayama, K., Nagai, T., 1999. Encapsulation of hydrophilic and lipophilic drugs in PLGA nanoparticles by the nanoprecipitation method. *Drug Dev. Ind. Pharm.*, 25(4), 471–476.

Bawarski, W.E., Chidlowsky, E., Bharali, D.J., Mousa, S.A., 2008. Emerging nanopharmaceuticals. *Nanomed. Nanotech. Biol. Med.*, 4(4), 273–282.

Bayat, A., Larijani, B., Ahmadian, S., Junginger, H.E., Rafiee-Tehrani, M., 2008. Preparation and characterization of insulin nanoparticles using chitosan and its quaternized derivatives. *Nanomed. Nanotech. Biol. Med.*, 4(2), 115–120.

Bekard, I.B. and Dunstan, D.E., 2009. Tyrosine autofluorescence as a measure of bovine insulin fibrillation. *Biophys. J.*, 97(9), 2521–2531.

Benita, S., 2005. *Microencapsulation: Methods and Industrial Applications*, 2nd ed., CRC Press, Boca Raton, FL.

Beta Cell Biology Consortium. "The Structure of Insulin". Available at: www.betacell.org/content/articleview/article_id/8/ (accessed 7 October 2014).

Bhattacharjee, S., Ershov, D., Gucht, J. van der, Alink, G.M., Rietjens, I.M.C.M., Zuilhof, H., Marcelis, A.T., 2013. Surface charge-specific cytotoxicity and cellular uptake of tri-block copolymer nanoparticles. *Nanotoxicology*, 7, 71–84.

Bilati, U., Allémann, E., Doelker, E., 2005a. Development of a nanoprecipitation method intended for the entrapment of hydrophilic drugs into nanoparticles. *Eur. J. Pharm. Sci.*, 24(1), 67–75.

Bilati, U., Allémann, E., Doelker, E., 2005b. Poly(D,L-lactide-co-glycolide) protein-loaded nanoparticles prepared by the double emulsion method--processing and formulation issues for enhanced entrapment efficiency. *J. Microencapsul.*, 22(2), 205–214.

Binks, B.P., 2002. Particles as surfactants—similarities and differences. *Curr. Opin. Colloid Interface Sci.*, 7, 21–41.

Bonduelle, S., Carrier, M., Pimienta, C., Benoit, J.P., Lenaerts, V., 1996. Tissue concentration of nanoencapsulated radiolabeled cyclosporin following peroral delivery in mice or ophthalmic application in rabbits. *Eur. J. Pharm. Biopharm.*, 42, 313–319.

Bradshaw, T.P., 2000. *A User's Guide: Introduction to peptide and protein HPLC*. Phenomenex, USA.

Brange, J., 1994. *Stability of insulin: studies on the physical and chemical stability of insulin in pharmaceutical formulation*. Kluwer Academic Publishers, Dordrecht, The Netherlands.

Brange, J., Andersen, L., Laursen, E.D., Meyn, G., Rasmussen, E., 1997. Toward understanding insulin fibrillation. *J. Pharm. Sci.*, 86(5), 517–525.

Brange, J. and Langkjaer, L., 1992. Chemical stability of insulin. 3. Influence of excipients, formulation, and pH. *Acta Pharm. Nord.*, 4(3), 149–158.

Bressolle, F., Bromet-Petit, M., Audran, M., 1996. Validation of liquid chromatographic and gas chromatographic methods Applications to pharmacokinetics. *J. Chromatogr. B Biomed. Sci. Appl.*, 686(1), 3–10.

British Pharmacopoeia Commission, G.B., 2007. *British Pharmacopoeia 2007*. Stationery Office, London, UK.

Budhian, A., Siegel, S.J., Winey, K.I., 2007. Haloperidol-loaded PLGA nanoparticles: systematic study of particle size and drug content. *Int. J. Pharm.*, 336(2), 367–375.

Bunjes, H., Drechsler, M., Koch, M.H.J., Westesen, K., 2001. Incorporation of the model drug ubidecarenone into solid lipid nanoparticles. *Pharm. Res.*, 18(3), 287–293.

Bunjes, H. and Koch, M.H.J., 2005. Saturated phospholipids promote crystallization but slow down polymorphic transitions in triglyceride nanoparticles. *J. Control. Release*, 107(2), 229–243.

Calvo, P., Alonso, M.J., Vila-Jato, J.L., Robinson, J.R., 1996. Improved ocular bioavailability of indomethacin by novel ocular drug carriers. *J. Pharm. Pharmacol.*, 48(11), 1147–1152.

Carino, G.P., Mathiowitz, E., 1999. Oral insulin delivery. *Adv. Drug Deliv. Rev.*, 35, 249–257.

Cassidy, O., Rowley, G., Fletcher, I., Davies, S., Briggs, D., 1999. Surface modification and electrostatic charge of polystyrene particles. *Int. J. Pharm.*, 182(2), 199–211.

Castelli, F., Puglia, C., Sarpietro, M.G., Rizza, L., Bonina, F., 2005. Characterization of indomethacin-loaded lipid nanoparticles by differential scanning calorimetry. *Int. J. Pharm.*, 304, 231–238.

Cavalli, R., Caputo, O., Gasco, M.R., 1993. Solid lipospheres of doxorubicin and idarubicin. *Int. J. Pharm.*, 89(1), R9–R12.

Cavalli, R., Peira, E., Caputo, O., Gasco, M.R., 1999. Solid lipid nanoparticles as carriers of hydrocortisone and progesterone complexes with β-cyclodextrins. *Int. J. Pharm.*, 182(1), 59–69.

Cedeno, F.O., Prieto, M.M., Espina, A., Garcia, J.R., 2001. Measurements of temperature and melting heat of some pure fatty acids and their binary and ternary mixtures by differential scanning calorimetry. *Thermochim. Acta*, 369, 39–50.

Chen, D.B., Yang, T.Z., Lu, W.L., Zhang, Q., 2001. *In vitro* and *in vivo* study of two types of long-circulating solid lipid nanoparticles containing paclitaxel. *Chem. Pharm. Bull. (Tokyo).*, 49, 1444–1447.

Chen, M.-C., Sonaje, K., Chen, K.-J., Sung, H.-W., 2011. A review of the prospects for polymeric nanoparticle platforms in oral insulin delivery. Biomaterials 32, 9826–38. doi:10.1016/j.biomaterials.2011.08.087

Ciszak, E. and Smith, G.D., 1994. Crystallographic evidence for dual coordination around zinc in the T3R3 human insulin hexamer. *Biochemistry*, 33, 1512–1517.

Clark, M., Jepson, M.A., Hirst, B.H., 2001. Exploiting M cells for drug and vaccine delivery. *Adv. Drug Deliv. Rev.*, 50, 81–106.

Clodfelter, D.K., Nussbaum, M.A., Reilly, J., 1999. Comparison of free solution capillary electrophoresis and size exclusion chromatography for quantitating non-covalent aggregation of an acylated peptide. *J. Pharm. Biomed. Anal.*, 19, 763–775.

Cortesi, R., Esposito, E., Luca, G., Nastruzzi, C., 2002. Production of lipospheres as carriers for bioactive compounds. *Biomaterials*, 23(11), 2283–2294.

Coustan, D.R., 2007. Pharmacological management of gestational diabetes: an overview. *Diabetes Care*, 30(2), S206–S208.

Couvreur, P., Kante, B., Roland, M., Speiser, P., 1979. Adsorption of antineoplastic drugs to polyalkylcyanoacrylate nanoparticles and their release in calf serum. *J. Pharm. Sci.*, 68(12), 1521–1524.

Craig, D.Q.M. and Reading, M., 2006. *Thermal analysis of pharmaceuticals.* CRC press, Boca Raton, FL.

Cui, F., Shi, K., Zhang, L., Tao, A., Kawashima, Y., 2006. Biodegradable nanoparticles loaded with insulin-phospholipid complex for oral delivery: preparation, *in vitro* characterization and *in vivo* evaluation. *J. Control. Release*, 114, 242–250.

Damgé, C., Maincent, P., Ubrich, N., 2007. Oral delivery of insulin associated to polymeric nanoparticles in diabetic rats. *J. Control. Release*, 117(2), 163–70.

Damgé, C., Michel, C., Aprahamian, M., Couvreur, P., 1988. New approach for oral administration of insulin with polyalkylcyanoacrylate nanocapsules as drug carrier. *Diabetes*, 37(2), 246–251.

Dapergolas, G., Gregoriadis, G., 1976. Hypoglycaemic effect of liposome-entrapped insulin administered intragastrically into rats. *Lancet*, 2, 824–827.

Darrington, R.T. and Anderson, B.D., 1995. Effects of insulin concentration and self-association on the partitioning of its A-21 cyclic anhydride intermediate to desamido insulin and covalent dimer. *Pharm. Res.*, 12(7), 1077–1084.

Deli, M.A., 2009. Potential use of tight junction modulators to reversibly open membranous barriers and improve drug delivery. *Biochim. Biophys. Acta (BBA)-Biomembranes*, 1788(4), 892–910.

Delie, F., 1998. Evaluation of nano- and microparticle uptake by the gastrointestinal tract. *Adv. Drug Deliv. Rev.*, 34(2), 221–233.

Delie, F., Berton, M., Allémann, E., Gurny, R., 2001. Comparison of two methods of encapsulation of an oligonucleotide into poly(D,L-lactic acid) particles. *Int. J. Pharm.*, 214(1), 25–30.

Demeule, B., Gurny, R., Arvinte, T., 2007. Detection and characterization of protein aggregates by fluorescence microscopy. *Int. J. Pharm.*, 329(1), 37–45.

Des Rieux, A., Fievez, V., Théate, I., Mast, J., Préat, V., Schneider, Y.J., 2007. An improved *in vitro* model of human intestinal follicle-associated epithelium to study nanoparticle transport by M cells. *Eur. J. Pharm. Sci.*, 30(5), 380–391.

Dinda, A., Biswal, I., Chowdhury, P., Mohapatra, R., 2013. Formulation development and evaluation of paclitaxel loaded solid lipid nanoparticles using glyceryl monostearate. *J. Appl. Pharm. Sci.*, 3(8), 133-138.

Doktorovova, S., Souto, E.B., Silva, A.M., 2014. Nanotoxicology applied to solid lipid nanoparticles and nanostructured lipid carriers–A systematic review of *in vitro* data. *Eur. J. Pharm. Biopharm*., 87(1), 1–18.

Dolan, J.W., 2002. Temperature selectivity in reversed-phase high performance liquid chromatography. *J. Chromatogr. A*, 965(1), 195–205.

Dufresne, M.H., Leroux, J.C., 2004. Study of the micellization behavior of different order amino block copolymers with heparin. *Pharm. Res.*, 21(1), 160–169.

Edge, S., Potter, U.J., Steele, D.F., Tobyn, M.J., Chen, A., Staniforth, J.N., 1999. The location of silicon dioxide in silicified microcrystalline cellulose. *Pharm. Pharmacol. Commun.*, 5(6), 371–376.

Eldem, T., Speiser, P., Hincal, A., 1991. Optimization of spray-dried and -congealed lipid micropellets and characterization of their surface morphology by scanning electron microscopy. *Pharm. Res.*, 8, 47–54.

Eldridge, J.H., Hammond, C.J., Meulbroek, J.A., Staas, J.K., Gilley, R.M., Tice, T.R., 1990. Controlled vaccine release in the gut-associated lymphoid tissues. I. Orally administered biodegradable microspheres target the Peyer's patches. *J. Control. Release*, 11(1), 205–214.

El-Etr, M., Slama, G., Desplanque, N., 1987. Preprandial intranasal insulin as adjuvant therapy in type II diabetics. *Lancet*, 330, 1085–1086.

Elvassore, N., Bertucco, A., Caliceti, P., 2001. Production of insulin-loaded poly (ethylene glycol)/poly (l-lactide)(PEG/PLA) nanoparticles by gas antisolvent techniques. *J. Pharm. Sci.*, 90(10), 1628–1636.

Fan, T., Chen, C., Guo, H., Xu, J., Zhang, J., Zhu, X., Yang, Y., Zhou, Z., Li, L., Huang, Y., 2014. Design and evaluation of solid lipid nanoparticles modified with peptide ligand for oral delivery of protein drugs. *Eur. J. Pharm. Biopharm.*, 88(2), 518-528.

Fangueiro, J.F., Gonzalez-Mira, E., Martins-Lopes, P., Egea, M.A., Garcia, M.L., Souto, S.B., Souto, E.B., 2013. A novel lipid nanocarrier for insulin delivery: production, characterization and toxicity testing. *Pharm. Dev. Technol.*, 18(3), 545–549.

Farid, N.A., Atkins, L.M., Becker, G.W., Dinner, A., Heiney, R.E., Miner, D.J., Riggin, R.M., 1989. Liquid chromatographic control of the identity, purity and "potency" of biomolecules used as drugs. *J. Pharm. Biomed. Anal.*, 7(2), 185–188.

Fernandez-Hervas, M.J., Holgado, M.A., Fini, A., Fell, J.T., 1998. *In vitro* evaluation of alginate beads of a diclofenac salt. *Int. J. Pharm.*, 163(1), 23–34.

Flood, T., 2006. Advances in insulin delivery systems and devices: beyond the vial and syringe. *Insulin*, 1(3), 99–108.

Florence, A.T., 2005. Nanoparticle uptake by the oral route: Fulfilling its potential? *Drug Discov. Today Technol.*, 2(1), 75–81.

Fogh, J., Fogh, J.M., Orfeo, T., 1977. One hundred and twenty-seven cultured human tumor cell lines producing tumors in nude mice. *J. Natl. Cancer Inst.*, 59(1), 221–226.

Folmer, J.C.W. and Franzen, S., 2003. Study of polymer glasses by modulated differential scanning calorimetry in the undergraduate physical chemistry laboratory. *J. Chem. Educ.*, 80(7), 813.

Frauman, A.G., Cooper, M.E., Parsons, B.J., Jerums, G., Louis, W.J., 1987. Long-term use of intranasal insulin in insulin-dependent diabetic patients. *Diabetes Care*, 10(5), 573–578.

Freshney, R.I., 2000. *Culture of animal cells: A manual of basic technique,* 4th ed., Wiley, NY.

Fukuda, Y., Tsuji, T., Fujita, T., Yamamoto, A., Muranishi, S., 1995. Susceptibility of insulin to proteolysis in rat lung homogenate and its protection from proteolysis by various protease inhibitors. *Biol. Pharm. Bull.*, 18(6), 891–894.

Garcia-Fuentes, M., Alonso, M.J., Torres, D., 2005a. Design and characterization of a new drug nanocarrier made from solid-liquid lipid mixtures. *J. Colloid Interface Sci.*, 285(2), 590–598.

Garcia-Fuentes, M., Torres, D., Alonso, M.J., 2005b. New surface-modified lipid nanoparticles as delivery vehicles for salmon calcitonin. *Int. J. Pharm.*, 296(1), 122–132.

Garcıa-Fuentes, M., Torres, D., Alonso, M.J., 2003. Design of lipid nanoparticles for the oral delivery of hydrophilic macromolecules. *Colloids Surf. B.*, 27(2), 159–168.

Garcia-Fuentes, M., Prego, C., Torres, D., Alonso, M.J., 2005c. A comparative study of the potential of solid triglyceride nanostructures coated with chitosan or poly(ethylene glycol) as carriers for oral calcitonin delivery. *Eur. J. Pharm. Sci.*, 25(1), 133–143.

Gedanken, A., 2004. Using sonochemistry for the fabrication of nanomaterials. *Ultrason. Sonochem.*, 11(2), 47–55.

Geng, X. and Wang, L., 2008. Liquid chromatography of recombinant proteins and protein drugs. *J. Chromatogr. B*, 866(1), 133–153.

Goeddel, D. V, Kleid, D.G., Bolivar, F., Heyneker, H.L., Yansura, D.G., Crea, R., Hirose, T., Kraszewski, A., Itakura, K., Riggs, A.D., 1979. Expression in Escherichia coli of chemically synthesized genes for human insulin. *Proc. Natl. Acad. Sci. USA*, 76(1), 106–110.

Gök, E. and Olgaz, S., 2004. Binding of fluorescein isothiocyanate to insulin: A fluorimetric labeling study. *J. Fluoresc.*, 14(2), 203–206.

Gualbert, J., Shahgaldian, P., Coleman, A.W., 2003. Interactions of amphiphilic calixarene-based solid lipid nanoparticles with bovine serum albumin. *Int. J. Pharm.*, 257, 69–73.

Hatziantoniou, S., Deli, G., Nikas, Y., Demetzos, C., Papaioannou, G.T., 2007. Scanning electron microscopy study on nanoemulsions and solid lipid nanoparticles containing high amounts of ceramides. *Micron*, 38(8), 819–823.

He, C., Hu, Y., Yin, L., Tang, C., Yin, C., 2010. Effects of particle size and surface charge on cellular uptake and biodistribution of polymeric nanoparticles. *Biomaterials*, 31(13), 3657–3666.

Heinemann, L., 2012. New ways of insulin delivery. *Int. J. Clin. Pract.*, 66(s175), 35–39.

Helgason, T., Awad, T.S., Kristbergsson, K., McClements, D.J., Weiss, J., 2009. Effect of surfactant surface coverage on formation of solid lipid nanoparticles (SLN). *J. Colloid Interface Sci.*, 334(1), 75–81.

Hertzog, D.L., McCafferty, J.F., Fang, X., Tyrrell, R.J., Reed, R.A., 2002. Development and validation of a stability-indicating HPLC method for the simultaneous determination of Losartan potassium, hydrochlorothiazide, and their degradation products. *J. Pharm. Biomed. Anal.*, 30(3), 747–760.

Heurtault, B., Saulnier, P., Pech, B., Proust, J.E., Benoit, J.P., 2003. Physico-chemical stability of colloidal lipid particles. *Biomaterials*, 24(23), 4283–4300.

Hidalgo, I.J., Raub, T.J., Borchardt, R.T., 1989. Characterization of the human colon carcinoma cell line (Caco-2) as a model system for intestinal epithelial permeability. *Gastroenterology*, 96, 736–749.

Hillaireau, H. and Couvreur, P., 2009. Nanocarriers' entry into the cell: relevance to drug delivery. *Cell. Mol. Life Sci.*, 66(17), 2873–2896.

Hoshino, A., Fujioka, K., Oku, T., Suga, M., Sasaki, Y.F., Ohta, T., Yasuhara, M., Suzuki, K., Yamamoto, K., 2004. Physicochemical Properties and Cellular Toxicity of Nanocrystal Quantum Dots Depend on Their Surface Modification. *Nano Lett.*, 4(11), 2163–2169.

Hoyer, G.L., Nolan Jr, P.E., LeDoux, J.H., Moore, L.A., 1995. Selective stability-indicating high-performance liquid chromatographic assay for recombinant human regular insulin. *J. Chromatogr. A*, 699(1), 383–388.

Hu, F.Q., Hong, Y., Yuan, H., 2004. Preparation and characterization of solid lipid nanoparticles containing peptide. *Int. J. Pharm.*, 273(1), 29–35.

Hu, F.Q., Jiang, S.P., Du, Y.Z., Yuan, H., Ye, Y.Q., Zeng, S., 2006. Preparation and characteristics of monostearin nanostructured lipid carriers. *Int. J. Pharm.,* 314(1), 83–89.

Hu, F.Q., Yuan, H., Zhang, H.H., Fang, M., 2002. Preparation of solid lipid nanoparticles with clobetasol propionate by a novel solvent diffusion method in aqueous system and physicochemical characterization. *Int. J. Pharm.*, 239(1), 121–128.

Hu, M., Chujo, S., Nishikawa, H., Yamaguchi, Y., Okubo, T., 2004. Spontaneous formation of large-area monolayers of well-ordered nanoparticles via a wet-coating process. *J. Nanoparticle Res.*, 6(5), 479–487.

Hubert, B., Atkinson, J., Guerret, M., Hoffman, M., Devissaguet, J.P., Maincent, P., 1991. The preparation and acute antihypertensive effects of a nanocapsular form of darodipine, a dihydropyridine calcium entry blocker. *Pharm. Res.*, 8(6), 734–738.

Hulspas, R., O'Gorman, M.R.G., Wood, B.L., Gratama, J.W., Robert Sutherland, D., 2009. Considerations for the control of background fluorescence in clinical flow cytometry. *Cytom. Part B - Clin. Cytom.*, 76(6), 355–364.

Hussain, A., Arnold, J.J., Khan, M.A., Ahsan, F., 2004. Absorption enhancers in pulmonary protein delivery. *J. Control. Release*, 94(1), 15–24.

Hussain, N., Jaitley, V., Florence, A.T., 2001. Recent advances in the understanding of uptake of microparticulates across the gastrointestinal lymphatics. *Adv. Drug Deliv. Rev.*, 50(1), 107–142.

IDF, 2013. *IDF Diabetes Atlas*, 6th ed., International Diabetes Federation, Brussels, Belgium.

Israelachvili, J.N., 2011. *Intermolecular and Surface Forces*, 3rd ed., Academic Press, Waltham, MA.

Jacob, S., Shirwaikar, A.A., Srinivasan, K.K., Alex, J., Prabu, S.L., Mahalaxmi, R., Kumar, R., 2006. Stability of proteins in aqueous solution and solid state. *Indian J. Pharm. Sci.*, 68(2), 154.

Jain, D., Majumdar, D.K., Panda, A.K., 2006. Insulin loaded eudragit L100 microspheres for oral delivery: preliminary *in vitro* studies. *J. Biomater. Appl*., 21(2), 195–211.

Jani, P., Halbert, G.W., Langridge, J., Florence, A.T., 1989. The uptake and translocation of latex nanospheres and microspheres after oral administration to rats. *J. Pharm. Pharmacol.*, 41(12), 809–812.

Jenning, V., Schäfer-Korting, M., Gohla, S., 2000. Vitamin A-loaded solid lipid nanoparticles for topical use: drug release properties. *J. Control. Release*, 66(2), 115–126.

Jiang, J., Oberdörster, G., Biswas, P., 2008. Characterization of size, surface charge, and agglomeration state of nanoparticle dispersions for toxicological studies. *J. Nanoparticle Res.*, 11(1), 77–89.

Jores, K., Mehnert, W., Bunjes, H., Drechsler, M., Mäder, K., 2003. From solid lipid nanoparticles (SLN) to nanospoons. Visions and reality of colloidal lipid dispersions, in: *Proceedings of the 30th Annual Meeting & Exposition of the Controlled Release Society*, 181.

Jorgensen, L. and Nielson, H.M., 2009. *Delivery technologies for biopharmaceuticals: peptides, proteins, nucleic acids and vaccines*, John Wiley & Sons, West Sussex, UK.

Karmarkar, A.B., Gonjari, I.D., Hosmani, A.H., 2008. Poloxamers and their applications. *Online Int. J. Pharmainfo.net*, 1–32.

Kaszuba, M., McKnight, D., Connah, M.T., McNeil-Watson, F.K., Nobbmann, U., 2008. Measuring sub nanometre sizes using dynamic light scattering. *J. Nanoparticle Res.*, 10(5), 823–829.

Kavimandan, N.J. and Peppas, N.A., 2008. Confocal microscopic analysis of transport mechanisms of insulin across the cell monolayer. *Int. J. Pharm.*, 354(1), 143–148.

Kavimandan, N.J., Peppas, N.A., Morishita, M., Goto, T., Nagai, T., Takayama, K., 2003. Experimental investigation of the effect of complexation hydrogels on insulin transport across model intestinal cell monolayers. *Drug Deliv. Syst.*, 18, 283.

Keck, C.M. and Müller, R.H., 2008. Size analysis of submicron particles by laser diffractometry-90% of the published measurements are false. *Int. J. Pharm.*, 355(1), 150–163.

Khan, N., Craig, D.Q.M., 2003. The influence of drug incorporation on the structure and release properties of solid dispersions in lipid matrices. *J. Control. Release*, 93(3), 355–368.

Kimura, T. and Higaki, K., 2002. Gastrointestinal Transit and Drug Absorption. *Biol. Pharm. Bull.*, 25(2), 149–164.

Kipp, J.E., 2004. The role of solid nanoparticle technology in the parenteral delivery of poorly water-soluble drugs. *Int. J. Pharm.*, 284(1), 109–122.

Klyushnichenko, V.E., Koulich, D.M., Yakimov, S.A., Maltsev, K. V, Grishina, G.A., Nazimov, I. V, Wulfson, A.N., 1994. Recombinant human insulin: III. High-performance liquid chromatography and high-performance capillary electrophoresis control in the analysis of step-by-step production of recombinant human insulin. *J. Chromatogr. A*, 661(1), 83–92.

Krentz, A.J. and Bailey, C.J., 2005. Oral antidiabetic agents: Current role in type 2 diabetes mellitus. *Drugs*, 65(3), 385–411.

Kuisma-Kursula, P., 2000. Accuracy , precision and detection limits of SEM–WDS, SEM–EDS and PIXE in the multi-elemental analysis of medieval glass. *X-Ray Spectrom.*, 29, 111–118.

Kunitake, T. and Okahata, Y., 1978. Synthetic bilayer membranes with anionic head groups. *Bull. Chem. Soc. Jpn.*, 51(6), 1877–1879.

Lai, M.C. and Topp, E.M., 1999. Solid-state chemical stability of proteins and peptides. *J. Pharm. Sci.*, 88(5), 489–500.

Laroui, H., Grossin, L., Léonard, M., Stoltz, J.-F., Gillet, P., Netter, P., Dellacherie, E., 2007. Hyaluronate-covered nanoparticles for the therapeutic targeting of cartilage. *Biomacromolecules*, 8(12), 3879–3885.

Lassmann-Vague, V. and Raccah, D., 2006. Alternatives routes of insulin delivery. *Diabetes Metab.*, 32(5), 513–522.

Leary, A.C., Stote, R.M., Cussen, K., O'Brien, J., Leary, W.P., Buckley, B., 2006. Pharmacokinetics and pharmacodynamics of intranasal insulin administered to patients with type 1 diabetes: a preliminary study. *Diabetes Technol. Ther.*, 8(1), 81–88.

Lee, H.J., McAuley, A., Schilke, K.F., McGuire, J., 2011. Molecular origins of surfactant-mediated stabilization of protein drugs. *Adv. Drug Deliv. Rev.*, 63(13), 1160–1171.

Lee, V.H., 1987. Enzymatic barriers to peptide and protein absorption. *Crit. Rev. Ther. Drug Carrier Syst.*, 5(2), 69–97.

Leichman, A.K., 2013. Groundbreaking insulin pill nearing market. *Israel21c*, [online] Available at http://www.israel21c.org/headlines/groundbreaking-insulin-pill-nearing-market/ (Accessed on 10th October 2014).

Liu, J., Gong, T., Fu, H., Wang, C., Wang, X., Chen, Q., Zhang, Q., He, Q., Zhang, Z., 2008. Solid lipid nanoparticles for pulmonary delivery of insulin. *Int. J. Pharm.*, 356(1), 333–344.

Liu, J., Gong, T., Wang, C., Zhong, Z., Zhang, Z., 2007. Solid lipid nanoparticles loaded with insulin by sodium cholate-phosphatidylcholine-based mixed micelles: preparation and characterization. *Int. J. Pharm.*, 340(1), 153–162.

Luo, Y., Chen, D., Ren, L., Zhao, X., Qin, J., 2006. Solid lipid nanoparticles for enhancing vinpocetine's oral bioavailability. *J. Control. Release*, 114(1), 53–59.

Ma, Z. and Lim, L.Y., 2003. Uptake of chitosan and associated insulin in Caco-2 cell monolayers: a comparison between chitosan molecules and chitosan nanoparticles. *Pharm. Res.*, 20(11), 1812–1819.

Mainardes, R.M. and Evangelista, R.C., 2005. PLGA nanoparticles containing praziquantel: Effect of formulation variables on size distribution. *Int. J. Pharm.*, 290(1), 137–144.

Malvern Instruments Ltd., 2014a. *Dynamic light scattering: An introduction in 30 Minutes*, 4th ed., Zetasizer Nano Series Technical Note, 1-15.

Malvern Instruments Ltd., 2014b. *Zeta potential - An introduction in 30 minutes*, 3rd ed., Zetasizer Nano Series Technical Note, 1-15.

Manconi, M., Sinico, C., Valenti, D., Loy, G., Fadda, A.M., 2002. Niosomes as carriers for tretinoin. I. Preparation and properties. *Int. J. Pharm.*, 234(1), 237–248.

Manning, M.C., Patel, K., Borchardt, R.T., 1989. Stability of protein pharmaceuticals. *Pharm. Res.*, 6(11), 903–918.

Mao, S., Cun, D., Kawashima, Y., 2009. Novel non-injectable formulation approaches of peptides and proteins. In *Deliv. Technol. Biopharm. Pept. Proteins, Nucleic Acids Vaccines*, John Wiley & Sons, Chichester, UK, 29–67.

Martins, S., Costa-Lima, S., Carneiro, T., Cordeiro-da-Silva, A., Souto, E.B., Ferreira, D.C., 2012. Solid lipid nanoparticles as intracellular drug transporters: an investigation of the uptake mechanism and pathway. *Int. J. Pharm.*, 430(1), 216–227.

Martins, S., Silva, A.C., Ferreira, D.C., Souto, E.B., 2009. Improving oral absorption of Salmon calcitonin by trimyristin lipid nanoparticles. *J. Biomed. Nanotechnol.*, 5(1), 76–83.

Mastrandrea, L.D. and Quattrin, T., 2006. Clinical evaluation of inhaled insulin. *Adv. Drug Deliv. Rev.*, 58(9), 1061–1075.

Mathieu, C. and Gale, E.A.M., 2008. Inhaled insulin: gone with the wind? *Diabetologia*, 51(1), 1–5.

McNally, E.J. and Hastedt, J.E., 2013. *Protein formulation and delivery*. CRC Press, Taylor & Francis Group, Boca Raton, FL.

Mehnert, W. and Mäder, K., 2001. Solid lipid nanoparticles Production, characterization and applications. *Adv. Drug Deliv. Rev.*, 47(2), 165–196.

Meier, J.J., Holst, J.J., Schmidt, W.E., Nauck, M.A., 2007. Reduction of hepatic insulin clearance after oral glucose ingestion is not mediated by glucagon-like peptide 1 or gastric inhibitory polypeptide in humans. *Am. J. Physiol. Endocrinol. Metab.*, 293(3), E849–E856.

Ministry of Health, 2012. *National Health Morbidity Survey 2011.* Institute of Public Health, Ministry of Health, Malaysia.

Morel, S., Terreno, E., Ugazio, E., Aime, S., Gasco, M.R., 1998. NMR relaxometric investigations of solid lipid nanoparticles (SLN) containing gadolinium (III) complexes. *Eur. J. Pharm. Biopharm.*, 45(2), 157–163.

Morishita, M., Lowman, A.M., Takayama, K., Nagai, T., Peppas, N.A., 2002. Elucidation of the mechanism of incorporation of insulin in controlled release systems based on complexation polymers. *J. Control. Release*, 81(1), 25–32.

Moslemi, P., Najafabadi, A.R., Tajerzadeh, H., 2003. A rapid and sensitive method for simultaneous determination of insulin and A21-desamido insulin by high-performance liquid chromatography. *J. Pharm. Biomed. Anal.*, 33(1), 45–51.

Mudshinge, S.R., Deore, A.B., Patil, S., Bhalgat, C.M., 2011. Nanoparticles: Emerging carriers for drug delivery. *Saudi Pharm. J.*, 19(3), 129–41.

Mühlen, Z.A. and Mehnert, W., 1998. Drug release and release mechanism of prednisolone loaded solid lipid nanoparticles. *Pharmazie*, 53, 552–555.

Mühlen, Z.A., Schwarz, C., Mehnert, W., 1998. Solid lipid nanoparticles (SLN) for controlled drug delivery - Drug release and release mechanism. *Eur. J. Pharm. Biopharm.*, 45(2), 149–155.

Mukherjee, S., Ray, S., Thakur, R., 2009a. Design and evaluation of itraconazole loaded solid lipid nanoparticulate system for improving the antifungal therapy. *Pak. J. Pharm. Sci.*, 22(2), 131–8.

Mukherjee, S., Ray, S., Thakur, R.S., 2009b. Solid lipid nanoparticles: a modern formulation approach in drug delivery system. *Indian J. Pharm. Sci.*, 71(4), 349–358.

Müller, R.H. and Keck, C.M., 2004. Challenges and solutions for the delivery of biotech drugs - A review of drug nanocrystal technology and lipid nanoparticles. *J. Biotechnol.*, 113(1), 151–170.

Müller, R.H., Mäder, K., Gohla, S., 2000. Solid lipid nanoparticles (SLN) for controlled drug delivery - a review of the state of the art. *Eur. J. Pharm. Biopharm.*, 50(1), 161–177.

Müller, R.H., Mehnert, W., Lucks, J.-S., Schwarz, C., Zur Mühlen, A., Meyhers, H., Freitas, C., Rühl, D., 1995. Solid lipid nanoparticles (SLN) : an alternative colloidal carrier system for controlled drug delivery. *Eur. J. Pharm. Biopharm.*, 41(1), 62–69.

Müller, R.H., Radtke, M., Wissing, S.A., 2002a. Solid lipid nanoparticles (SLN) and nanostructured lipid carriers (NLC) in cosmetic and dermatological preparations. *Adv. Drug Deliv. Rev.*, 54, S131-155.

Müller, R.H., Radtke, M., Wissing, S.A., 2002b. Nanostructured lipid matrices for improved microencapsulation of drugs. *Int. J. Pharm.*, 242(1), 121–128.

Mundargi, R.C., Babu, V.R., Rangaswamy, V., Patel, P., Aminabhavi, T.M., 2008. Nano/micro technologies for delivering macromolecular therapeutics using poly(D,L-lactide-co-glycolide) and its derivatives. *J. Control. Release*, 125(3), 193–209.

Nihant, N., Schugens, C., Grandfils, C., Jerome, R., Teyssie, P., 1994. Polylactide microparticles prepared by double emulsion/evaporation technique. I. Effect of primary emulsion stability. *Pharm. Res.*, 11(10), 1479–1484.

Obeidat, W.M., Schwabe, K., Müller, R.H., Keck, C.M., 2010. Preservation of nanostructured lipid carriers (NLC). *Eur. J. Pharm. Biopharm.*, 76(1), 56–67.

Okumura, K., Iwakawa, S., Yoshida, T., Seki, T., Komada, F., 1992. Intratracheal delivery of insulin absorption from solution and aerosol by rat lung. *Int. J. Pharm.*, 88(1), 63–73.

Olbrich, C., Kayser, O., Müller, R.H., 2002. Lipase degradation of Dynasan 114 and 116 solid lipid nanoparticles (SLN) - Effect of surfactants, storage time and crystallinity. *Int. J. Pharm.*, 237(1), 119–128.

Oliva, A., Fariña, J., Llabrés, M., 1996. Influence of temperature and shaking on stability of insulin preparations: degradation kinetics. *Int. J. Pharm.*, 143(2), 163–170.

Oliva, A., Fariña, J., Llabrés, M., 2000. Development of two high-performance liquid chromatographic methods for the analysis and characterization of insulin and its degradation products in pharmaceutical preparations. *J. Chromatogr. B Biomed. Sci. Appl.*, 749(1), 25–34.

Owens, D.R., 2002. New horizons—alternative routes for insulin therapy. *Nat. Rev. Drug Discov.*, 1(7), 529–540.

Paliwal, R., Rai, S., Vaidya, B., Khatri, K., Goyal, A.K., Mishra, N., Mehta, A., Vyas, S.P., 2009. Effect of lipid core material on characteristics of solid lipid nanoparticles designed for oral lymphatic delivery. *Nanomedicine Nanotechnology Biol. Med.*, 5(2), 184–191.

Parhi, R. and Suresh, P., 2010. Production of solid lipid nanoparticles-drug loading and release mechanism. *J. Chem Pharm Res*, 2(1), 211–227.

Park, T.G., 1999. Temperature modulated protein release from pH/temperature-sensitive hydrogels. *Biomaterials*, 20(6), 517–521.

Passerini, N., Albertini, B., González-Rodríguez, M.L., Cavallari, C., Rodriguez, L., 2002. Preparation and characterisation of ibuprofen–poloxamer 188 granules obtained by melt granulation. *Eur. J. Pharm. Sci.*, 15(1), 71–78.

Pathak, Y., Thassu, D., Deleers, M., 2007. Pharmaceutical applications of nanoparticulate drug-delivery systems, in: *Nanoparticulate Drug Delivery Systems*, Taylor & Francis Group, Boca Raton, FL., 185–212.

Patton, J.S., 1996. Mechanisms of macromolecule absorption by the lungs. *Adv. Drug Deliv. Rev.*, 19(1), 3–36.

Pearlman, R., 1993. *Stability and characterization of protein and peptide drugs: case histories*, Plenum Press, NY.

Pecora, R., 2000. Dynamic light scattering measurement of nanometer particles in liquids. *J. Nanoparticle Res.*, 2(2), 123–131.

Permyakov, E.A., Yarmolenko, V. V, Burstein, E.A., Gerday, C., 1982. Intrinsic fluorescence spectra of a tryptophan-containing parvalbumin as a function of thermal, pH and urea denaturation. *Biophys. Chem.*, 15(1), 19–26.

Petersen, S., Steiniger, F., Fischer, D., Fahr, A., Bunjes, H., 2011. The physical state of lipid nanoparticles influences their effect on *in vitro* cell viability. *Eur. J. Pharm. Biopharm.*, 79(1), 150–161.

Pillai, O., Panchagnula, R., 2001. Polymers in drug delivery. *Curr. Opin. Chem. Biol.*, 5(4), 447–451.

Pinto, M., Robine-Leon, S., Appay, M.-D., Kedinger, M., Triadou, N., Dussaulx, E., Lacroix, B., Simon-Assmann, P., Haffen, K., Fogh, J., Zweibaum, A., 1983. Enterocyte-like differentiation and polarization of the human colon carcinoma cell line Caco-2 in culture. *Biol. Cell*, 47, 323–330.

Plapied, L., Duhem, N., des Rieux, A., Préat, V., 2011. Fate of polymeric nanocarriers for oral drug delivery. *Curr. Opin. Colloid Interface Sci.*, 16(3), 228–237.

Purcell, A.W., Aguilar, M.I., Hearn, M.T.W., 1995. Conformational effects in reversed-phase high-performance liquid chromatography of polypeptides I. Resolution of insulin variants. *J. Chromatogr. A*, 711(1), 61–70.

Quintanar-Guerrero, D., Tamayo-Esquivel, D., Ganem-Quintanar, A., Allémann, E., Doelker, E., 2005. Adaptation and optimization of the emulsification-diffusion technique to prepare lipidic nanospheres. *Eur. J. Pharm. Sci.*, 26(2), 211–218.

Rader, R.A., 2005. What is a biopharmaceutical. *Part 1, BioExecutive International*, 60–65.

Rader, R.A., 2008. (Re) defining biopharmaceutical. *Nat. Biotechnol.*, 26(7), 743–751.

Rajan, Ds., Gowda, Kv., Mandal, U., Ganesan, M., Bose, A., Sarkar, A., Pal, T., 2006. Development of RP-HPLC for analysis of human insulin. *Indian J. Pharm. Sci.*, 68(5), 662.

Rang, H.P., Dale, M.M., Ritter, J.M., Moore, P.K., 2003. *Pharmacology*, Churchill Livingstone, NY.

Rekha, M.R. and Sharma, C.P., 2009. Synthesis and evaluation of lauryl succinyl chitosan particles towards oral insulin delivery and absorption. *J. Control. Release*, 135(2), 144–151.

Roach, P., Farrar, D., Perry, C.C., 2005. Interpretation of protein adsorption: surface-induced conformational changes. *J. Am. Chem. Soc.*, 127(22), 8168–8173.

Ruckmani, K., Sivakumar, M., Ganeshkumar, P.A., 2006. Methotrexate loaded solid lipid nanoparticles (SLN) for effective treatment of carcinoma. *J. Nanosci. Nanotechnol.*, 6(9-10), 2991–2995.

Salmaso, S., Elvassore, N., Bertucco, A., Caliceti, P., 2009. Production of solid lipid submicron particles for protein delivery using a novel supercritical gas-assisted melting atomization process. *J. Pharm. Sci.*, 98(2), 640–650.

Sambuy, Y., De Angelis, I., Ranaldi, G., Scarino, M.L., Stammati, A., Zucco, F., 2005. The Caco-2 cell line as a model of the intestinal barrier: Influence of cell and culture-related factors on Caco-2 cell functional characteristics. *Cell Biol. Toxicol.*, 21(1), 1–26.

Sarmento, B., Martins, S., Ferreira, D., Souto, E.B., 2007a. Oral insulin delivery by means of solid lipid nanoparticles. *Int. J. Nanomedicine*, 2(4), 743–749.

Sarmento, B., Ribeiro, A., Veiga, F., Ferreira, D., 2006. Development and validation of a rapid reversed-phase HPLC method for the determination of insulin from nanoparticulate systems. *Biomed. Chromatogr.*, 20(9), 898–903.

Sarmento, B., Ribeiro, A., Veiga, F., Ferreira, D., Neufeld, R., 2007b. Oral bioavailability of insulin contained in polysaccharide nanoparticles. *Biomacromolecules*, 8(10), 3054–3060.

Satake, S., Moore, M.C., Igawa, K., Converse, M., Farmer, B., Neal, D.W., Cherrington, A.D., 2002. Direct and indirect effects of insulin on glucose uptake and storage by the liver. *Diabetes*, 51(6), 1663–1671.

Sauter, C., Emin, M.A., Schuchmann, H.P., Tavman, S., 2008. Influence of hydrostatic pressure and sound amplitude on the ultrasound induced dispersion and de-agglomeration of nanoparticles. *Ultrason. Sonochem.*, 15(4), 517–523.

Schmiele, M., Gehrer, S., Westermann, M., Steiniger, F., Unruh, T., 2014. Formation of liquid crystalline phases in aqueous suspensions of platelet-like tripalmitin nanoparticles. *J. Chem. Phys.*, 140(21), 214905.

Schubert, M.A. and Müller-Goymann, C.C., 2005. Characterisation of surface-modified solid lipid nanoparticles (SLN): influence of lecithin and nonionic emulsifier. *Eur. J. Pharm. Biopharm.*, 61(1), 77–86.

Schwarz, C., Mehnert, W., Lucks, J.S., Müller, R.H., 1994. Solid lipid nanoparticles (SLN) for controlled drug delivery. I. Production, characterization and sterilization. *J. Control. Release*, 30(1), 83–96.

Severino, P., Andreani, T., Jäger, A., Chaud, M. V, Santana, M.H.A., Silva, A.M., Souto, E.B., 2014. Solid lipid nanoparticles for hydrophilic biotech drugs: Optimization and cell viability studies (Caco-2 & HEPG-2 cell lines). *Eur. J. Med. Chem.*, 81, 28–34.

Severino, P., Pinho, S.C., Souto, E.B., Santana, M.H.A., 2012. Crystallinity of Dynasan® 114 and Dynasan® 118 matrices for the production of stable Miglyol®-loaded nanoparticles. *J. Therm. Anal. Calorim.*, 108(1), 101–108.

Shah, P., Jogani, V., Bagchi, T., Misra, A., 2006. Role of Caco-2 Cell Monolayers in Prediction of Intestinal Drug Absorption. *Biotechnol. Prog.*, 22(1), 186–198.

Sharma, P., Ganta, S., Denny, W.A., Garg, S., 2009. Formulation and pharmacokinetics of lipid nanoparticles of a chemically sensitive nitrogen mustard derivative: Chlorambucil. *Int. J. Pharm.*, 367(1), 187–194.

Siekmann, B. and Westesen, K., 1996. Investigations on solid lipid nanoparticles prepared by precipitation in o/w emulsions. *Eur. J. Pharm. Biopharm.*, 42(2), 104–109.

Sonaje, K., Lin, K.J., Wang, J.J., Mi, F.L., Chen, C.T., Juang, J.H., Sung, H.W., 2010a. Self-assembled pH-sensitive nanoparticles: A platform for oral delivery of protein drugs. *Adv. Funct. Mater.*, 20(21), 3695–3700.

Sonaje, K., Lin, K.J., Wey, S.P., Lin, C.K., Yeh, T.H., Nguyen, H.N., Hsu, C.W., Yen, T.C., Juang, J.H., Sung, H.W., 2010b. Biodistribution, pharmacodynamics and pharmacokinetics of insulin analogues in a rat model: Oral delivery using pH-responsive nanoparticles vs. subcutaneous injection. *Biomaterials*, 31, 6849–6858.

Soppimath, K.S., Aminabhavi, T.M., Kulkarni, A.R., Rudzinski, W.E., 2001. Biodegradable polymeric nanoparticles as drug delivery devices. *J. Control. Release*, 70(1), 1–20.

Souto, E.B. and Müller, R.H., 2006. Investigation of the factors influencing the incorporation of clotrimazole in SLN and NLC prepared by hot high-pressure homogenization. *J. Microencapsul.*, 23(4), 377–388.

Souto, E. and Müller, R.H., 2007. Lipid nanoparticles (SLN and NLC) for drug delivery. *Nanoparticles Pharm. Appl.*, 103–122.

Souto, E. and Müller, R.H., 2010. Lipid Nanoparticles: Effect on bioavailability and pharmacokinetic changes. In *Drug Deliv., Handbook of Experimental Pharmacology*, Springer, Heidelberg, 115–141.

Souto, E.B., Doktorovova, S., Boonme, P., 2011. Lipid nanocarriers-based semisolids: review on materials and end product formulations. *J. Drug Deliv. Sci. Technol.*, 21, 43–54.

Sundram, K., Sambanthamurthi, R., Tan, Y.A., 2003. Palm fruit chemistry and nutrition. *Asia Pac. J. Clin. Nutr.*, 12(3), 355–362.

Sze, A., Erickson, D., Ren, L., Li, D., 2003. Zeta-potential measurement using the Smoluchowski equation and the slope of the current–time relationship in electroosmotic flow. *J. Colloid Interface Sci.*, 261(2), 402–410.

Tauzin, B., 2008. Biotechnology research continues to bolster arsenal against disease with 633 medicines in development. *Med. Dev. Biotechnol.*, 1–59.

Teale, F.W.J., 1960. The ultraviolet fluorescence of proteins in neutral solution. *Biochem. J.*, 76(2), 381.

Trotta, M., Carlotti, M.E., Gallarate, M., Zara, G.P., Muntoni, E., Battaglia, L., 2011. Insulin-loaded SLN prepared with the emulsion dilution technique: *in vivo* tracking of nanoparticles after oral administration to rats. *J. Dispers. Sci. Technol.*, 32(7), 1041–1045.

Trotta, M., Cavalli, R., Carlotti, M.E., Battaglia, L., Debernardi, F., 2005. Solid lipid micro-particles carrying insulin formed by solvent-in-water emulsion–diffusion technique. *Int. J. Pharm.*, 288(2), 281–288.

Trotta, M., Debernardi, F., Caputo, O., 2003. Preparation of solid lipid nanoparticles by a solvent emulsification-diffusion technique. *Int. J. Pharm.*, 257(1), 153–160.

Uner, M. and Yener, G., 2007. Importance of solid lipid nanoparticles (SLN) in various administration routes and future perspectives. *Int. J. Nanomedicine*, 2(3), 289–300.

Unwin, N., 2009. *IDF diabetes atlas*. International Diabetes Federation Executive Office.

Van Breemen, R.B. and Li, Y., 2005. Caco-2 cell permeability assays to measure drug absorption. *Expert Opin. Drug Metab. Toxicol.*, 1, 175–185.

Vandervoort, J. and Ludwig, A., 2002. Biocompatible stabilizers in the preparation of PLGA nanoparticles: a factorial design study. *Int. J. Pharm.*, 238(1), 77–92.

Varshosaz, J., Sadrai, H., Alinagari, R., 2004. Nasal delivery of insulin using chitosan microspheres. *J. Microencapsul.*, 21(7), 761–774.

Vemuri, S. and Rhodes, C., 1995. Preparation and characterization of liposomes as therapeutic delivery systems: a review. *Pharm. Acta Helv.*, 70, 95–111.

Venkateswarlu, V. and Manjunath, K., 2004. Preparation, characterization and *in vitro* release kinetics of clozapine solid lipid nanoparticles. *J. Control. Release*, 95(3), 627–638.

Verma, A. and Stellacci, F., 2010. Effect of surface properties on nanoparticle-cell interactions. *Small*, 6(1), 12–21.

Verspohl, E.J., 2012. Novel pharmacological approaches to the treatment of type 2 diabetes. *Pharmacol. Rev.*, 64(2), 188–237.

Vitorino, C., Carvalho, F.A., Almeida, A.J., Sousa, J.J., Pais, A.A.C.C., 2011. The size of solid lipid nanoparticles: an interpretation from experimental design. *Colloids Surf. B.*, 84(1), 117–130.

Vonarbourg, A., Passirani, C., Saulnier, P., Benoit, J.P., 2006. Parameters influencing the stealthiness of colloidal drug delivery systems. *Biomaterials*, 27(24), 4356–4373.

Wakankar, A.A. and Borchardt, R.T., 2006. Formulation considerations for proteins susceptible to asparagine deamidation and aspartate isomerization. *J. Pharm. Sci.*, 95(11), 2321–2336.

Walsh, G., 2010. Biopharmaceutical benchmarks 2010. *Nat. Biotechnol.*, 28(9), 917-924.

Wang, J., Wang, B.M., Schwendeman, S.P., 2002. Characterization of the initial burst release of a model peptide from poly (D, L-lactide-co-glycolide) microspheres. *J. Control. Release*, 82(2), 289–307.

Warheit, D.B., Laurence, B.R., Reed, K.L., Roach, D.H., Reynolds, G.A.M., Webb, T.R., 2004. Comparative pulmonary toxicity assessment of single-wall carbon nanotubes in rats. *Toxicol. Sci.*, 77(1), 117–125.

Weiss, J., Decker, E.A., McClements, D.J., Kristbergsson, K., Helgason, T., Awad, T., 2008. Solid lipid nanoparticles as delivery systems for bioactive food components. *Food Biophys*., 39(2), 146–154.

Westesen, K., Bunjes, H., Koch, M.H.J., 1997. Physicochemical characterization of lipid nanoparticles and evaluation of their drug loading capacity and sustained release potential. *J. Control. Release*, 48(2), 223–236.

Westesen, K., Siekmann, B., Koch, M.H.J., 1993. Investigations on the physical state of lipid nanoparticles by synchrotron radiation X-ray diffraction. *Int. J. Pharm.*, 93(1), 189–199.

Whittingham, J.L., Scott, D.J., Chance, K., Wilson, A., Finch, J., Brange, J., Guy Dodson, G., 2002. Insulin at pH 2: structural analysis of the conditions promoting insulin fibre formation. *J. Mol. Biol.*, 318(2), 479–490.

Woitiski, C.B., Neufeld, R.J., Ribeiro, A.J., Veiga, F., 2009. Colloidal carrier integrating biomaterials for oral insulin delivery: Influence of component formulation on physicochemical and biological parameters. *Acta Biomater.*, 5, 2475–2484.

Woitiski, C.B., Sarmento, B., Carvalho, R.A., Neufeld, R.J., Veiga, F., 2011. Facilitated nanoscale delivery of insulin across intestinal membrane models. *Int. J. Pharm.*, 412, 123–131.

Woodley, J.F., 1993. Enzymatic barriers for GI peptide and protein delivery. *Crit. Rev. Ther. Drug Carrier Syst.*, 11(2-3), 61–95.

Xie, S., Wang, S., Zhao, B., Han, C., Wang, M., Zhou, W., 2008. Effect of PLGA as a polymeric emulsifier on preparation of hydrophilic protein-loaded solid lipid nanoparticles. *Colloids Surf. B.*, 67(2), 199–204.

Xie, S., Zhu, L., Dong, Z., Wang, X., Wang, Y., Li, X., Zhou, W., 2011a. Preparation, characterization and pharmacokinetics of enrofloxacin-loaded solid lipid nanoparticles: influences of fatty acids. *Colloids Surf. B.*, 83(2), 382–387.

Xie, S., Zhu, L., Dong, Z., Wang, Y., Wang, X., Zhou, W., 2011b. Preparation and evaluation of ofloxacin-loaded palmitic acid solid lipid nanoparticles. *Int. J. Nanomedicine*, 6, 547–555.

Xu, F.H. and Zhang, Q., 2007. Recent advances in the preparation progress of protein/peptide drug loaded PLA/PLGA microspheres. *Acta Pharmaceutica Sinica*, 42(1), 1–7.

Xu, X., Fu, Y., Hu, H., Duan, Y., Zhang, Z., 2006. Quantitative determination of insulin entrapment efficiency in triblock copolymeric nanoparticles by high-performance liquid chromatography. *J. Pharm. Biomed. Anal.*, 41(1), 266–273.

Xue, M., Yang, M., Zhang, W., Li, X., Gao, D., Ou, Z., Li, Z., Liu, S., Li, X., Yang, S., 2013. Characterization, pharmacokinetics, and hypoglycemic effect of berberine loaded solid lipid nanoparticles. *Int. J. Nanomedicine*, 8, 4677–4687.

Yanagawa, A., Iwayama, T., Saotome, T., Shoji, Y., Takano, K., Oka, H., Nakagawa, T., Mizushima, Y., 1989. Selective transfer of cyclosporin to thoracic lymphatic systems by the application of lipid microspheres. *J. Microencapsul.*, 6(2), 161–164.

Yang, R., Gao, R., Li, F., He, H., Tang, X., 2011. The influence of lipid characteristics on the formation, *in vitro* release, and *in vivo* absorption of protein-loaded SLN prepared by the double emulsion process. *Drug Dev. Ind. Pharm.*, 37(2), 139–148.

Yang, S., Zhu, J., Lu, Y., Liang, B., Yang, C., 1999. Body distribution of camptothecin solid lipid nanoparticles after oral administration. *Pharm. Res.*, 16(5), 751–757.

Yang, Y.Y., Chia, H.H., Chung, T.S., 2000. Effect of preparation temperature on the characteristics and release profiles of PLGA microspheres containing protein fabricated by double-emulsion solvent extraction/evaporation method. *J. Control. Release*, 69(1), 81–96.

Yazan, Y., 2008. Solid lipid nanoparticle systems for drug delivery, in: Kumar, M.N.V.R. (Ed.), *Handbook of particulate drug delivery*. American Scientific Publishers, CA, 245–265.

Yin, L., Ding, J., He, C., Cui, L., Tang, C., Yin, C., 2009. Drug permeability and mucoadhesion properties of thiolated trimethyl chitosan nanoparticles in oral insulin delivery. *Biomaterials*, 30, 5691–5700.

Yin, L., Wang, Y., Pang, G., Koltypin, Y., Gedanken, A., 2002. Sonochemical synthesis of cerium oxide nanoparticles-effect of additives and quantum size effect. *J. Colloid Interface Sci.*, 246(1), 78–84.

Yomota, C., Yoshii, Y., Takahata, T., Okada, S., 1996. Separation of B-3 monodesamidoinsulin from human insulin by high-performance liquid chromatography under alkaline conditions. *J. Chromatogr. A*, 721(1), 89–96.

York, P. and Grant, D.J.W., 1985. A disruption index for quantifying the solid state disorder induced by additives or impurities. I. Definition and evaluation from heat of fusion. *Int. J. Pharm.*, 25(1), 57–72.

Zambaux, M.F., Bonneaux, F., Gref, R., Dellacherie, E., Vigneron, C., 1999. Preparation and characterization of protein C-loaded PLA nanoparticles. *J. Control. Release*, 60(2), 179–188.

Zara, G.P., Bargoni, A., Cavalli, R., Fundar, A., Vighetto, D., Gasco, M.R., 2002. Pharmacokinetics and tissue distribution of idarubicin-loaded solid lipid nanoparticles after duodenal administration to rats. *J. Pharm. Sci.*, 91(5), 1324–1333.

Zhang, N., Ping, Q., Huang, G., Xu, W., Cheng, Y., Han, X., 2006. Lectin-modified solid lipid nanoparticles as carriers for oral administration of insulin. *Int. J. Pharm.*, 327(1), 153–159.

Zhang, Z., Lv, H., Zhou, J., 2009. Novel solid lipid nanoparticles as carriers for oral administration of insulin. *Pharmazie*, 64(9), 574–578.